2. Bioenhancement of Atenolol

Atenolol is a cardio selective β blocker, widely used in the management of hypertension, angina pectoris, cardiac arrhythmia's, and myocardial infarction (1). It is always a choice of molecule when β blockers are used for the treatment.

Atenolol is a hydrophilic drug that is transported via the paracellular route through tight junctions (2). After oral administration, about 46–62 % of the dose is absorbed (1). Peak plasma concentrations are reached within 2–4 hr after administration of a single dose. It is excreted almost unchanged in the feces and urine (3). Food intake significantly shortened the time to peak concentration and also caused a significant reduction in AUC values (about 20 %), while elimination half-life remained essentially unaffected (4). It has very low protein binding. Excretion is essentially complete within 48 hr after administration of a single dose. The elimination half-life is 6–9 hr (5).

Atenolol is a BCS class III drug, i.e. it has high permeability and low solubility (6). In last few years various methods have been applied to get a better formulation with good permeation of atenolol. Different sophisticated novel drug delivery approaches and variety of synthetic bioenhancers have been used to improve the absorption characteristics of atenolol (7). Use of natural bioenhancers with poor permeable drugs is a new concept. These natural bioenhancers are effective, less toxic and more stable than the synthetic bioenhancers.

Piperine is used in the form of medications, bioenhancer, spices and condiments. It increases the bioavailability of drugs such as rifampicin, pyrazinamide, propranolol, theophylline, nimesulide and other nutrients such as beta-carotene, enzyme Q10 and vitamins (8,9,10). Glycyrrhizic acid ammonium salt and its derivatives are effectively used as bioenhancer for antibiotics, anti-infective agents, anti-cancer agents and nutritional compounds (11). It is even reported as an oral absorption enhancer of calcitonin, insulin, and Low molecular weight heparin (12,13). In the present chapter piperine and glycyrrhizic acid ammonium salt were incorporated with atenolol. Effect of both bioenhancers on the permeability of atenolol was determined by various methods such as *ex vivo* permeation studies, *in vitro* permeation experiments across epithelial cell monolayers, and *in vivo* pharmacokinetic studies in rats. Optimized binary system was formulated in single oral dosage form.

2.1 ATENOLOL-PIPERINE BINARY SYSTEMS

In the present section piperine (PI) was incorporated with atenolol. Effect of PI on atenolol permeability was determined. PI was incorporated with atenolol (AT), using three different concentrations of PI, by means of three methods such as physical mixture, solvent evaporation method and kneading method. Binary systems with each weight ratio, of three methods were evaluated by following parameters,

- FTIR – to determine physical interaction of PI–AT
- DSC – to determine compatibility of PI with AT
- *Ex vivo* permeation study – to determine the effect of PI on permeation of AT

2.1.1 Materials

The Model drug atenolol (AT) was procured as a gift sample from Wockhardt Ltd., Mumbai, India. Piperine (PI) was purchased from Sigma Aldrich Ltd., Mumbai, India. Potassium bromide, potassium dihydrogen orthophosphate, pancreatin and methanol were purchased from Qualigence fine chemicals, Mumbai, India. All the other chemicals and solvents were of analytical grade and were used without any further purification. Deionized double distilled water was used through out the study.

2.1.2 Methods

AT – PI binary systems were prepared at three different weight ratios (AT: PI – 5:1, 5:2, and 5:3 w/w). Three different methods such as physical mixture, solvent evaporation method and kneading method were used to prepare AT – PI binary systems. All three methods are described in detail below,

Physical Mixtures (**PM**):

The required and accurately weighed amounts of AT and PI were prepared by simply mixing the powders in a polythene bag.

Solvent Evaporation Method (**SE**):

The required amounts of AT and PI were accurately weighed and dissolved in methanol. Both solutions were mixed uniformly followed by allowing the solvent evaporated to get a dried powder.

Kneading Method (**KE**):

The required amount of AT was dissolved in sufficient amount of double distilled water, PI was dissolved in methanol. Methanolic solution of PI was drop wise mixed in the AT solution with continuous trituration, which leads precipitations. The solvent was allowed to evaporate to get a dried powder.

2.1.3 Evaluation Parameters

2.1.3.1 Fourier Transform Infrared Spectroscopy (FTIR)

The FTIR studies were performed to get an idea about the possible physical interaction of AT and PI. FTIR transmission spectra of a pure AT, PI and AT – PI binary systems of PM method, SE method and KE method were obtained using a Fourier Transform infrared spectrophotometer (Avatar™ 360 E.S.P™ FTIR spectrometer, Thermo Nicolet Corp., Madison, WI, USA). A total of 2 % (w/w) of sample (with respect to the potassium bromide-KBr) was mixed with dry KBr. The mixture was ground into a fine powder using an agate mortar before compressing into KBr disc under a hydraulic press at 10,000 psi. Each KBr disc was scanned 16 times at 4 mm s^{-1} at a resolution of 2 cm^{-1} over a wave number region of 500–4000 cm^{-1}. The characteristic peaks were recorded.

2.1.3.2 Differential Scanning Calorimetry (DSC)

Differential scanning calorimetric analysis was used to characterize thermal behaviour of AT, PI and AT-PI binary systems and to check compatibility of PI with AT. DSC thermograms were obtained using an automatic thermal analyzer system (DSC 822e, Mettler Toledo, Columbus, OH, USA). Temperature calibration was performed using indium as a standard. Samples (2.5 to 5 mg) were crimped in a standard aluminium pan and heated from 30–250 °C at a heating rate of 10 °C min^{-1} under constant purging of dry nitrogen at 40 ml min^{-1}. An empty pan,

crimped in same manner as sample, was used as a reference. The characteristic endothermic peaks and specific heat of the melting endotherm were recorded.

2.1.3.3 *Spectrophotometric analysis and standard curves*

Shimadzu, UV-1700 Double beam UV, Visible spectrophotometer, Kyoto (Japan) was used for the spectrophotometric analysis of AT in presence of PI in simulated intestinal fluid (pH 7.4). An analysis was done at 273.6 nm which was previously established as the wavelength of the AT's maximum absorbance (14). Standard curves were constructed by serially diluting a stock solution of AT to obtain concentrations in the range of 0.5-100 µg/ml using simulated intestinal fluid (SIF) as diluent. Each concentration was analyzed in triplicate against reference blank containing PI.

2.1.3.4 *Ex Vivo permeation studies*

All the binary systems containing AT and PI were assessed for *ex vivo* permeation studies. The permeation study was carried out using initial part of goat intestinal membrane, which has similar morphology as human intestine. Intestinal tissue of goat was collected from slaughterhouse where it was removed after sacrificing the animal and was stored in normal saline. Tissue was cleaned and intestinal content was removed by a slow infusion of normal saline and air. Then after the tissue was immediately transferred to experimental set up. Study was conducted using specific diffusion cell with an area of 3.80 cm^2. The tissue was mounted between donor and receiver chamber of cell. Temperature of medium was maintained at 37±1 °C by means of a surrounding jacket. Receptor compartment was filled with simulated intestinal fluid (SIF) which was continuously stirred at 600 rpm with a teflon-coated bar magnet. AT concentration in donor compartment was taken to maintain sink condition (2 mg/ml). Samples were withdrawn from receptor compartment at predetermined time interval 5, 15, 30, 60, 90, 120, 180, and 240 min and replaced with same volume of fresh medium to maintain sink condition. The withdrawn samples were filtered through 0.45 µm whatman filter paper and diluted suitably and analyzed spectrophotometrically at 273.6 nm for AT. Absorbance values were transformed to concentration by reference to a standard calibration curve obtained experimentally. Amount of drug permeated was determined and plotted as a function of time. The

permeability coefficients (P_{eff}) were calculated from the linear part of the curves as per equation 2.1.1,

Equation 2.1.1

$$Peff(cm/\sec) = \frac{dQ/dt}{A * Cd}$$

Where, A = the surface area, dQ/dt = amount of drug permeated per unit time at steady state and C_d = donor drug concentration. Permeation coefficient (P_{eff}) was calculated for AT (control) and the binary systems as above. These studies were performed in triplicate for each of control and binary systems average values were considered for data analysis.

Permeation enhancement ratios were calculated from P_{eff} values according to the equation 2.1.2. (15)

Equation 2.1.2

$$R = \frac{Papp(sample)}{Papp(control)}$$

The results of experiments performed (n = 3) are presented as mean $\pm$ SD. Significance between the mean values was calculated using ANOVA using SPSS version 15.0. Tukey HSD post-hoc multiple comparison test was done to detect significant differences ($p<0.05$) between the permeability of AT in presence and absence of PI.

2.1.4 Results and Discussion

2.1.4.1 Fourier Transform Infrared Spectroscopy (FTIR)

FTIR spectra of AT, PI and AT-PI binary systems of PM method, SE method and KE method are shown in Figure 2.1.1. FTIR spectrum of pure AT has characteristic peak of carbonyl band of 1725 – 1685 cm^{-1} (16). Absorption band between 3300-3100 cm^{-1} ascribed to combine peaks of N-H and O-H stretching. While absorption bands between 3000-2800 cm^{-1} ascribed to C-H stretching. Peak at 1514 cm^{-1} is of N-H bending and peak at 1243 is of C-N stretching. All these peaks of AT remain unaffected in the IR spectrum of binary systems of each method. The slight change in the intensity is there which is not having any significant difference than the pure AT. Thus FTIR spectra remains unchanged, explained that there was no interaction between AT and PI in any of the binary system of each of three methods. This confirms that PI is not interacting with AT, at molecular level.

Figure 2.1.1 The FTIR spectra of AT, PI, AT-PI binary systems of each method.

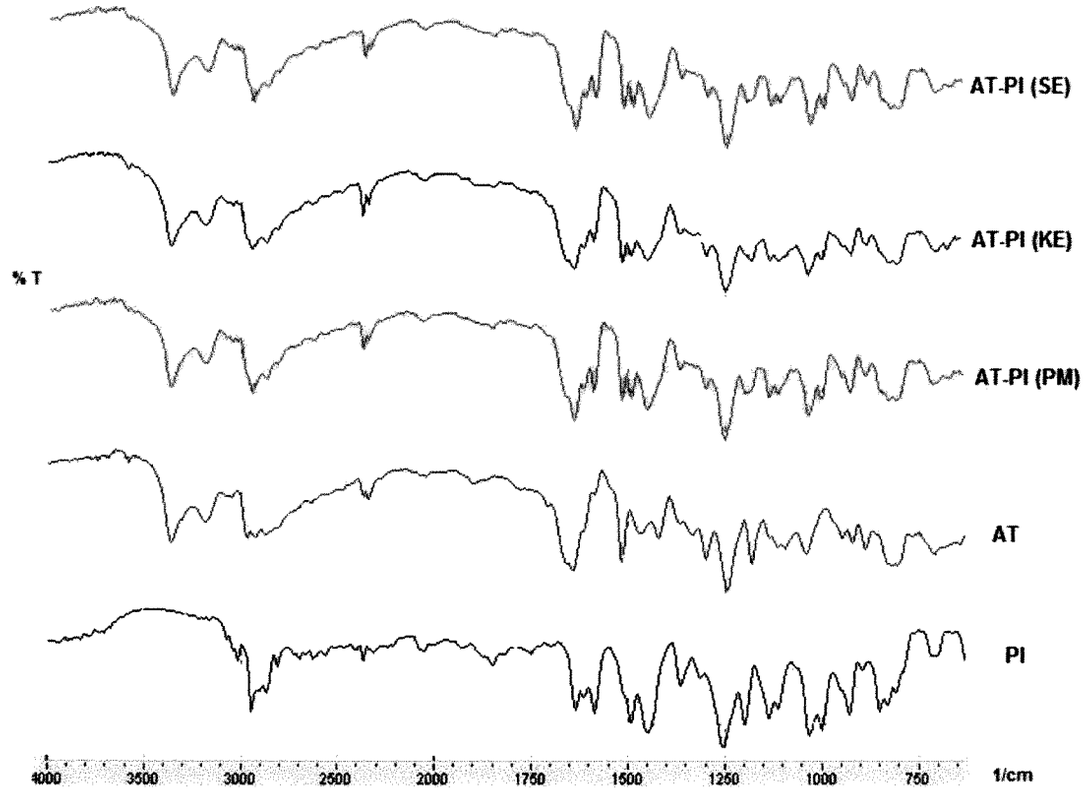

2.1.4.2 *Differential Scanning Calorimetry (DSC)*

The thermograms of pure AT, PI and AT-PI binary systems of PM, SE and KE method are shown in Figure 2.1.2. The thermogram of pure AT showed a sharp endothermic peak at 154.60 °C (17), which is due to a melting point as it consumes energy. Thermogram of PI indicates a sharp endothermic peak at 131.39 °C. In the thermogram of binary systems of PM method, endothermic peak of AT found at 148.43 °C, shift in peak to lower temperature which may be explained by weak interaction between AT and PI. Binary systems of SE method has endothermic peak at 147.91 °C and KE method has endothermic peak at 142.6 °C. Shift in peak to lower temperature is due to conversion of AT in amorphous form. Thus all thermograms prove that almost negligible interaction between AT and PI in all binary systems of each method.

Figure 2.1.2 The thermograms of pure AT, PI and AT-PI binary systems of each method.

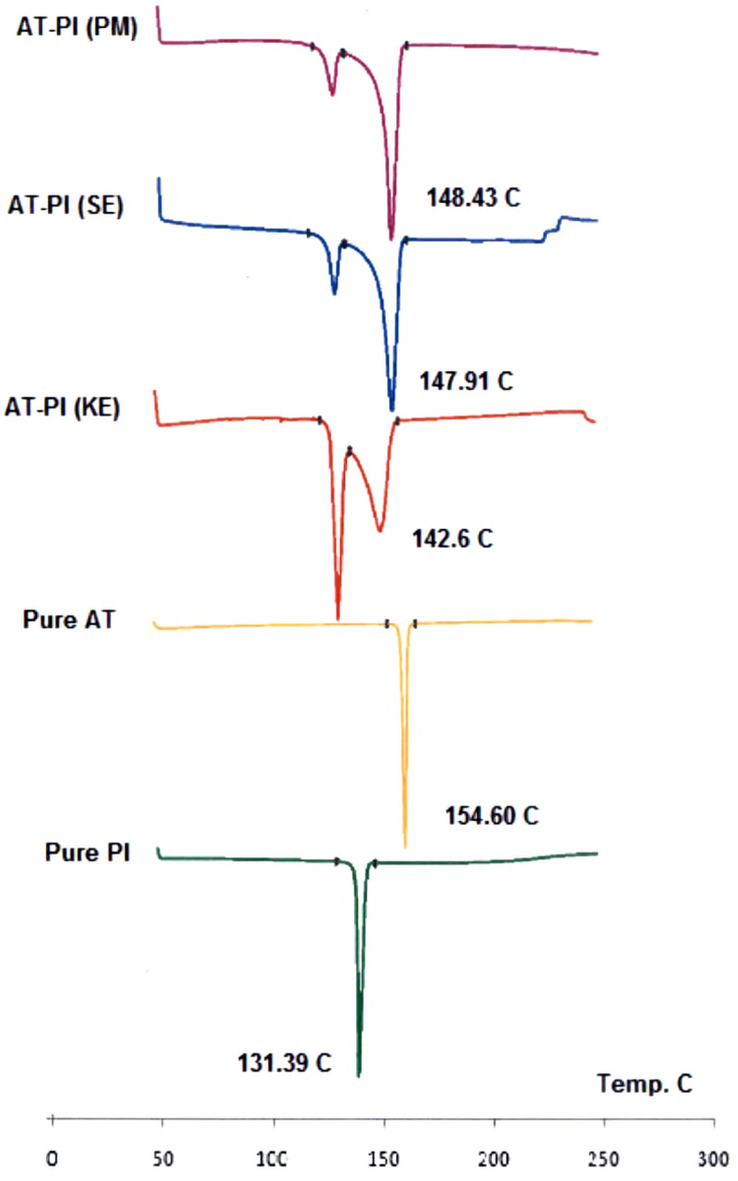

2.1.4.3 *Spectrophotometric analysis and standard curves*

UV spectrophotometric method was successfully applied for determining permeated AT content in *ex-vivo* permeation study without interference of PI. All the validation parameters for determination of AT in presence of PI is shown in Table 2.1.1. UV spectra of AT in presence of PI is shown in Figure 2.1.3. The method is rapid, simple and sensitive enough to measure the AT content in *ex-vivo* permeation study.

Table 2.1.1 The spectral and statistical data for determination of AT in presence of PI by spectrophotometric method.

Parameters	Values
Wavelength	273.6 nm
Range	0.5-100 µg/ml
Linearity	0.9990
Intercept	0.0165
Slope	0.0121
LOD	0.13 µg/ml
LOQ	0.39 µg/ml
Intra day precision	% RSD < 2
Inter day precision	% RSD < 2

Figure 2.1.3 The representative spectra of AT in presence of PI.

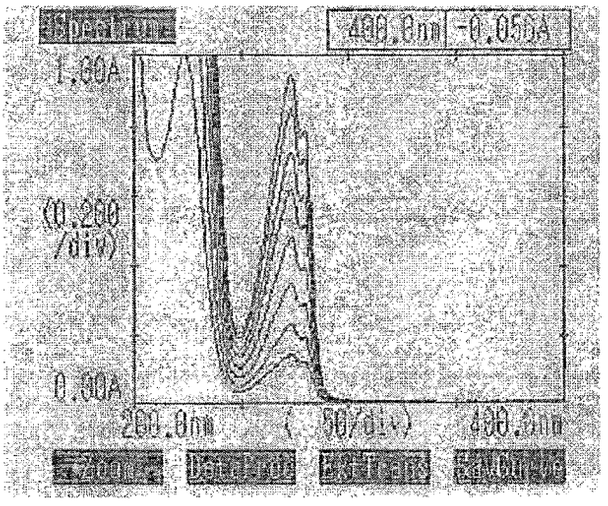

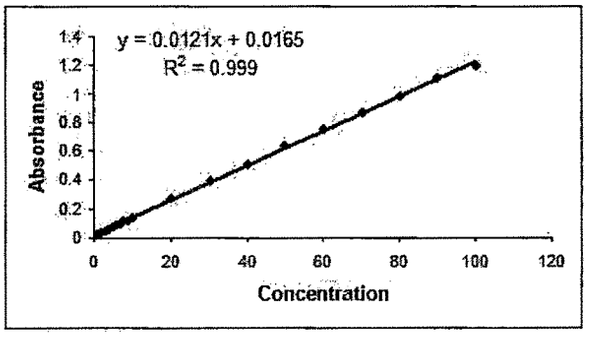

2.1.4.4 *Ex Vivo permeation studies*

Permeability can be determined by permeation study with excised human or animal intestinal tissue (18). In the present *ex vivo* permeation studies were carried out using goat intestine as permeation membrane (11). Permeation coefficient (P_{eff}) was calculated for AT and AT-PI binary systems of PM, SE and KE methods as per equation 2.1.1. Table 2.1.2 summarised the mean permeation coefficient ± SD of AT in absence (control) and presence of PI in binary systems of each method. Release profile of AT in each binary system with ratio of AT: PI- 5:1, 5:2 and 5:3 is represented respectively in Figure 2.1.4, Figure 2.1.5 and Figure 2.1.6.

Table 2.1.2 Mean permeation coefficient ± SD of AT in absence (control) and presence of PI for binary systems of methods.

Ratio of AT:PI	**Mean Permeation coefficient ± SD of AT, P_{eff} x 10^{-5} (cm/sec)(n=3)**		
AT (control)		2.085 ± 0.002, ER – 1.00	
	PM Method*	**SE Method***	**KE Method***
AT: PI 5:1	2.506 ± 0.003	**4.752 ± 0.004**	3.34 ± 0.004
	ER – 1.20	**ER – 2.28**	ER – 1.60
AT: PI 5:2	**4.697 ± 0.001**	2.367 ± 0.001	2.102 ± 0.002
	ER – 2.25	ER – 1.13	ER – 1.09
AT: PI 5:3	3.351 ± 0.001	2.295 ± 0.001	2.137 ± 0.001
	ER – 1.61	ER – 1.10	ER – 1.02

*p value < 0.001; significant difference from control (Tukey's multiple comparison test)

ER (R) – Enhancement Ratio (as per equation 2.1.2)

Each binary system of all three methods has higher permeation than control AT. i.e. PI significantly ($p<0.05$) increasing the permeation coefficient (P_{eff} cm/sec) of AT. All three methods corroborate increase in permeation, but SE method (AT: PI - 5:1) and PM method (AT: PI - 5:2) show almost twice (ER – more than 2.00) increase in permeation coefficient of AT than control (AT without PI). KE method can be used for permeation enhancement but SE and PM methods are more prone to increase permeation. SE method has more

permeation enhancing effect can be explained by reduction in the size of the particles after solvent evaporation.

There are various known and unknown causes, by which PI increases the permeation of AT in *ex-vivo* permeation study. The probable mechanism could be, PI modulates membrane dynamics, cause increase in intestinal surface and its brush border effect (19).

Figure 2.1.4 The release profile of AT with ratio AT: PI- 5:1 for each method.

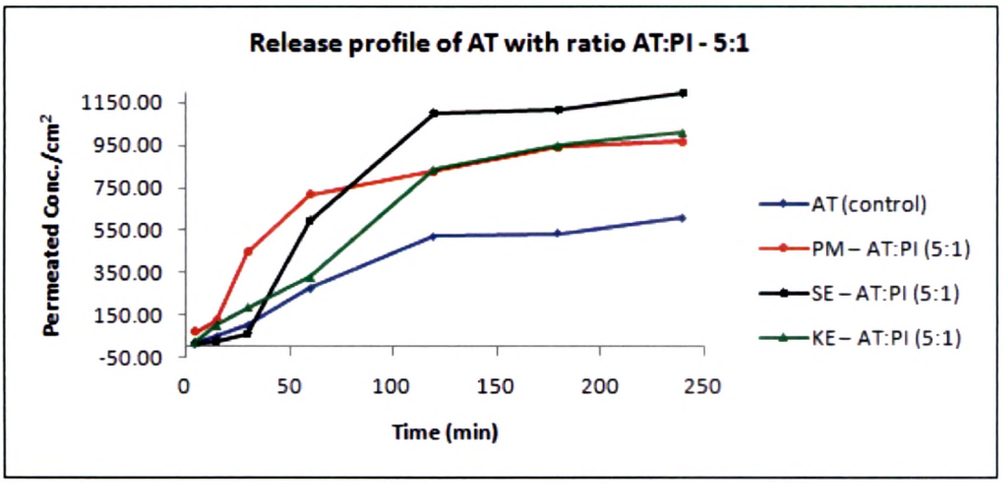

Figure 2.1.5 The release profile of AT with ratio AT: PI- 5:2 for each method.

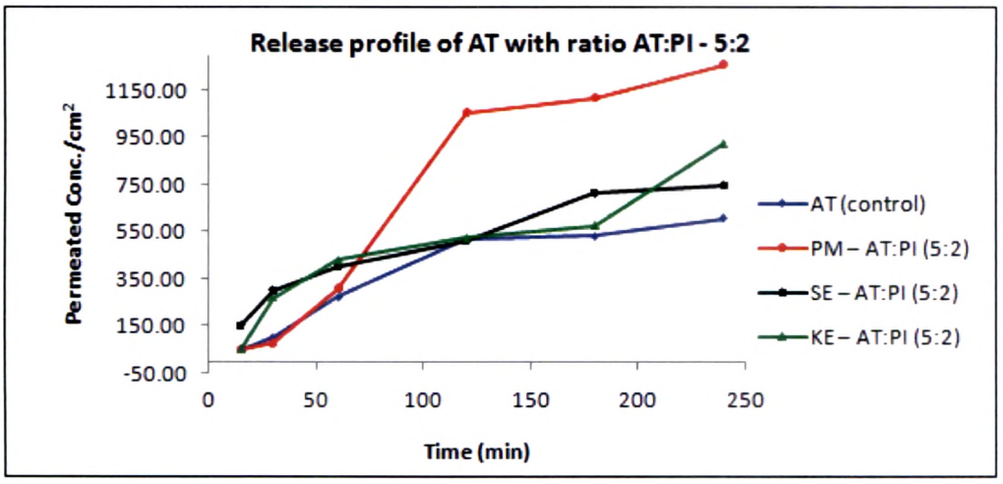

Figure 2.1.6 The release profile of AT with ratio AT: PI- 5:3 for each method.

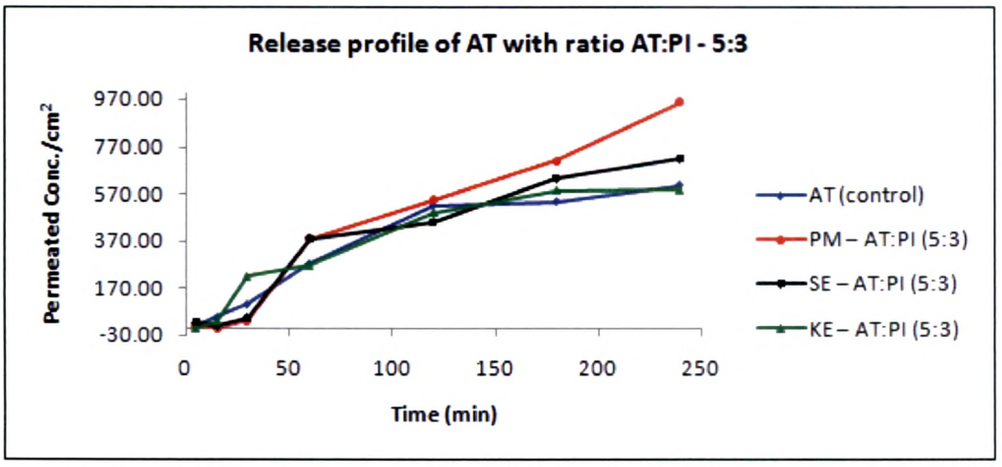

2.1.5 Conclusion

The results of DSC and IR of each binary systems of PM, SE and KE method suggests that there is no physical interaction between AT and PI. The results of *ex-vivo* permeation showed almost 2 fold increase in permeation coefficient of AT in presence of PI than without PI (i.e pure AT). All three methods are useful to increase permeation than pure drug, but permeation is not dependent on concentration of PI. i.e. even low concentration of PI is sufficient to increase the permeation of AT.

KE method also showed permeation enhancement but comparatively less than PM and SE method. The probable reason for marked increase with SE may be due to size reduction of drug particles after solvent evaporation.

SE and PM methods have almost similar pattern of increment in permeation of AT. It is concluded from all these studies, there will be use of only PM method for permeation evaluation for further studies such as Caco-2 cell line and pharmacokinetics.

2.1.6 References

1 Martindale, The extra pharmacopoeia, Ed. 31, Royal Pharmaceutical Society, London, UK, **2003**.

2 H. Lennerna¨s, Human intestinal permeability, J Pharm Sci., **1998**, 87(4), 403–410.

3 W. Kirch, K. Gorg, Clinical pharmacokinetics of atenolol. A review. Eur J Drug Metab Pharmacokin., **1982**, 7, 81–91.

4 A. Melander, P. Stenberg, H. Liedholm, B. Schersten, Food induced reduction in bioavailability of atenolol, Eur J Pharmacol., **1979**, 16, 327–330.

5 R. Mehvar,M. E. Gross, R. N. Kreamer, Pharmacokinetics of atenolol enantiomers in humans and rats, J Pharm Sci., **1990**, 79(10), 881–885.

6 H. Vogelpoel, J. Welink, G.L. Amidon, H.E. Junginger, K.K. Midha, M. Olling, V.P. Shah, Bio-waiver Monographs for Immediate Release Solid Oral Dosage Forms Based on Biopharmaceutics Classification System (BCS) Literature Data: Verapamil Hydrochloride, Propranolol Hydrochloride, and Atenolol, J Pharm Sci., **2004**, 93(8), 1945-1956.

7 S. V. Sastry, M. A. Khan, Aqueous based polymeric dispersion: Plackett–Burman design for screening of formulation variables of Atenolol Gastrointestinal Therapeutic System, Pharm Acta Helvetiae., **1998**, 73, 105–112.

8 R. K. Zutshi, R. Singh, U Zutshi, R. K. Johri, C. K. Atal, Influence of piperine on rifampicin blood levels in patients of pulmonary tuberculosis, J Assoc Physicians India., **1985**, 33, 223–224.

9 U. Zutsi, A process for preparation of pharmaceutical combination with enhanced activity for treatment of tuberculosis and leprosy, Indian Patent 1 232/DEV89, **1989**.

10 S. K. Gupta, P. Bansal, R. K. Bhardway, T. Velpandian, Comparative anti-nociceptive, anti-inflammatory and toxicity profile of nimesulide vs. nimesulide and piperine in combination, Pharmacol Res., **2000**, 41, 657–662.

11 S. P. S. Khanuja, S. A. Kumar, M. Singh, Composition comprising pharmaceutical /nutraceutical agent and a bio-enhancer obtained from Glycyrrhiza glabra, U.S. Pat. No. 6, 979, 471, **2005**.

12 T. Imai, M. Sakai, H. Ohtake, H. Azuma, M. Otagiri, In vitro and in vivo evaluation of the enhancing activity of glycyrrhizin on the intestinal absorption of drugs, Pharm Res., **1999**, 16, 80–86.

13 N. A. Motlekar, K. S. Srivenugopal, M. S. Wachtel, B. C. Youan, Evaluation of the Oral Bioavailability of Low Molecular Weight Heparin Formulated With Glycyrrhetinic Acid as Permeation Enhancer, Drug Dev Res., **2006**, 67(2), 166–174.

14 Indian Pharmacopoeia, Ministry of Health & Family welfare, Government of India, The controller of Publications, Delhi, **1996**, 1, 73–75.

15 M. Thanou, J. C. Verhoef, M. T. Nihot, J. H. Verheijden, H. E. Junginger, Enhancement of the intestinal absorption of low molecular weight heparin (LMWH) in rats and pigs using Carbopol 934P, Pharm Res., **2001**, 18, 1638–1641.

16 R. Ficarra, P. Ficarra, M.R. Di Bella, D. Raneri, S. Tommasini, Study of the inclusion complex of atenolol with b-cyclodextrins, J Pharm Bio Ana., **2000**, 23, 231–236.

17 M. Moneghini, A. Carcano, G. Zingone, B. Perissutti, Studies in dissolution enhancement of atenolol, Int J Pharm, **1998**, 175, 177–183.

18 CDER Waiver of In Vivo Bioavailability and Bioequivalence Studies for Immediate Release Solid Oral Dosage Forms Based on a Biopharmaceutics Classification System, Food and Drug Administration, Rockville, MD, USA, **2000.**

19 A. Khajuria, N. Thusu, U. Zutshi, Piperine modulates permeability characteristics of intestine by inducing alterations in membrane dynamics: influence on brush border membrane fluidity, ultrastructure and enzyme kinetics, Phytomedicine., **2002**, 9, 224–231.

2.2 ATENOLOL-GLYCYRRHIZIC ACID AMMONIUM SALT BINARY SYSTEMS

In the present section glycyrrhizic acid ammonium salt (GA) was incorporated with atenolol. Effect of GA on atenolol permeability was determined. GA was incorporated with atenolol (AT), using three different concentrations of GA, by means of two methods such as physical mixture and solvent evaporation method. Binary systems with each weight ratio, of two methods were evaluated by following parameters,

- FTIR – to determine physical interaction of GA–AT
- DSC – to determine compatibility of GA with AT
- *Ex vivo* permeation study – to determine the effect of GA on permeation of AT

2.2.1 Materials

The Model drug atenolol (AT) was procured as a gift sample from Wockhardt Ltd., Mumbai, India. Glycyrrhizic acid ammonium salt (GA) was purchased from Sigma Aldrich Ltd., Mumbai, India. Potassium bromide, potassium dihydrogen orthophosphate, pancreatin and methanol were purchased from Qualigence fine chemicals, Mumbai, India. All the other chemicals and solvents were of analytical grade and were used without any further purification. Deionized double distilled water was used through out the study.

2.2.2 Methods

AT – GA binary systems were prepared at three different ratios, where GA was taken as 1 %, 5 % and 10 % of w/w of AT dose (25 mg). Two methods such as physical mixture method and solvent evaporation method were used to prepare the AT – GA binary systems with three ratios. Both methods are described in detail below,

Physical Mixtures (**PM**):

The required and accurately weighed amounts of AT and GA were prepared by simply mixing the powders in a polythene bag.

 # Solvent Evaporation Method (SE):

The required amounts of AT and GA were accurately weighed and dissolved in methanol. Both solutions were mixed uniformly followed by allowing the solvent evaporated to get a dried powder.

2.2.3 Evaluation Parameters

2.2.3.1 Fourier Transform Infrared Spectroscopy (FTIR)

The FTIR studies were performed to get an idea about the possible physical interaction of AT and GA. The FTIR transmission spectra of a pure AT, GA and AT – GA binary systems of PM method and SE method were obtained using a FTIR spectrophotometer (Avatar™ 360 E.S.P™ FTIR spectrometer, Thermo Nicolet Corp., Madison, WI, USA). A total of 2 % (w/w) of sample (with respect to the potassium bromide-KBr) was mixed with dry KBr. The mixture was ground into a fine powder using an agate mortar before compressing into KBr disc under a hydraulic press at 10,000 psi. Each KBr disc was scanned 16 times at 4 mm s^{-1} at a resolution of 2 cm^{-1} over a wave number region of 500–4000 cm^{-1}. The characteristic peaks were recorded.

2.2.3.2 Differential Scanning Calorimetry (DSC)

Differential scanning calorimetric analysis was used to characterize thermal behaviour of AT, GA and AT-GA binary systems and to check compatibility of GA with AT. DSC thermograms were obtained using an automatic thermal analyzer system (DSC-60, Shimadzu, Japan). Temperature calibration was performed using indium as a standard. Samples (2.5 to 5 mg) were crimped in a standard aluminium pan and heated from 30–250 °C at a heating rate of 10 °C min^{-1} under constant purging of dry nitrogen at 40 ml min^{-1}. An empty pan, crimped in same manner as sample, was used as a reference. The characteristic endothermic peaks and specific heat of the melting endotherm were recorded.

2.2.3.3 *Spectrophotometric analysis and standard curves*

Shimadzu, UV-1700 Double beam UV, Visible spectrophotometer, Kyoto (Japan) was used for the spectrophotometric analyses of AT in presence of GA in simulated intestinal fluid (pH 7.4). AT and GA is having very closely overlapping spectra, which prevents the use of zero-order UV-Vis spectrophotometry for determination of AT in presence of GA. Therefore AT analysis was done using derivative spectrophotometry which is very useful tool (1) for determination of drugs in combine dosage forms. The absorbance spectra of samples (AT with GA) were recorded between 200 nm and 400 nm against a reagent blank (the same of the samples without the AT) using a 1.0 cm quartz cell. The zero-order spectra of pure AT and GA were stored individually within the concentration ranges to be determined and were derivatized in first order using delta lambda 4 and scaling factor 10 for both AT and GA. The first derivative amplitudes were recorded at 258.1 nm for determination of AT. Standard curves were constructed by serially diluting a stock solution of AT to obtain concentrations in the range of 1 to 100 µg/ml using simulated intestinal fluid (SIF) as the diluent. Each concentration was analyzed in triplicate.

2.2.3.4 *Ex Vivo permeation studies*

All the binary systems containing AT and GA were assessed for *ex vivo* permeation studies. The permeation study was carried out same as described in section 2.1.3.4 using goat intestinal membrane. AT concentration in donor compartment was taken to maintain sink condition (2 mg/ml). Samples were withdrawn from receptor compartment at predetermined time interval 5, 15, 30, 60, 90, 120, 180, and 240 min and replaced with same volume of fresh medium to maintain sink condition. The withdrawn samples were filtered through 0.45 µm whatman filter paper and diluted suitably and analyzed spectrophotometrically with first derivative method at 258.1 nm for AT. The absorbance values were transformed to concentration by reference to a standard calibration curve obtained experimentally. The amount of drug permeated was determined and plotted as a function of time. The permeability coefficients (P_{eff}) and permeation enhancement ratio were calculated from the linear part of the curves as described in section 2.1.3.4. These studies were performed in triplicate for each of control and binary systems and average values were considered for data analysis.

The results of experiments performed (n = 3) are presented as mean ± SD. Significance between the mean values was calculated using ANOVA using SPSS version 15.0. Tukey HSD post-hoc multiple comparison test was done to detect significant differences ($p<0.05$) between the permeability of AT in presence and absence of GA.

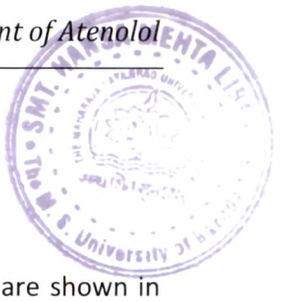

2.2.4 Results and Discussion

2.2.4.1 Fourier Transform Infrared Spectroscopy (FTIR)

FTIR spectra of AT, GA, AT-GA binary system of PM method and SE method are shown in Figure 2.2.1. The FTIR spectrum of pure AT has characteristic peak of carbonyl band of 1725 – 1685 cm^{-1} (2). Absorption band between 3300-3100 cm^{-1} ascribed to combine peaks of N-H and O-H stretching. While absorption bands between 3000-2800 cm^{-1} ascribed to C-H stretching. Peak at 1514 cm^{-1} is of N-H bending and peak at 1243 is of C-N stretching. Same as AT-PI, all these peaks remain unaffected in the IR spectrum of binary systems of each method of AT-GA. The slight change in the intensity is there which is not having any significant difference than the pure AT. Thus FTIR spectra remains unchanged, explained that there was no interaction between AT and GA in any of the binary system of both methods. This confirms the GA is not interacting with AT, at molecular level.

Figure 2.2.1 The FTIR spectra of AT, GA, AT-GA binary systems of each method.

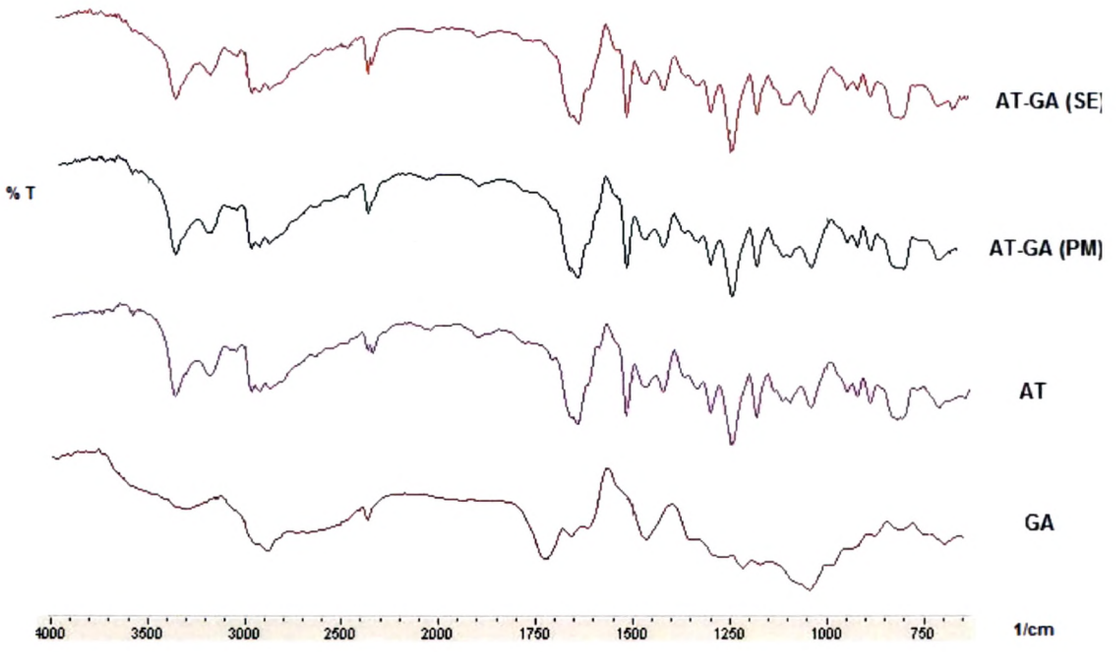

2.2.4.2 *Differential Scanning Calorimetry (DSC)*

The thermograms of pure AT, GA and AT-GA binary systems of PM and SE method are shown in Figure 2.2.2. The thermogram of pure AT has a sharp endothermic peak at 154.60 °C (3), which is due to a melting point as it consumes the energy. The thermogram of GA indicates an endothermic peak at 209 °C. In the binary system of PM method endothermic peak of AT found at 154.6 °C, thus there is no interaction between AT and GA. Binary system of SE method has endothermic peak at 154.16 °C, the peak intensity is same as pure AT. Thus all thermograms prove that there is no interaction between AT and GA in all binary systems of each method.

Figure 2.2.2 The thermograms of pure AT, GA and AT-GA binary systems of each method.

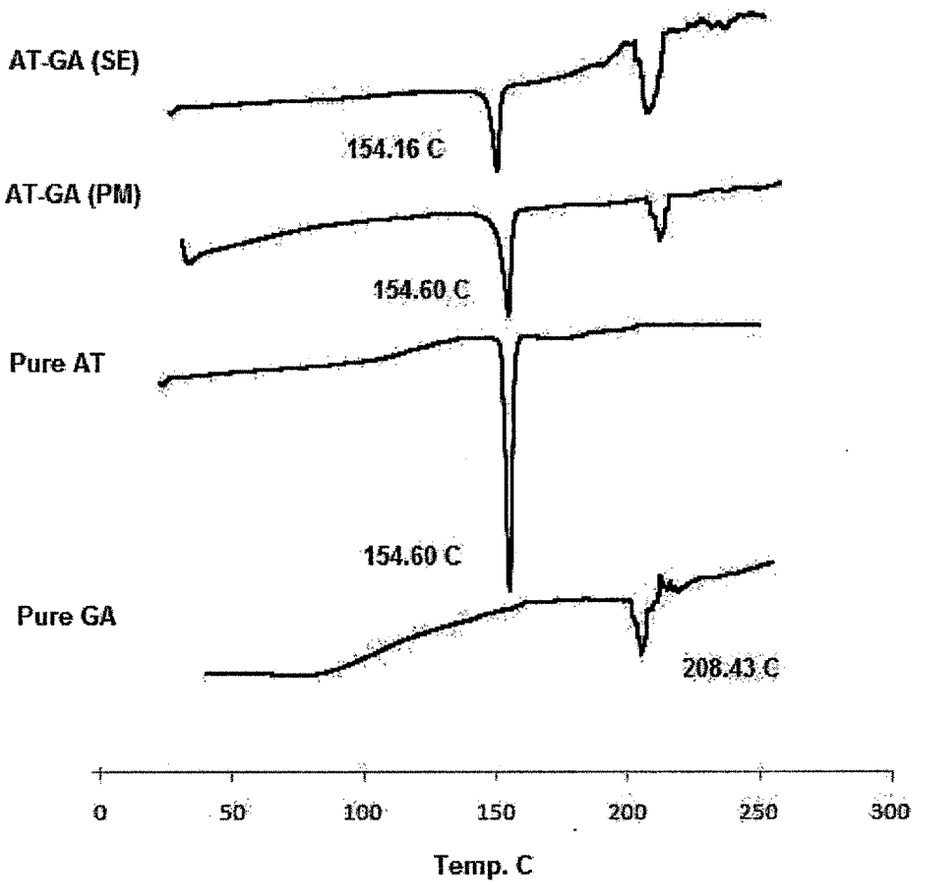

2.2.4.3 *Spectrophotometric analysis and standard curves*

The method was successfully applied for determining permeated AT in *ex-vivo* permeation study without interference of GA with first derivative zero crossing spectrophotometric method. In contrast to zero order spectra (Figure 2.2.3), first derivative UV spectra (Figure 2.2.4) of AT in presence of GA shows more resolution. It is clearly indicates that GA has zero absorbance at 258.1 nm where AT was determined. All the validation parameters for determination of AT is shown in Table 2.2.1. The method is rapid, simple and sensitive enough to measure the AT content in *ex-vivo* permeation study.

Table 2.2.1 The spectral and statistical data for determination of AT by first derivative zero crossing spectrophotometric method.

Parameters	AT in presence of GA
Wavelength	258.1 nm
Range	1-100 µg/ml
Linearity	0.9992
Intercept	0.0007
Slope	0.0015
LOD	0.3 µg/ml
LOQ	1.0 µg/ml
Intra day precision	% RSD < 2
Inter day precision	% RSD < 2

Figure 2.2.3 The representative zero order overlain spectra of AT and GA.

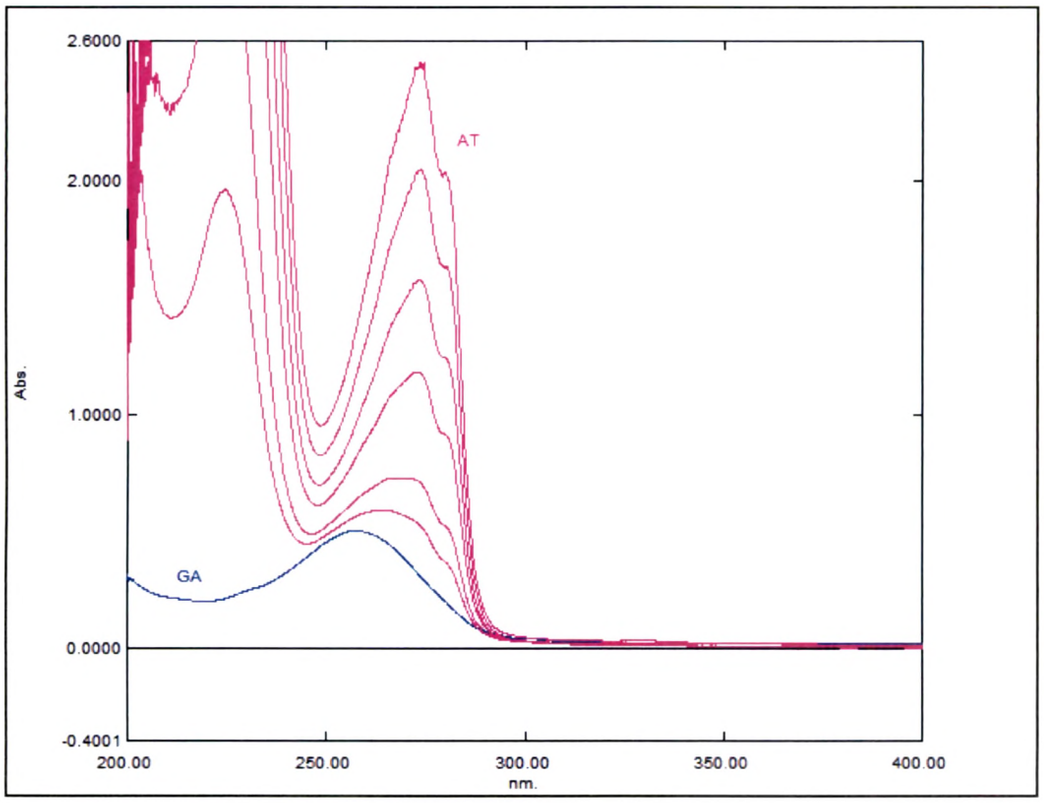

Figure 2.2.4 The representative first derivative zero crossing spectra of AT and GA.

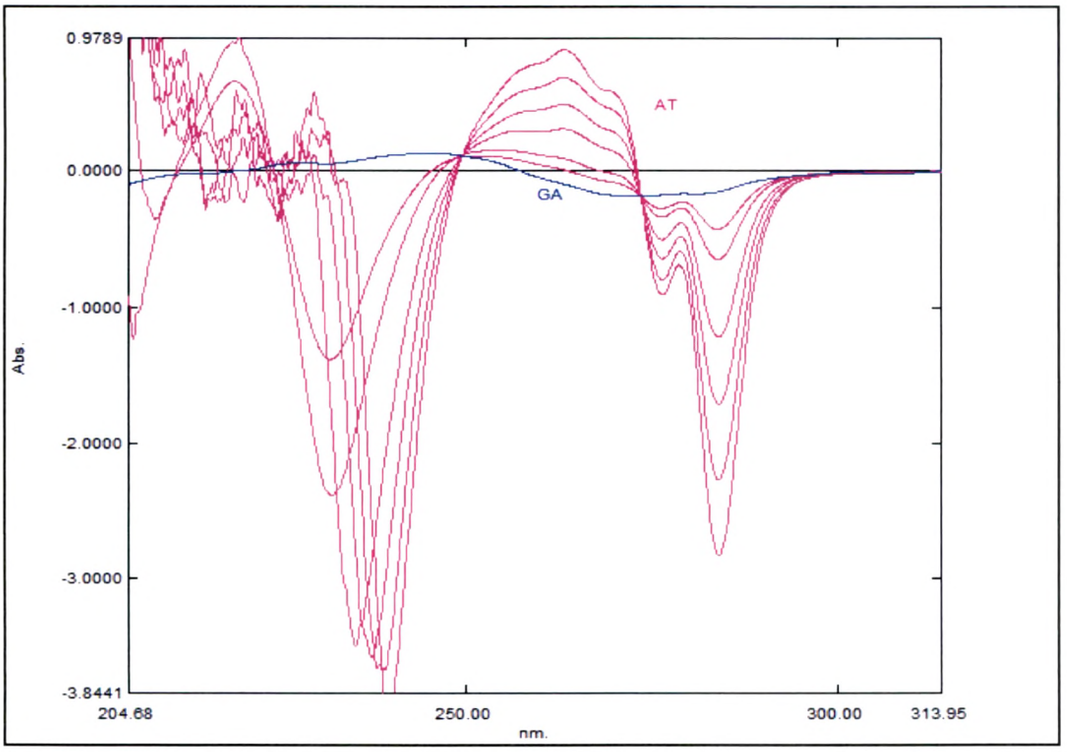

2.2.4.4 *Ex Vivo permeation studies*

It has been found that GA increases permeation in the region of small intestine than large intestine, therefore small intestine was taken for the studies (4). Permeation coefficient (P_{eff}) was calculated for AT and AT-GA binary systems of both methods. Table 2.2.2 summarised the mean permeation coefficient ± SD of AT in absence (control) and presence of GA in binary systems of both methods. Release profile of AT in each binary system with ratio of AT: GA – 1:0.01, 1:0.05 and 1:0.1 is represented respectively in Figure 2.2.5, Figure 2.2.6 and Figure 2.2.7.

Table 2.2.2 Mean permeation coefficient ± SD of AT in absence (control) and presence of GA for binary systems of methods.

Ratio of AT:GA	**Mean Permeation coefficient ± SD of AT, P_{eff} x 10^{-5} (cm/sec)(n=3)**		**Enhancement Ratio (ER)**	
AT (control)	1.967 ± 0.24*		1.00	
	PM Method*	**SE Method***	**PM Method**	**SE Method**
AT:GA 1:0.01	4.393 ± 0.211	3.00 ± 0.247	2.23	1.53
AT:GA 1:0.05	**4.776 ± 0.192**	**5.292 ± 0.108**	**2.43**	**2.69**
AT:GA 1:0.1	3.342 ± 0.529	2.566 ± 0.340	1.70	1.30

*Note: p value < 0.05; significant difference from control (Tukey's multiple comparison test)

Each Binary system of both methods has higher permeation than control AT. i.e. GA significantly ($p \leq 0.05$) increasing the permeation coefficient (P_{eff} cm/sec) of AT. Both methods confirm increase in permeation with each ratio, but binary systems with AT: GA (1:0.05) ratio of PM and SE method shows almost 2.5 fold increase in the permeation coefficient of AT than control (AT without GA).

There are various known and unknown causes, by which GA increases permeation of AT in *ex-vivo* permeation studies (5). The probable mechanism could be: GA which can act on paracellular pathways (4) modulates opening of same, cause increase in permeation of AT.

Figure 2.2.5 The release profile of AT with ratio AT: GA - 1:0.01 for both methods.

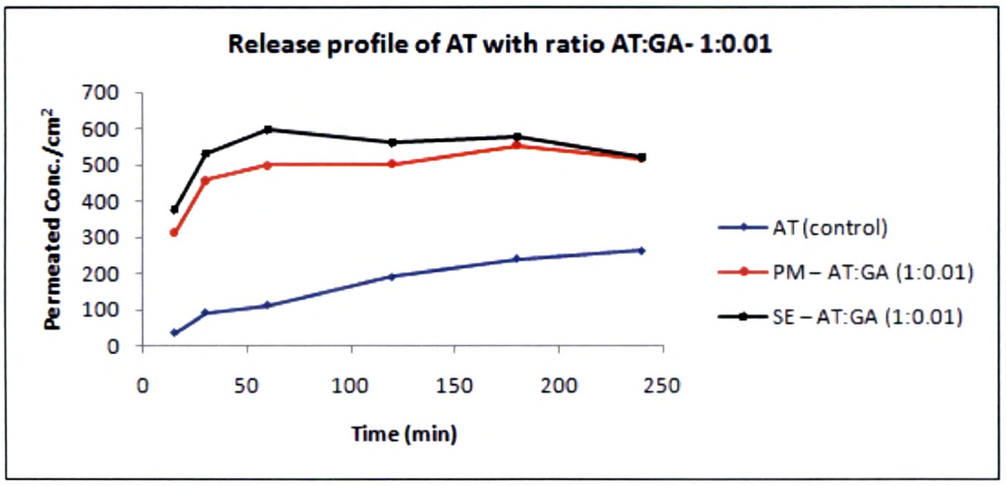

Figure 2.2.6 The release profile of AT with ratio AT: GA - 1:0.05 for both methods.

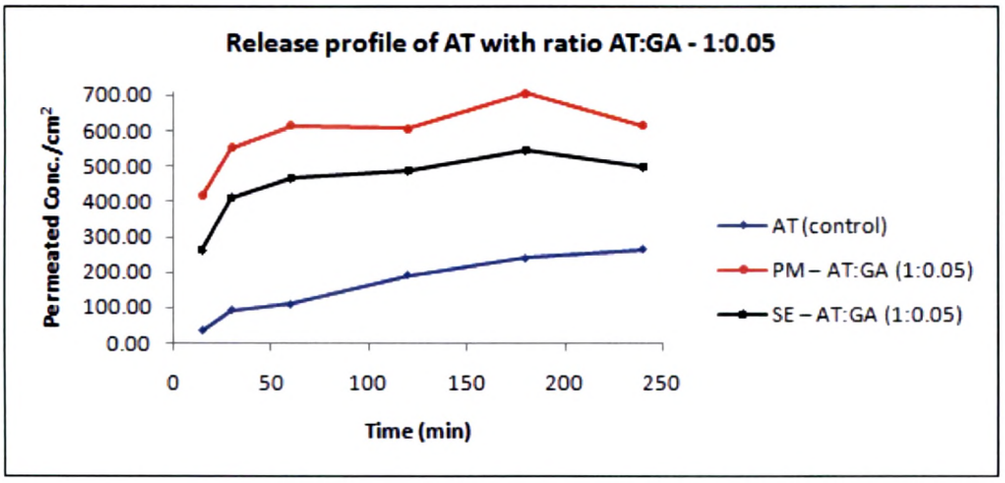

Figure 2.2.7 The release profile of AT with ratio AT: GA - 1:0.1 for both methods.

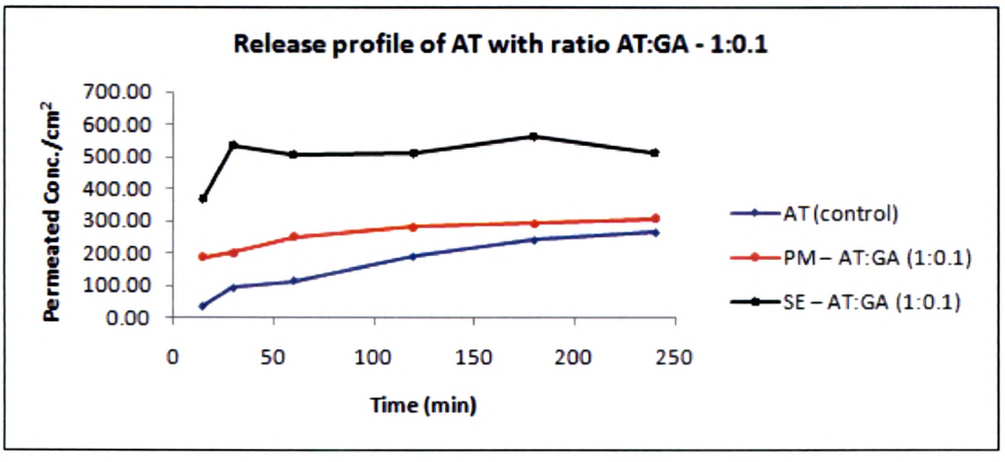

2.2.5 Conclusion

Results of DSC and IR suggests that there is no physical interaction between AT and GA in each of binary systems of PM and SE method. The results of *ex-vivo* permeation showed incredible increase in permeation coefficient of AT in presence of GA when compared with pure drug AT. Both methods are useful to increase permeation than pure drug. Specifically binary systems with AT: GA (1:0.05) ratio of PM and SE method cause 2.5 fold increase in the permeation of AT.

SE method have similar pattern of increment in permeation of AT. Therefore it is concluded that only PM method will be used for further studies.

2.2.6 References

1 H. N. Dave, R. C. Mashru, A. R. Thakkar, Simultaneous determination of salbutamol sulphate, bromhexine hydrochloride and etofylline in pharmaceutical formulations with the use of four rapid derivative spectrophotometric methods, Anal Chimica Acta., **2007**, 597 (1), 113–120.

2 R. Ficarra, P. Ficarra, M.R. Di Bella, D. Raneri, S. Tommasini, Study of the inclusion complex of atenolol with b-cyclodextrins, J Pharm Bio Ana., **2000**, 23, 231–236.

3 M. Moneghini, A. Carcano, G. Zingone, B. Perissutti, Studies in dissolution enhancement of atenolol, Int J Pharm, **1998**, 175, 177–183.

4 N. A. Motlekar, K. S. Srivenugopal, M. S. Wachtel, B. C. Youan, Evaluation of the Oral Bioavailability of Low Molecular Weight Heparin Formulated With Glycyrrhetinic Acid as Permeation Enhancer, Drug Dev Res., **2006**, 67(2), 166–174.

5 S. P. S. Khanuja, S. A. Kumar, M. Singh, Composition comprising pharmaceutical /nutraceutical agent and a bio-enhancer obtained from Glycyrrhiza glabra, U.S. Pat. No. 6, 979, 471, **2005**.

2.3 ATENOLOL TRANSPORT STUDIES ACROSS Caco-2 CELL MONOLAYERS

The present work was done at Cell culture Lab, Pharmaceutical Science Division, King's College of London, London, UK under supervision of Dr Ben Forbes, Head, Drug Delivery Group, Pharmaceutical Science Division, King's College of London, UK.

In the present chapter, atenolol transport studies were performed in presence of bioenhancers. Caco-2 cells were used to perform the transport study. Transport experiments were performed using radiolabelled atenolol. The analysis of permeated radiolabelled drug was determined with liquid scintillator.

The prime objectives of present study was,

(i) To perform the permeability study of paracellularly absorbing Mannitol in presence of various concentrations of EDTA

(ii) To optimize the concentration of EDTA and use optimized concentration as standard bioenhancer

(iii) To perform permeability studies of atenolol in presence of bioenhancer piperine and glycyrrhizic acid ammonium salt

(iv) To determine the effect of both bioenhancers on the epithelium and integrity of tight junctions.

(v) To access the influence of bioenhancers on atenolol permeation

Intestinal Absorption

Small intestine represents principal site of absorption for any ingested compound. The main barrier for drug absorption is an epithelium of intestine. Intestinal epithelium contains different types of cells, amongst all cells the enterocyte (absorptive cells-Figure 2.3.2) is most abundant cells and account for majority of absorption in the small intestine (1). The columnar appearance obtained during differentiation which leads to formation of microvilli (Figure 2.3.1a). These microvilli reside on luminal cell membrane which is called as an apical cell membrane. Opposite this membrane is basal plasma membrane, which is separated by lamina propria by a basement membrane (2). The columnar cells of microvilli together form a tight protective barrier through several different intercellular junctions (Figure 2.3.1b). The junctional complex includes several well defined structures including gap junctions, desmosomes, adherens junctions, and the tight junction (TJ). The TJ is most apical component of junctional complex and functions as major paracellular barrier (3).

Figure 2.3.1 The schematic structure of an intestinal villus with epithelial cells (enterocytes) and mucus producing cells (goblet cells) (a), and the epithelial cell junctional complex with a tight junction, an adherent junction and a desmosome (b).

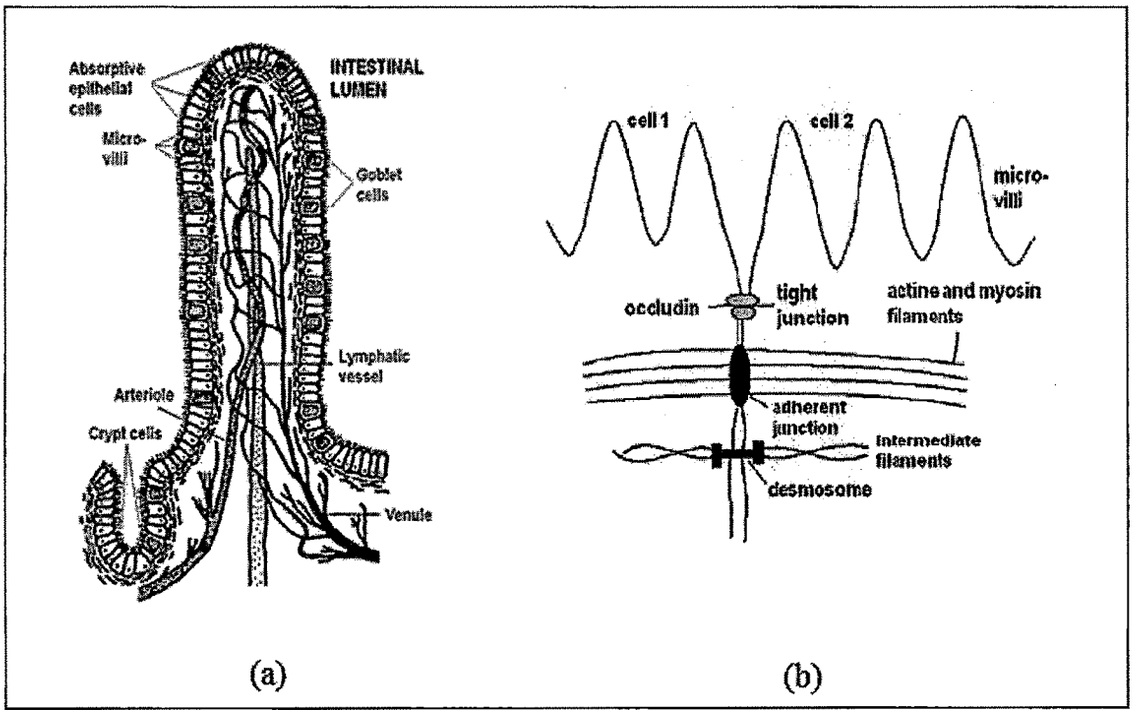

Figure 2.3.2 The diagram of typical intestinal epithelial cell (enterocyte). The cells are joined tightly by neighbouring cells by tight junctions. The microvilli on apical surface give appearance of brush border.

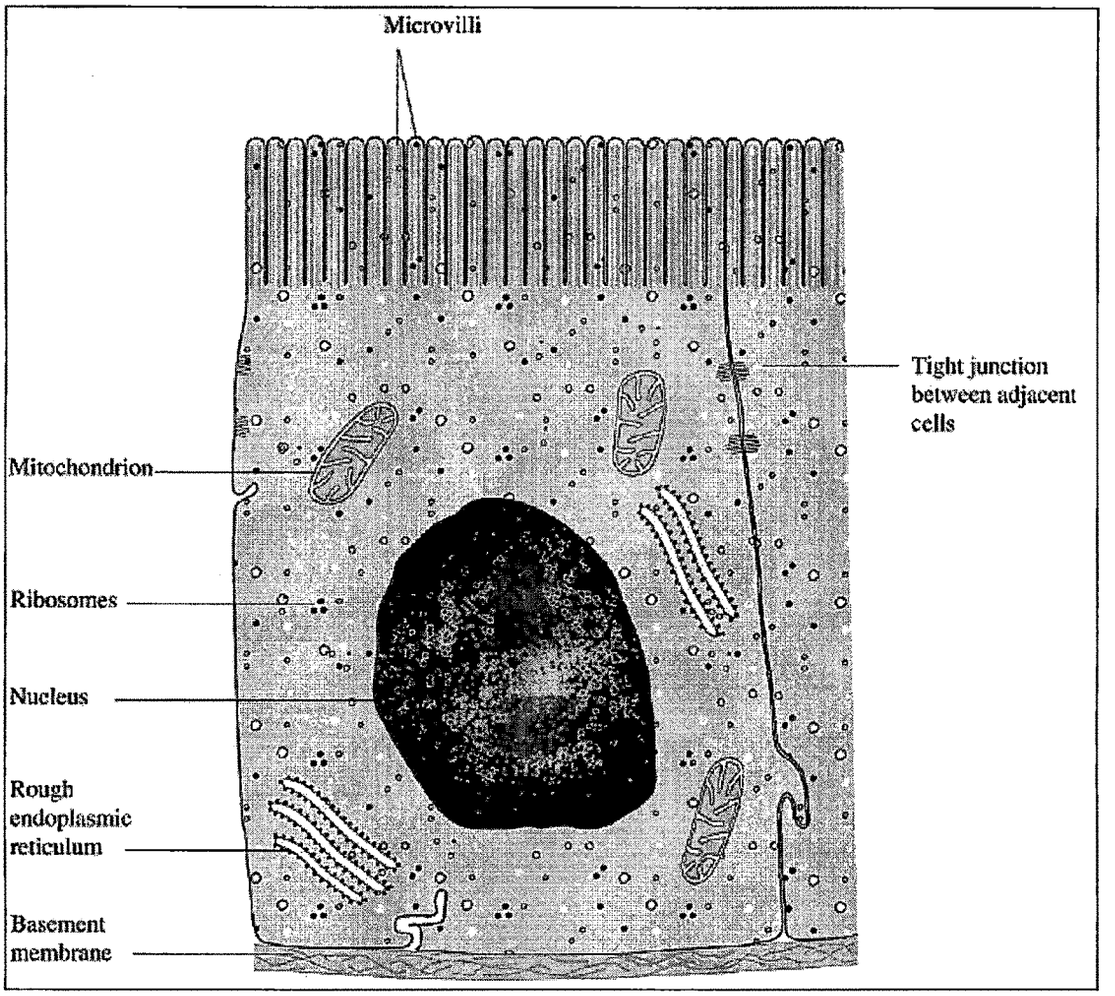

Route of Absorption

The absorption of solute in intestinal epithelium occurs via two principal route, paracellular or transcellular (Figure 2.3.3a). A number of small hydrophilic, ionised drugs are absorbed via paracellular pathway (4).Transcellular absorption from lumen to blood requires uptake across an apical membrane, followed by transport across cytosol, then exit across basolateral membrane and into blood. Transcellular absorption of hydrophilic drugs may be facilitated via specific carrier-mediated pathways by means of utilising the same route of absorption followed by nutrients and micronutrients (Figure 2.3.3b). Most drugs permeate mainly transcellularly, but a variable contribution of the paracellular route is possible (5,6).

The capacity of the paracellular route is limited because of the spaces between absorbing enterocytes are small compared to total absorptive area (7).

Figure 2.3.3 The schematic structure of intestinal epithelium as a selective barrier against the entry of compounds to circulation. **a:** passive trans and paracellular diffusion; **b:** carrier mediated absorption at apical and basolateral membranes; **c:** active efflux transporter on apical membrane, acting during absorption; **d:** active efflux transporter on apical membrane, offering an additional route for drug clearance from the circulation; **e:** intracellular metabolising enzymes localized inside the enterocytes, possibly combined with an active efflux transporter on apical and basolateral membranes. (Modified from8)

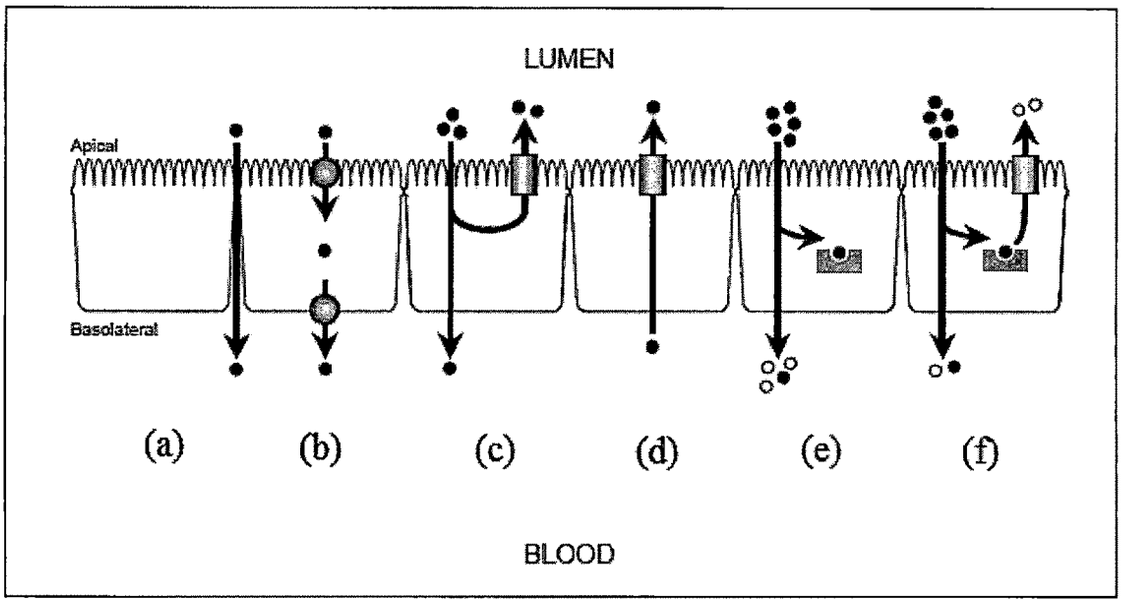

Active transport of drugs and nutrients is mediated by several membrane transporter proteins located in the cell membranes (Figure 2.3.3b, c, d, and e). Membrane transporter carriers can be classified based on their energy requirements to facilitated diffusion, primary active and secondary active transport. Facilitated diffusion does not require energy for its function while primary active transport is an energy demanding process. Many orally administered drugs that cross the apical membrane may be substrates for apical efflux transporters, which extrude compounds back into the lumen (9,10) (Figure 2.3.3c). These apical efflux transporters are principally ABC proteins such as P-glycoprotein (P-gp) and Multi-drug Resistance Protein (MRP). Compounds that are already present in the blood may

undergo active blood-to-lumen secretion facilitated by these transporters (Figure 2.3.3d). As well as efflux pumps, the transcellular route of absorption exposes drugs to intracellular metabolic systems; small intestinal enterocytes provide the first site for cytochrome P450 (CYP)-mediated metabolism of orally ingested drugs and xenobiotics (Figure 2.3.3e,f) (11).

Methods for Predicting Intestinal Absorption

As described earlier various methods are available for predicting intestinal absorption of drugs. Amongst all methods the *in vitro* model systems are advantageous as able to examine large number of samples with clear interpretation and in less quantity of drugs. Many *in vitro* studies examining drug uptake and transport in the intestinal epithelium have utilized such models as everted sac, brush border membrane vesicles, isolated cells and intestinal rings. All these systems lacks in tissue viability and polarity. In the 1980s when difficulties encountered in obtaining human intestinal differentiated cell lines in culture from normal tissue, interest and development leads to use human colon adenocarcinoma cell lines which appeared to undergo enterocyte like differentiation in culture.

Cell Cultures

The isolated human intestinal cells of normal tissue don't differentiated normally; attention was directed to the specific intestinal properties of some of the tumoral cell lines. In most cases partial differentiation could be induced by treatment with synthetic or biological factors added to the medium (12). One of the cell lines, Caco-2 showed a spontaneous differentiation pathway in long term culture. First studies on Caco-2 cell line demonstrated that these cells, upon differentiation, express several morphological and biochemical characteristics of small intestinal enterocytes (12). Therefore, during past few years Caco-2 cell monolayers have been widely accepted by pharmaceutical companies and regulatory authorities (13) as a potent and standard permeability screening membrane for prediction of drug permeability (14,15,16,17). Many other cell lines are also used by various pharmaceuticals laboratories. The cell lines such as HT29, HT29-18 and HT29-H (18,19), and T84 (20), have been used for permeability experiments by several laboratories around the world because of their capability to differentiate in culture. Cell lines from animals, such as MDCK (Madin Darby canine kidney), CHO (Chinese hamster ovary), and 2/4/A1 (rat), are also intensively used as *in vitro* model for intestinal absorption (21,22).

Caco-2 cells

Caco-2 cell model has been the most popular and extensively characterized cell-based model in examining permeability of drugs in both pharmaceutical industries and academia. Caco-2 cell line was established from a moderately well differentiated colon adenocarcinoma obtained from a 72-year-old patient (13). Caco-2 cells, a human colon adenocarcinoma, undergo spontaneous enterocytic differentiation in culture and become polarized cells with well-established tight junctions, resembling intestinal epithelium in humans. Caco-2 cells reach confluency within 3-6 days and reach stationary growth phase after 10 days in culture (23). The differentiation is completed within 20 days (13). Electrical measurement made it possible to define the epithelial properties of Caco-2 cells, which may resemble those of colonic crypt or fetal cells (24). These measurements also confirmed that functional differentiation is homogeneous in Caco-2 cells.

When cells grown with standard conditions, it exhibit epithelial characteristics such as brush-border microvilli, tight junctions, and dome formation on an impermeable support. Sucrase, alkaline phosphatase, and aminopeptidase, brush-border enzymes peculiar to the adult human small intestine, are increasingly produced during growth. Several active transport systems that are located in the intestinal epithelium (e.g. sugars, amino acids, dipeptides, bile acids, and cobalamin intrinsic factor) are also expressed in Caco-2 cells (25,26,27). The enzymes found in the brush border membranes (e.g. aminopeptidase, alkaline phosphatase, sucrase, dipeptidyl aminopeptidase, and y-glutamyl transpeptidase) of the enterocytes are also present in the Caco-2 cells (13). The existence of phase I metabolizing enzyme CYPl Al (28,29) and phase II metabolizing enzymes glutathione S-transferase, glucuronidase, and sulfotransferase in this cell system has been reported. Even evidence has been presented for existence of a microsomal cytochrome P-450 isozyme in Caco-2 cells (30) which resembles CYP3A found in human enterocytes (11). These biochemical and morphological properties prompts to use Caco-2 cells as an *in vitro* tool for evaluating permeability property of discovery compounds and for conducting in depth mechanistic studies.

To better reproduce the steric conditions existing in intestine *in vivo*, Caco-2 cells were cultured on permeable filter support that allow free access of ions and nutrients to both sides of cell monolayer (Figure 2.3.4 and 2.3.5).

Figure 2.3.4 The schematic structure of well containing Caco-2 cells.

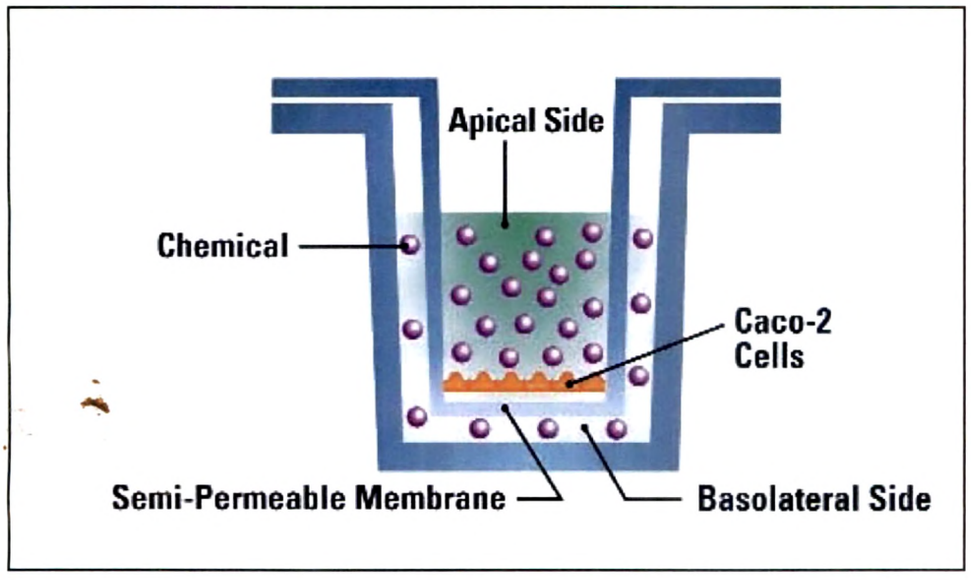

Figure 2.3.5 The diagram of Transwell (12 wells, 1.13 cm^2 polyester, 0.4 μm pore size) containing Caco-2 cells with culture media.

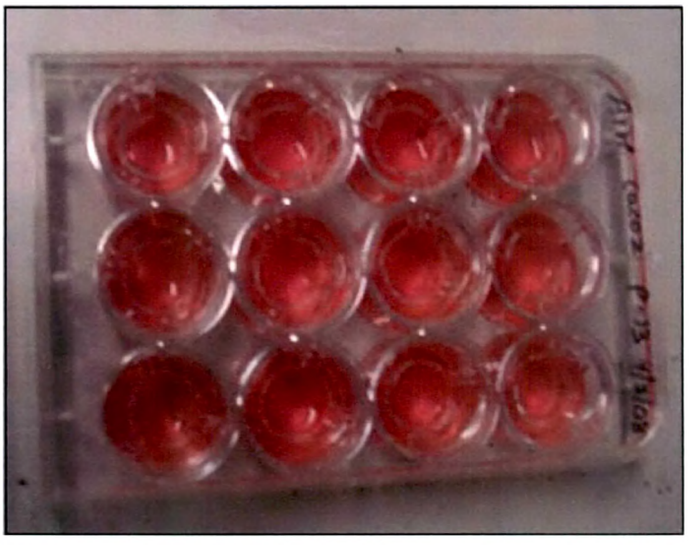

The basic constituents required to make culture media includes inorganic salts, carbohydrates, amino acids, vitamins, fatty acid and lipids, protein and peptides and serum (mixture of albumins, growth factors and growth inhibitors). Over the last thirty years various defined basal media types have been developed and are available commercially such as Dulbecco's Modified Eagle Medium (DMEM) (Figure 2.3.5). Trans-epithelial electrical resistance (TEER) after confluence and permeability of marker molecule have been utilized to monitor integrity of the cell layer. The monolayers exhibit a barrier function as judged by high TEER values (200-600 Ω cm^2, grown on polycarbonate filters). While ultra structural morphology, by transmission electron microscopy, have been utilized to check for morphological differentiation. Various factors affecting performance of Caco-2 cells have been described in Table 2.3.1.

Table 2.3.1 Various factors which influencing performance of Caco-2 cells.

Passage No ↓	Medium ↓		Support ↓		
Brush border enzyme activities	pH ↓	Composition ↓	Material ↓	Pore size ↓	Matrix ↓
Morphology	Motility	Permeability	Non-specific adsorption	Dome formation	Attachment
TEER	Proliferation	Differentiation	Cell density	Growth	Spreading
Proliferation rate	Differentiation		Morphology	Transport	Density
Cell density Glucose transport expression	permeability		TEER Transport		Differentiation

Caco-2 cell monolayers have been used for studying mechanisms of passive paracellular (31,32) and passive transcellular permeability (17), carrier mediated absorptive transport of amino acids (33), amino acid analogues (34), oligo-peptides, ß-lactam antibiotics and ACE-inhibitors, and peptidomimetic thrombin inhibitors. Carrier mediated efflux (combined with metabolism inside the enterocytes) of several drugs has been intensively studied over last few years (35,36,37), as well as cocktail dosing of several different drugs (38).

Advantages of Caco-2 cells

→ It can serve as a rapid screening tool for drug absorption studies

→ It provides information at a cellular level on absorption, metabolism and transport of drug molecules across intestinal mucosa, an advantage over intestinal loops and everted sacs which are more suitable for study of drug uptake into the mucosal cells

→ It provides information on possible mucosal toxicity caused by therapeutic agents

→ As it is of human origin, it does not suffer from interspecies differences in morphological and physiological characteristics of intestinal cells

→ Unlike many other in vitro intestinal absorption models, it does not require use of animals.

Limitations of Caco-2 cells

→ The tight junctions in appropriately differentiated Caco-2 cell monolayers are more characteristic of those in colon than in small intestine (i.e. higher transepithelial resistance (TEER) than is normally found across small intestinal epithelium) (15,17)

→ Caco-2 cell monolayers are devoid of mucin producing goblet cells, and therefore are devoid of mucus layer found on intestinal epithelium (39)

→ Role of physiological parameters, such as intestinal motility or transit time, in absorption of drug molecules can not be accounted for with use of this model

→ It is not always possible to relate rates of transport across Caco-2 cells to the extent of intestinal absorption

Despites of these limitations, Caco-2 cells constitute an excellent model to study drug transport across this barrier, provided that its limitations are taken into account in interpreting results.

Atenolol being hydrophilic molecule transported via paracellular route through tight junctions (40,41). The pH of transport solution plays an important role, while the pH of basolateral solution of Caco-2 monolayers corresponds to the pH of interstitial fluid in the villi of the small intestine. Under this region the pH value is 7.4. Therefore, in the present

study permeability of atenolol across Caco-2 cell monolayers was performed at pH 7.4 at apical and basolateral as atenolol has higher P_{app} at the same pH condition (42).

Many synthetic permeation enhancers show significant promise as a solution to low permeability issues of the intestinal epithelium. EDTA is very commonly studied bioenhancer (43). Permeation enhancement effect of EDTA was studied on D-[1-^{14}C] Mannitol, which is used as role model compound for permeation enhancers acting on paracellular route. Optimum concentration of EDTA obtained after permeation studies, was selected as a standard concentration in atenolol permeation study.

2.3.1 Materials

Dulbecco's modified Eagle medium (DMEM), non-essential amino acids (NEAA), fetal bovine serum (FBS), L-glutamine, gentamicin solution, and DMSO were purchased from Sigma Aldrich Ltd. (Ayrshire, UK). Disodium EDTA was purchased from VWR International Ltd. (UK). Cell culture flasks (162 cm^2 with ventilated caps) and Transwell cell culture systems (12 wells, 1.13 cm^2 polyester, 0.4 µm pore size) were from Costar, Corning Inc. (through Fisher Scientific, Leicestershire, UK). Cell culture reagents included trypsin EDTA solution (2.5 g/L trypsin, 0.5 g/L EDTA), trypan blue solution (0.4 % w/v), Hanks balanced salt solution [HBSS, no phenol red, including $NaHCO_3$ at 0.33 g/L with 10 mM 4-(2-hydroxyethyl) piperazine-1-ethanesulfonic acid (HEPES)], and phosphate buffered saline (PBS) were from Oxoid, Hampshire, UK.

Radiolabelled D-[1-^{14}C] Mannitol 250 µCi, 9.25 mBq in 1.25 ml with 61 mCi /mmol specific activity was obtained from GE Healthcare (UK). Radiolabelled [^{3}H] Atenolol 250 µCi, 9.25 mBq in 0.25 ml with 7.3 Ci/mmol specific activity was procured from Moravek Biochemicals (Brea, CA). Atenolol was kindly gifted from Wockhardt Ltd. (Mumbai, India). Piperine (PI) and Glycyrrhizic acid ammonium salt (GA) were purchased from Sigma Aldrich Ltd. (Mumbai, India). All the other chemicals and solvents were of analytical grade and were used without any further purification. Deionized double distilled water was used through out the study.

2.3.2 Methods

2.3.2.1 Caco-2 Cell Culture

Caco-2 cells, were obtained from European collection for cell cultures (ECACC, Wiltshire, UK) at passage 4, were maintained as described previously (44) using Fetal bovine serum. Caco-2 cells were used at passages 7-13 for all the studies. Cells were cultured in 162 cm^2 flasks using 25 ml medium and maintained in a humidified, 5 % CO_2, 95 % atmospheric air incubator at 37°C. Cell cultured medium was pre-warmed to 37 °C and comprised of 500 ml Dulbecco's modified Eagle medium (D-MEM), 10 % fetal bovine Serum, 5 ml nonessential amino acid solution (X100), 5 ml L-glutamine solution (200 mM), and 0.5 ml of gentamycin solution (50 mg/ml). The medium was changed every other day until the flask reached 90 % confluence.

Confluent cells were detached using trypsin–EDTA solution. The cell layer was washed twice with 6 ml of pre-warmed (at 37 °C) PBS. After removal of PBS, 6 ml of trypsin–EDTA was gently dripped down side of the flask to distribute trypsin–EDTA solution all over surface of the culture. Flask was kept in incubator shaker with 30 rpm speed till the cells are loosened properly. Trypsination was stopped by addition of propagation medium to neutralize trypsin, and then cells were pelleted by centrifugation at 1500 rpm for 5 min. Supernatants were removed and cell pellets were re-suspended in assay medium and counted using a hemocytometer. Cells were seeded onto the Transwells with seeding density 1 X 10^5 cells/cm^2. Cells were introduced to the apical surface of transwell cell culture support in 0.5 ml medium and 1.5 ml medium was added to the basolateral chamber. Cells were incubated at 37 °C with 5 % CO_2 and 90 % relative humidity, and media was changed every 48 hr. The cells used for transport studies between 21 and 28 days. The integrity of monolayer was checked by measuring TEER after each week till transport studies done.

2.3.2.2 Cell Monolayer Integrity

The initial and final values of transepithelial electrical resistance (TEER) of the Caco-2 cell monolayers grown on permeable supports were measured with an epithelial volt-ohmmeter (EVOM), equipped with an STX-2 electrode (World Precision Instruments, Stevenage, UK). The monolayers were equilibrated for 25-35 min before TEER measurements. Only cell

monolayers with TEER values over 200 Ω cm^2 were used. TEER was calculated by subtracting the resistance of a cell-free culture insert and correcting for surface area of the Transwell cell culture support.

2.3.3 Transport Studies

To prepare cell layers on the day of transport studies, TEER was measured and medium on the apical and basolateral chambers was aspirated and cell layers washed twice with pre-warmed (37 °C) HBSS. The cells were allowed to equilibrate in pre-warmed HBSS/10 mM HEPES buffer pH 7.4 for half and hour to one hour in the incubator at 37 °C. The TEER was measured prior to experimentation. For absorptive permeability, transport studies initiated by adding 0.5 ml of respective test solution (as per section 2.3.6.3 to 2.3.6.5) to the apical chamber and 1.0 ml to the basolateral chamber. All experiments were performed at 37 °C. The plates were stirred using an orbital shaker (at 37 °C) to avoid problem of unstirred water layer. Samples (100 µl) were withdrawn from the basolateral chamber at 0, 15, 30, 45, 60, 90, 120, 150 and 180 min and from the apical chamber 20 µl sample withdrawn at 0 and 180 min. The withdrawn volume was replaced with fresh transport media. For all instances, each experiment was performed three times to get n = 9 for control and experimental wells, samples were appropriately measured and averaged. TEER was also measured after final sample withdrawal. After completion of the experiment, cell monolayer with insert membrane was removed with help of scraper to measure the amount of drug retained in the cell monolayer.

2.3.3.1 Sample Analysis

The amount of drug transported was determined from radioactivity content in the samples using scintillation counter (Beckman Coulter LS6000TA, Buckinghamshire, UK). Withdrawn samples (100 µl) were mixed with 5 ml of StarScint scintillation cocktail and analyzed.

2.3.3.2 Calculations of Permeability Coefficients and Statistical Analysis

The transport rate is described by the equation 2.3.1 obtained from Fick's law

Equation 2.3.1

$$\frac{dQ}{dt} = \frac{dCr(t)}{dtVr} = Papp \cdot A \cdot (Cd(t) - Cr(t))$$

Where *Q* [mg] is the amount transported over cell monolayer, $C_r(t)$ [µmol/ml] receiver concentration, $C_d(t)$ [µmol/ml] donor concentration, *Vr* [ml] receiver volume, P_{app} [cm/sec] apparent permeability coefficient, A [cm^2] area of filter and t [sec] time.

All the experiments were performed under 'sink' conditions, the apparent permeability coefficients were calculated according to equation 2.3.2,

Equation 2.3.2

$$Papp(cm/\sec) = \frac{dQ/dt}{A * Cd(0)}$$

Where, transport rate (*dQ/dt*) was determined as the slope obtained by linear regression of cumulative fraction absorbed-time profiles. Equation 2.3.2 is obtained from equation 2.3.1, where $C_d(t)$ have been approximated constant and *Cr(t)* on the left side of equation 2.3.1 has been approximated as zero.

Transport enhancement ratios were calculated from P_{app} values according to the equation 2.3.3. (45)

Equation 2.3.3

$$R = \frac{Papp(sample)}{Papp(control)}$$

The results of experiments performed (n = 9) are presented as mean ± SD. Significance between the mean values was calculated using ANOVA using SPSS version 15.0. Tukey HSD post-hoc multiple comparison test was done to detect significant differences ($p < 0.05$) between the permeability in presence of bioenhancer as compared with control (without bioenhancer).

2.3.3.3 Effect of EDTA on [^{14}C] Mannitol Flux

To optimize the concentration of EDTA six different concentrations such as 1 mM, 2 mM, 4 mM, 8 mM, 16 mM and 24 mM were used. Each of EDTA solutions were taken in three wells (n=3). The concentration of D-[1-^{14}C] Mannitol was 10 µM in each well. Each of test solutions of EDTA and D-[1-^{14}C] Mannitol was prepared in HBSS/10 mM HEPES buffer pH 7.4.

Experiment Design for D-[1-^{14}C] Mannitol flux measurement:

Transwell 1 (D-[1-^{14}C] Mannitol flux with 1, 2 mM EDTA and control)			
A1 HBSS (Blank)	**A2** 10 µM Mannitol (Control)	**A3** 10 µM Mannitol **1 mM** EDTA	**A4** 10 µM Mannitol **2 mM** EDTA
B1 HBSS (Blank)	**B2** 10 µM Mannitol (Control)	**B3** 10 µM Mannitol **1 mM** EDTA	**B4** 10 µM Mannitol **2 mM** EDTA
C1 HBSS (Blank)	**C2** 10 µM Mannitol (Control)	**C3** 10 µM Mannitol **1 mM** EDTA	**C4** 10 µM Mannitol **2 mM** EDTA

Transwell 2 (D-[1-^{14}C] Mannitol flux with 4, 8, 16, 24 mM EDTA)			
A1 10 µM Mannitol **4 mM** EDTA	**A2** 10 µM Mannitol **8 mM** EDTA	**A3** 10 µM Mannitol **16 mM** EDTA	**A4** 10 µM Mannitol **24 mM** EDTA
B1 10 µM Mannitol **4 mM** EDTA	**B2** 10 µM Mannitol **8 mM** EDTA	**B3** 10 µM Mannitol **16 mM** EDTA	**B4** 10 µM Mannitol **24 mM** EDTA
C1 10 µM Mannitol **4 mM** EDTA	**C2** 10 µM Mannitol **8 mM** EDTA	**C3** 10 µM Mannitol **16 mM** EDTA	**C4** 10 µM Mannitol **24 mM** EDTA

2.3.3.4 *Effect of PI on [^{3}H] Atenolol Flux*

To estimate the effect of PI on permeation of Atenolol, optimized concentration of EDTA was used as standard bioenhancer. Amongst six different concentrations, EDTA with 8 mM was used for PI effect on Atenolol flux. Each of PI solutions was taken in three wells. This experiment was repeated more two times i.e. (n=9). The concentration of [^{3}H] Atenolol was taken together with unlabelled Atenolol giving final concentration of 0.8 µCi/ml. Each of test solutions was prepared in HBSS/10 mM HEPES buffer pH 7.4. PI was prepared as 5 mM stock solutions in DMSO and diluted with HBSS/HEPES buffer pH 7.4 as needed. In each experiment, the final concentration of DMSO in the medium was kept constant at 0.5 %. Permeation of [^{3}H] Atenolol was measured in presence of five different concentrations of PI (1 µM, 10 µM, 50 µM, 100 µM and 250 µM).

Experiment Design for [^{3}H] Atenolol flux measurement:

Transwell 3 ([^{3}H] Atenolol flux with 1, 10, 50 µM PI)			
A1 0.8 µCi/ml Atenolol	**A2** 0.8 µCi/ml Atenolol **1 µM** PI	**A3** 0.8 µCi/ml Atenolol **10 µM** PI	**A4** 0.8 µCi/ml Atenolol **50 µM** PI
B1 0.8 µCi/ml Atenolol	**B2** 0.8 µCi/ml Atenolol **1 µM** PI	**B3** 0.8 µCi/ml Atenolol **10 µM** PI	**B4** 0.8 µCi/ml Atenolol **50 µM** PI
C1 0.8 µCi/ml Atenolol	**C2** 0.8 µCi/ml Atenolol **1 µM** PI	**C3** 0.8 µCi/ml Atenolol **10 µM** PI	**C4** 0.8 µCi/ml Atenolol **50 µM** PI

Transwell 4 ([^{3}H] Atenolol flux with 8 mM EDTA and 100, 250 µM PI)			
A1 HBSS (Blank)	**A2** 0.8 µCi/ml Atenolol **8 mM** EDTA	**A3** 0.8 µCi/ml Atenolol **100 µM** PI	**A4** 0.8 µCi/ml Atenolol **250 µM** PI
B1 HBSS (Blank)	**B2** 0.8 µCi/ml Atenolol **8 mM** EDTA	**B3** 0.8 µCi/ml Atenolol **100 µM** PI	**B4** 0.8 µCi/ml Atenolol **250 µM** PI
C1 HBSS (Blank)	**C2** 0.8 µCi/ml Atenolol **8 mM** EDTA	**C3** 0.8 µCi/ml Atenolol **100 µM** PI	**C4** 0.8 µCi/ml Atenolol **250 µM** PI

2.3.3.5 Effect of GA on [^{3}H] Mannitol Flux

GA was evaluated for its efficacy as an absorption enhancer of hydrophilic molecule Atenolol. Same as PI optimized concentration of EDTA (8 mM) was used as standard bioenhancer. Each of GA solutions was taken in three wells. This experiment was repeated more two times i.e. (n=9). The concentration of [^{3}H] Atenolol and preparation of each test solutions were as per section 2.3.6.4. Permeation of [^{3}H] Atenolol was measured in presence of five different concentrations of GA (0.01 mM, 0.05 mM, 0.1 mM, 2.5 mM and 24 mM).

Experiment Design for [^{3}H] Atenolol flux measurement:

Transwell 5 ([^{3}H] Atenolol flux with 0.01, 0.05, 0.1 mM GA)			
A1 0.8 µCi/ml Atenolol	**A2** 0.8 µCi/ml Atenolol **0.01 mM** GA	A3 0.8 µCi/ml Atenolol **0.05 mM** GA	A4 0.8 µCi/ml Atenolol **0.1 mM** GA
B1 0.8 µCi/ml Atenolol	**B2** 0.8 µCi/ml Atenolol **0.01 mM** GA	B3 0.8 µCi/ml Atenolol **0.05 mM** GA	B4 0.8 µCi/ml Atenolol **0.1 mM** GA
C1 0.8 µCi/ml Atenolol	**C2** 0.8 µCi/ml Atenolol **0.01 mM** GA	C3 0.8 µCi/ml Atenolol **0.05 mM** GA	C4 0.8 µCi/ml Atenolol **0.1 mM** GA

Transwell 6 ([^{3}H] Atenolol flux with 8 mM EDTA and 2.5, 24 mM GA)			
A1 HBSS (Blank)	**A2** 0.8 µCi/ml Atenolol **8 mM** EDTA	A3 0.8 µCi/ml Atenolol **2.5 mM** GA	A4 0.8 µCi/ml Atenolol **24 mM** GA
B1 HBSS (Blank)	**B2** 0.8 µCi/ml Atenolol **8 mM** EDTA	B3 0.8 µCi/ml Atenolol **2.5 mM** GA	B4 0.8 µCi/ml Atenolol **24 mM** GA
C1 HBSS (Blank)	**C2** 0.8 µCi/ml Atenolol **8 mM** EDTA	C3 0.8 µCi/ml Atenolol **2.5 mM** GA	C4 0.8 µCi/ml Atenolol **24 mM** GA

2.3.4 Results and Discussion

2.3.4.1 Effect of EDTA on [^{14}C] Mannitol Flux

The release profile of [^{14}C] Mannitol in presence of different concentrations of EDTA is represented in Figure 2.3.6. It clearly indicates that each EDTA concentration increasing the permeation of [^{14}C] Mannitol. Table 2.3.2 represents transport parameters and enhancement ratios of Mannitol permeation. P_{app} values and enhancement ratio of Mannitol is almost twice with 4 mM and higher concentration of EDTA than control Mannitol (without EDTA). The enhancement of permeation with 1 and 2 mM EDTA is almost not seen for [^{14}C] Mannitol, but when concentration rise to 4 mM almost twice increment in the permeation is observed. Increase in permeation is significantly high than control [^{14}C] Mannitol (Figure 2.3.7). Presence of EDTA is causing decrease in % TEER values (Table 2.3.3) of Caco-2 monolayers during [^{14}C] Mannitol permeation. This decrease in % TEER suggests that EDTA causing opening of tight junctions and allows more permeation of [^{14}C] Mannitol which is absorbs by paracellular pathway (Figure 2.3.8). EDTA is widely studied bioenhancer, which acts as chelating agent. It has an enhancing effect via a paracellular route by chelating Ca^{+2} to open tight junctions of epithelium. It has low interaction with membrane which leads to lack of high toxicity of membrane. Higher concentration of EDTA can act on transcellular route (46). All results suggest that after 4 mM of concentration of EDTA all tight junctions are opened completely so after that higher concentrations causes much more similar increase in permeation. There may be saturation of paracellular pathway which is not allowing more enhancement of permeation after certain level of concentration. An optimum concentration was selected as 8 mM; as such there is no much significance difference in P_{app} values of [^{14}C] Mannitol with 4 mM and 8 mM EDTA. The reason to optimize 8 mM of EDTA, as decrease in % TEER values suggests there is more opening of tight junctions of monolayers than with 4 mM of EDTA.

Figure 2.3.6 The Release profile of Mannitol in presence of different concentrations of EDTA.

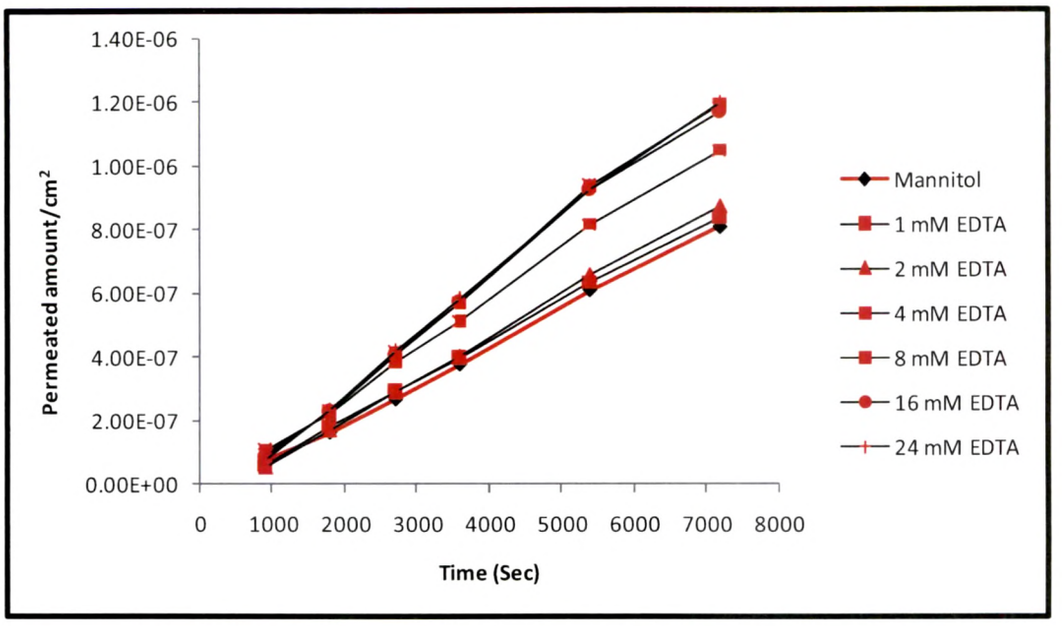

Figure 2.3.7 Mannitol P_{apps} in presence of different concentrations of EDTA.

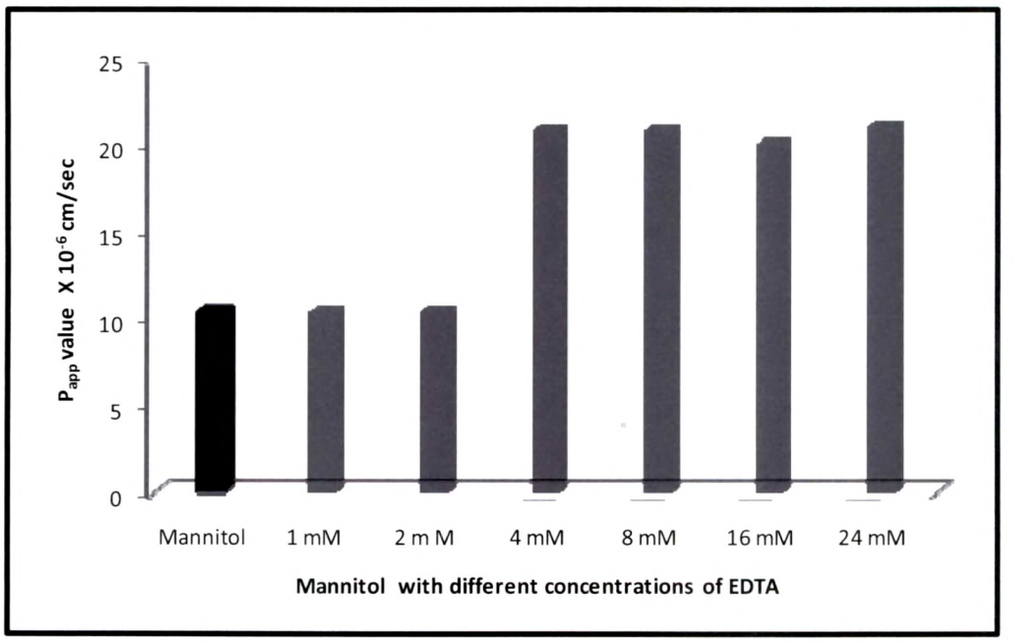

Table 2.3.2 Effect of EDTA on [^{14}C] Mannitol fluxes across Caco-2 cell monolayer.

EDTA (mM)	P_{app} of [^{14}C] Mannitol (P_{app} x 10^{-6} cm/sec)	Enhancement ratio (ER)	p Value
0	10.36 ± 0.05	1.00	
1	10.34 ± 0.07	1.00	p > 0.05
2	10.37 ± 0.14	1.00	p > 0.05
4	**20.77 ± 0.09**	**2.01**	0.0001*
8	**20.82 ± 0.07**	**2.00**	0.0001*
16	20.03 ± 1.17	1.93	0.0001*
24	21.03 ± 0.11	2.03	0.0001*

Note: Data were calculated from the results of transport experiments and present the means ± SD. (n = 3)

*p < 0.05; significant difference from control i.e. Mannitol (One way ANOVA, Tukey's multiple comparison test)

Table 2.3.3 The effects of various concentrations of EDTA on post % TEER (at 180 min) of Caco-2 monolayers and P_{app} values during Mannitol flux.

EDTA (mM)	Post % TEER (at 180 min)	P_{app} of [^{14}C] Mannitol (P x 10^{-6} cm/sec)
0	100.00	10.36 ± 0.05
1	95.68	10.34 ± 0.07
2	90.13	10.37 ± 0.14
4	78.34	20.77 ± 0.09
8	**71.32**	**20.82 ± 0.07**
16	70.05	20.03 ± 1.17
24	69.45	21.03 ± 0.11

Data represents Mean ± SD (n = 3)

Figure 2.3.8 The effect of various concentrations of EDTA on TEER and P_{apps} of Mannitol.

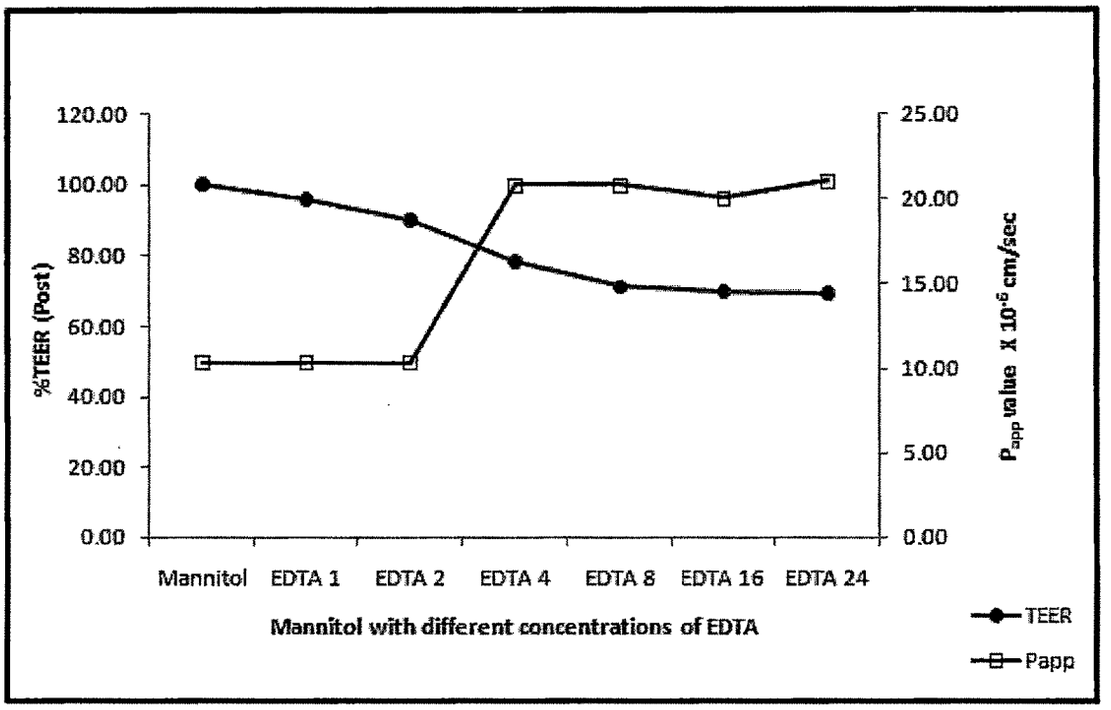

2.3.4.2 *Effect of PI on [^{3}H] Atenolol Flux*

The release profile of [^{3}H] Atenolol in presence of optimized concentration of EDTA (8 mM) and different concentrations of PI is represented in Figure 2.3.9. It clearly indicates that higher concentrations of PI are not increasing permeation but with lower concentrations the release i.e. fluxes value of [^{3}H] Atenolol is increasing. While EDTA optimized concentration which was taken as standard bioenhancer shows more release of [^{3}H] Atenolol than PI concentrations.

Table 2.3.4 represents transport parameters and enhancement ratios of the [^{3}H] Atenolol permeation. P_{app} values and enhancement ratio of [^{3}H] Atenolol is higher with 1, 10 and 50 µM concentrations of PI and with 8 mM EDTA. Enhancement of permeation with each lower concentrations of PI is significantly different ($p < 0.05$) than the control (Figure 2.3.10).

The presence of PI is decreasing % TEER values (Figure 2.3.11) of Caco-2 monolayers. [^{3}H] Atenolol which absorbs by paracellular route has less permeation across the membrane in

absence of PI. While PI affects the permeation of [^{3}H] Atenolol, this reflects PI may have paracellular opening effect that might be related to ready permeation across the apical membrane.

Figure 2.3.9 The Release profile of [^{3}H] Atenolol in presence of EDTA and different concentrations of PI.

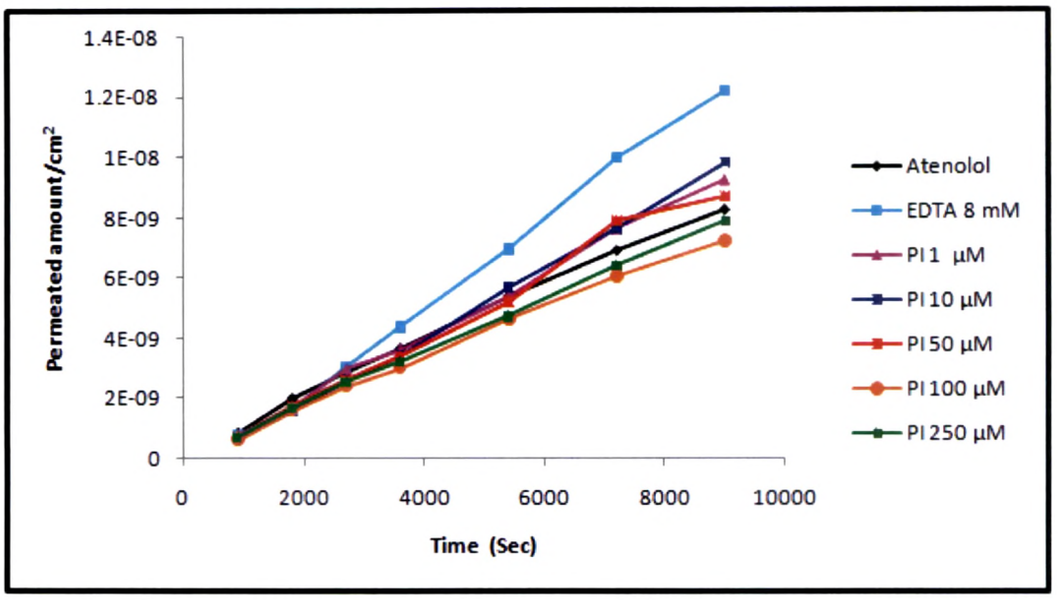

Figure 2.3.10 [^{3}H] Atenolol P_{apps} in presence of EDTA and different concentrations of PI.

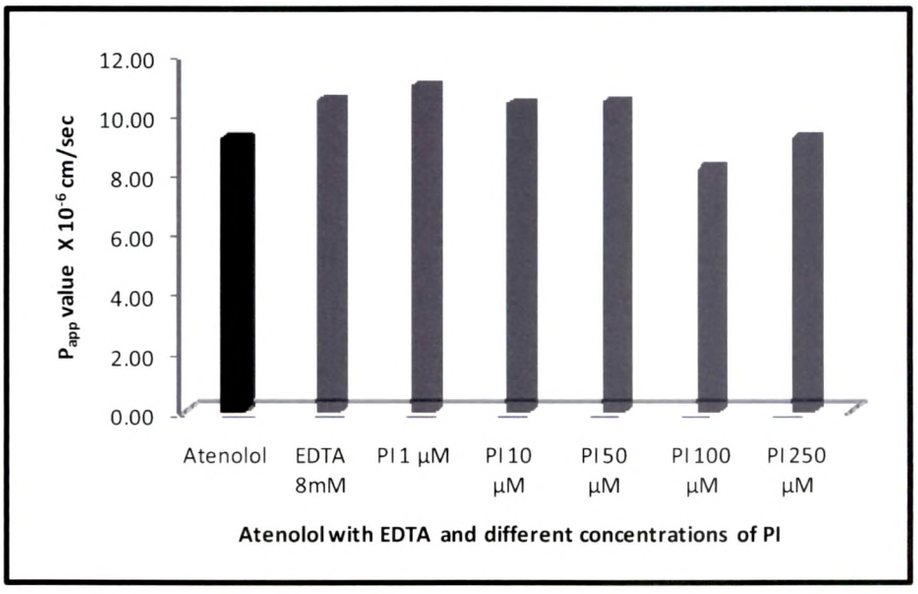

Table 2.3.4 The effects of EDTA and various concentrations of PI on [^{3}H] Atenolol fluxes across Caco-2 cell monolayer.

Concen. of Bioenhancer	**P_{app} of [^{3}H] Atenolol (P_{app} x 10^{-6} cm/sec)**	**Enhancement ratio (ER)**	**p Value**
0 (Control)	9.20 ± 0.01	1.00	
EDTA (8 mM)	10.48 ± 0.23	1.14	0.001*
PI (μM)			
1	**11.01 ± 0.06**	**1.20**	0.001*
10	10.39 ± 0.06	1.13	0.001*
50	10.45 ± 0.03	1.14	0.001*
100	8.20 ± 0.00	0.90	0.001*
250	9.25 ± 0.01	1.04	p > 0.05

Note: Data were calculated from the results of transport experiments and present the means ± SD. (n = 9)

*p < 0.05; significant difference from control i.e. Atenolol (One way ANOVA, Tukey's multiple comparison test)

Figure 2.3.11 The effects of EDTA and various concentrations of PI on pre and post % TEER (at 180 min) of Caco-2 monolayers containing [^{3}H] Atenolol.

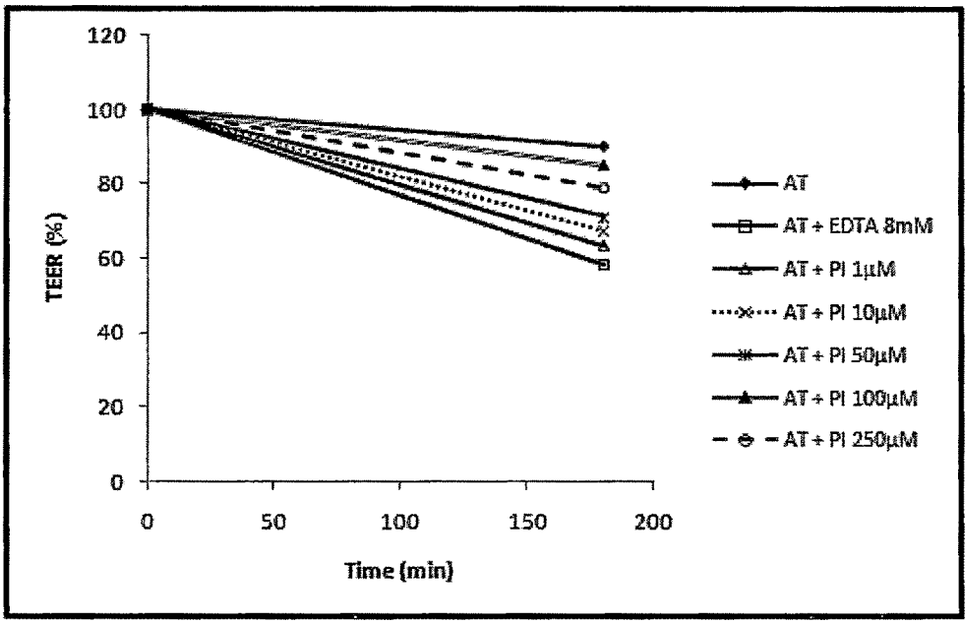

Although atenolol is expected to cross monolayer by paracellular pathways, but it has been also found in previous studies that atenolol may have transport mediated flux through P-glycoprotein. PI is postulated as inhibitor of efflux transporter P-glycoprotein, (47) thus increase in permeation of atenolol may be due to inhibition of P-glycoprotein by PI. There is reduction in % TEER of monolayer in presence of bioenhancers and increase in P_{app} values (Figure 2.3.12) supports there are opening of paracellular pathways by PI in monolayers allowing atenolol to cross the monolayer. The detailed explanation of TEER reduction and mechanism of action of PI through paracellular pathway remain to be elucidated but it is believed that subtle changes in cell membrane caused by cytoskeletal changes result in TEER reduction and enhanced permeability of atenolol. Permeation reduction effect of higher concentrations of PI remains still unclear but it may be due to saturation of paracellular pathways. EDTA is also causing decrease in % TEER which is due to its action as chelating agent which described in section 2.3.4.1.

Figure 2.3.12 The effect of EDTA and various concentrations of PI on TEER and P_{apps} of Atenolol.

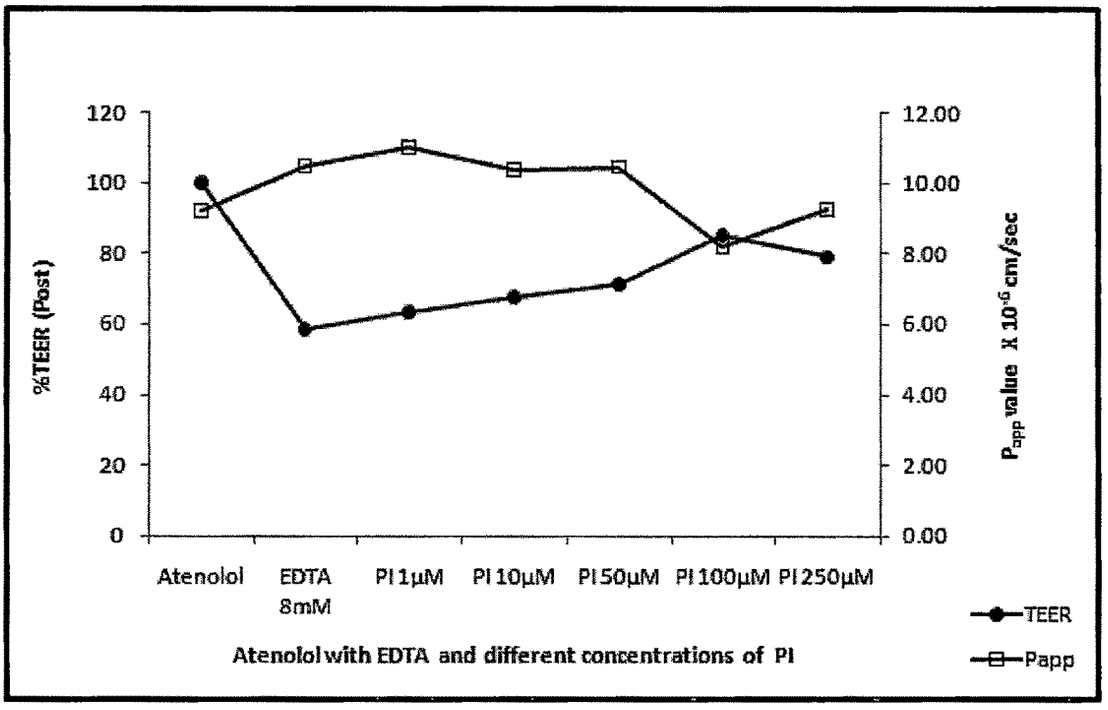

Thus it seems from the P_{app} values and TEER of cell monolayers that, PI along with *paracellular openings*, also inhibits *P-glycoprotein* which plays minor role in the permeation of atenolol. This synergistic action (paracellular opening and P-glycoprotein inhibition) increases permeation of atenolol significantly in presence of PI.

2.3.4.3 *Effect of GA on [^{3}H] Atenolol Flux*

The release profile of [^{3}H] Atenolol in presence of optimized concentration of EDTA (8 mM) and different concentrations of GA is represented in Figure 2.3.13. It clearly indicates that higher concentrations of GA decrease permeation of [^{3}H] Atenolol through Caco-2 cell monolayers. While lower concentrations are increasing permeation (Figure 2.3.14). While EDTA optimized concentration which was taken as standard bioenhancer shows more release of [^{3}H] Atenolol than control.

Table 2.3.5 represents transport parameters and enhancement ratios of the [^{3}H] Atenolol permeation. P_{apps} values and enhancement ratio is higher with 0.01 and 0.05 mM concentrations of GA and with 8 mM EDTA. The enhancement with each concentrations of GA is significantly different ($p < 0.05$) than the control (Table 2.3.5).

Figure 2.3.13 The Release profile of [^{3}H] Atenolol in presence of EDTA and different concentrations of GA.

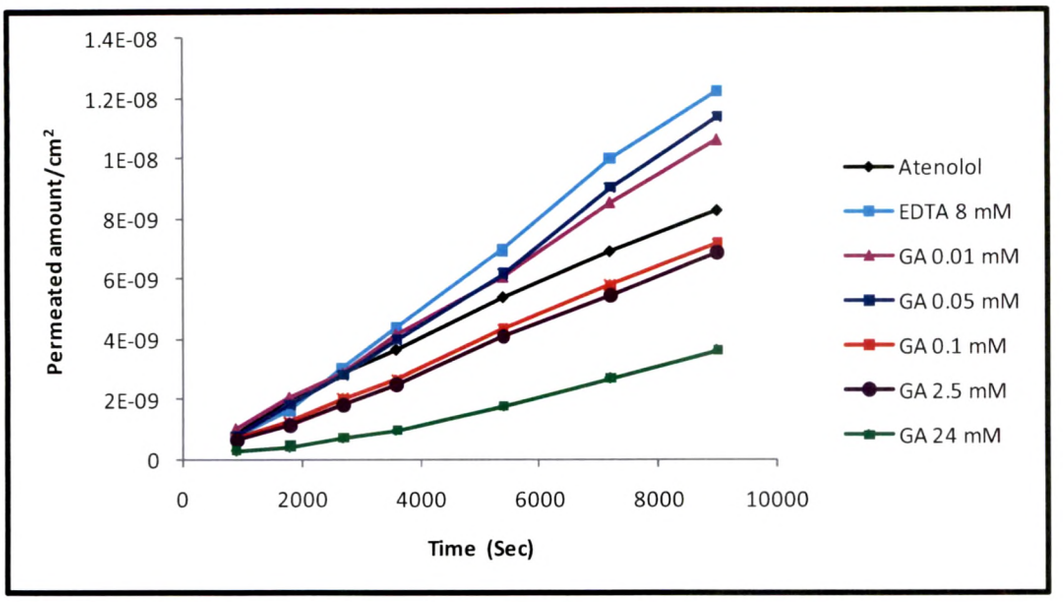

Figure 2.3.14 [^{3}H] Atenolol flux in presence of EDTA and different concentrations of GA.

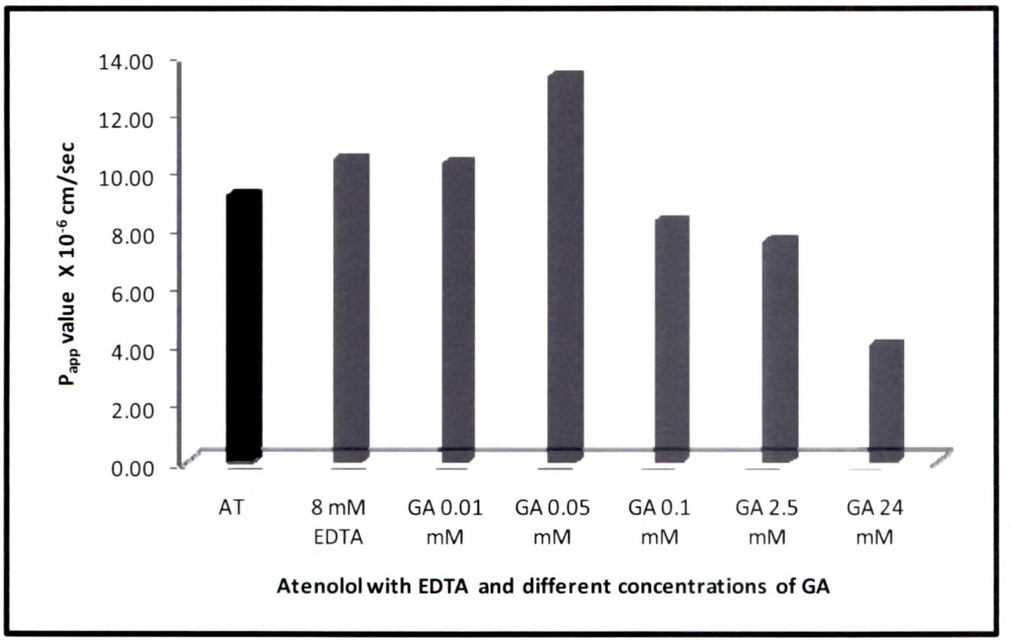

Table 2.3.5 The effects of EDTA and various concentrations of GA on [^{3}H] Atenolol fluxes across Caco-2 cell monolayer.

Concen. of Bioenhancer	**P_{app} of [^{3}H] Atenolol (P_{app} x 10^{-6} cm/sec)**	**Enhancement ratio (ER)**	**p Value**
0 (Control)	9.20 ± 0.01	1.00	
EDTA (8 mM)	10.48 ± 0.23	1.14	$p < 0.001$*
GA (mM)			
0.01	10.31 ± 0.08	1.12	$p < 0.001$*
0.05	**13.32 ± 0.14**	**1.45**	$p < 0.001$*
0.1	8.31 ± 0.02	0.90	$p < 0.001$*
2.5	7.62 ± 0.59	0.83	$p < 0.001$*
24	4.04 ± 0.10	0.44	$p < 0.001$*

Note: Data were calculated from the results of transport experiments and present the means ± SD. (n = 9)

*$p < 0.05$; significant difference from control i.e. Atenolol (One way ANOVA, Tukey's multiple comparison test)

The presence of GA in lower concentrations is decreasing % TEER values (Figure 2.3.15) which may be due to, surfactant like action of GA. Thus it may be increasing permeation via its solubilizing activity and increase intracellular calcium ion concentrations resulting in opening of paracellular route. This increase in intracellular calcium has activated calmodulin dependent kinase, which leads phosphorylation of myosin chain, followed by the contraction of actin-myosin ring, which open the paracellular route (48).There is reduction in the % TEER of monolayer in presence of bioenhancers and increase in P_{app} values (Figure 2.3.16) supports there are opening of paracellular pathways by lower concentrations of GA allowing atenolol to cross the monolayer.

While the higher concentrations of GA are causing decrease (49) in permeation of atenolol which is absorbs through paracellular route. The % TEER increase and decrease (Figure 2.3.15) in permeation of atenolol with higher concentrations may be due to inactivation of GA than its aglycon part, which is said to be acing on paracellular route (47)

Figure 2.3.15 The effects of EDTA and various concentrations of GA on pre and post % TEER (at 180 min) of Caco-2 monolayers containing [^{3}H] Atenolol.

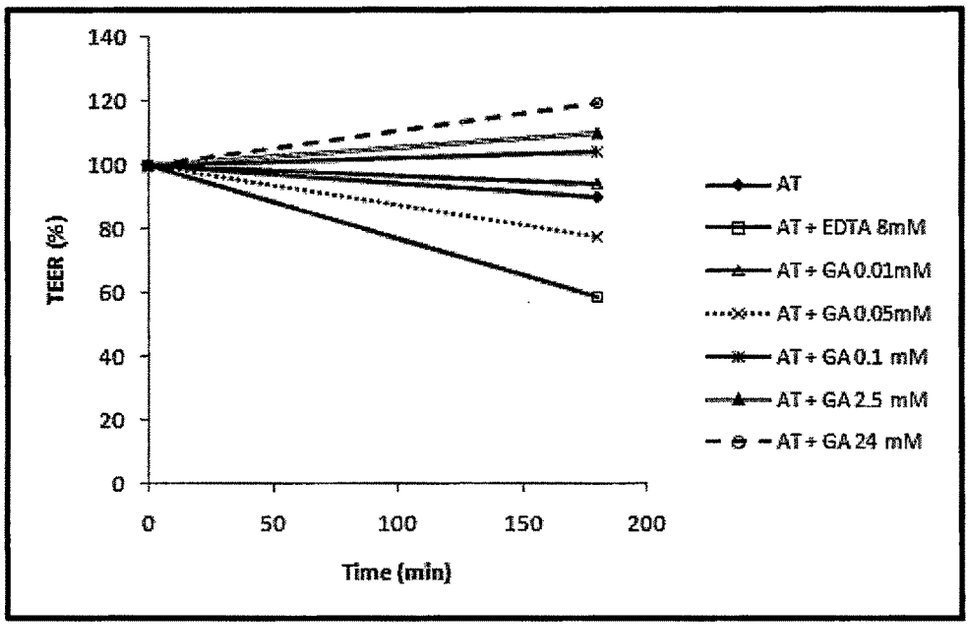

Figure 2.3.16 The effect of EDTA and various concentrations of GA on TEER and P_{apps} of Atenolol.

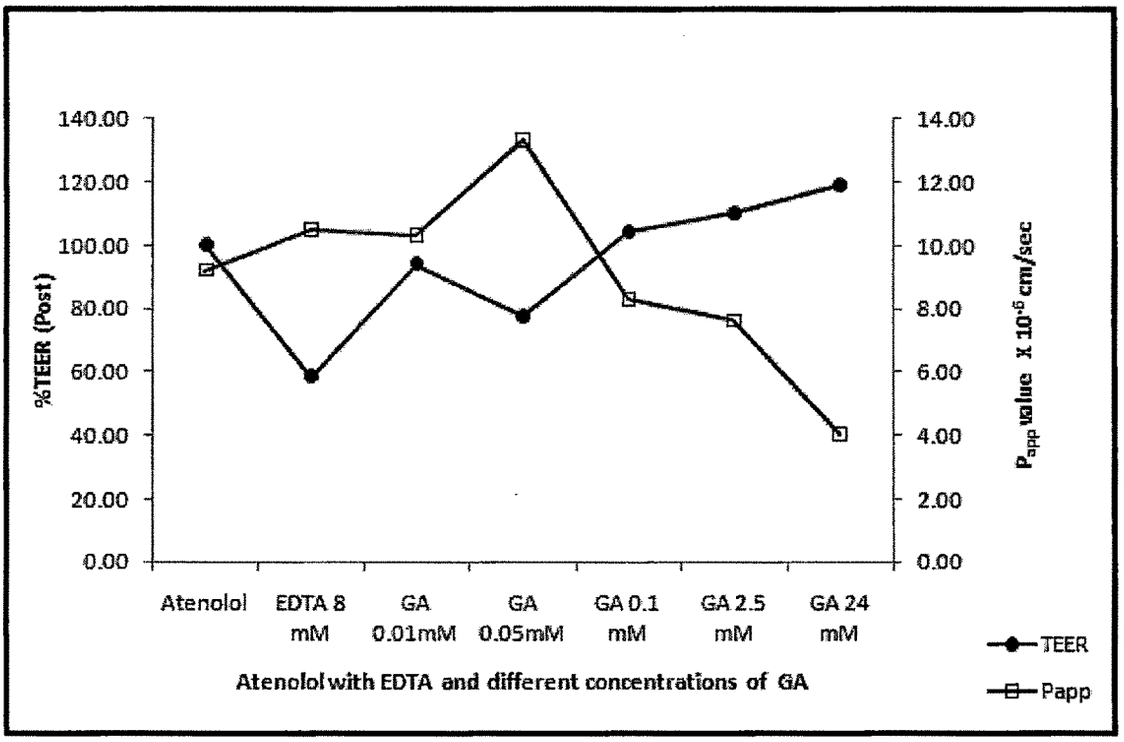

2.3.5 Conclusion

The results of Mannitol permeation studies showed that 8 mM concentration of EDTA is sufficient enough to open paracellular pathway and leads to more permeation of Mannitol. In permeation study of atenolol it is found that PI and GA both significantly improve permeation of AT in lower concentrations than the higher concentrations of bioenhancers. PI with 1 µM concentration cause 1.2 fold increases in permeation, while 0.05 mM of GA is sufficient to cause 1.45 fold enhancement in permeation of AT. PI and GA seems to cause opening of paracellular pathway which can lead to more permeation of AT across cell monolayers. These all studies indicates both bioenhancers PI and GA are most effective as bioenhancers in lowest concentrations only. Higher concentrations may cause reduction in permeation of AT.

The results obtained in atenolol transport across Caco-2 cell monolayers supports the results obtained in *ex vivo* permeation studies. Although the permeation is less across cell monolayers that may be due to lack of mucus producing goblet cells in monolayers, as intestine has mucus producing goblet cells, which influence the tight junctions and allows more permeation. PI can modulate membrane dynamics, and cause increase in intestinal surface and its brush border effect allows more permeation of atenolol. Thus more permeation in *ex vivo* permeation studies than *in vitro* cell line studies is fairly obvious.

2.3.6 References

1 A. R. Hilgers, R. A. Conradi, P. S. Burton, Caco-2 cell monolayers as a model for drug transport across the intestinal mucosa, Pharm Res., **1990**, 7 (9), 902–910.

2 M. Mayersohn, Principles of drug absorption, Morden Pharmaceutics, Edn 4, Marcel & Dekker, New York, USA, **2002**, 22–44.

3 B. M, Denker, S. K. Nigam, Molecular structure and assembly of the tight junctions, Am J Physiol., **1998**, 274(43), F1–F9.

4 I. Hidalgo, Cultured intestinal epithelial cell models, Models for assessing drug absorption and metabolism, Plenum Press, New York, USA, **1996**, 35–50.

5 V. Pade, S. Stavchansky, Estimation of the relative contribution of the transcellular and paracellular pathway to the transport of passively absorbed drugs in the Caco-2 cell culture model, Pharm Res., **1997**, 14, 1210–1215.

6 S. D. Flanagan, L. H. Takahashi, X. Liu, L. Z. Benet, Contributions of saturable active secretion, passive transcellular, and paracellular diffusion to the overall transport of furosemide across adenocarcinoma (Caco-2) cells. J Pharm Sci., **2002b**, 91, 1169–1177.

7 J. R. Pappenheimer, K. Z. Reiss, Contribution of solvent drag through intercellular junctions to absorption of nutrients by the small intestine of the rat, J Membr Biol., **1987**, 100 123–136.

8 L. M. Chan, S. Lowes, B. H. Hirst, The ABCs of drug transport in intestine and liver: efflux proteins limiting drug absorption and bioavailability. Eur J Pharm Sci., **2004**, 21, 25–51.

9 J. Hunter, M. Jepson, T. Tsuruo, N. Simmons, B. Hirst, Functional expression of P-glycoprotein in apical membranes of human intestinal Caco-2 cells, J Biol Chem., **1993a**, 268, 14991–14997.

10 R. Evers, M. de Haas, R. Sparidans, J. Beijnen, P. R. Wielinga, J. Lankelma, P. Borst, Vinblastine and sulfinpyrazone export by the multidrug resistance protein MRP2 is associated with glutathione export, Br J Cancer., **2000**, 83, 375–383.

11 P. B. Watkins, Drug metabolism by cytochromes P450 in the liver and small bowel, Gastrointest Pharmacol., **1992**, 21, 511–526.

12 M. Pinto, S. Robine-Leon, M. Appay, M. Kedinger, N. Triadou, E. Dussaulx, B. Lacroix, A. Zweibaum, Enterocyte-like differentiation and polarization of the human colon carcinoma cell line Caco-2 in culture, Biol Cell., **1983**, 47, 323–330.

13 CDER Waiver of In Vivo Bioavailability and Bioequivalence Studies for Immediate Release Solid Oral Dosage Forms Based on a Biopharmaceutics Classification System, Food and Drug Administration, Rockville, MD, USA, **2000**. http://www.fda.gov/cder/guidance/3618fnl.pdf

14 J. Fogh, T. Orfeo, One hundred and twenty seven cultured human tumor cell lines producing tumors in nude mice, J Natl Cancer Inst., 1977, 59, 221–226.

15 I. J. Hidalgo, T. J. Raub, R. T. Borchardt, Characterization of the human colon carcinoma cell line (Caco-2) as a model system for intestinal epithelial permeability, Gastroenterology, **1989**, 96, 736–749.

16 J. N. Cogburn, M. G. Donovan, C. S. Schaasteen, A model of human small intestinal absorptive cells 1. Transport barrier, Pharm Res., **1991**, 8, 210–216.

17 P. Artursson, Epithelial transport of drugs in cell culture. I: A model for studying the passive diffusion of drugs over intestinal absorptive (Caco-2) cells, J Pharm Sci., **1990**, 79, 476–482.

18 C. Huet, C. Sahuquillo-Merino, E. Coudrier, D. Louvard, Absorptive and mucus-secreting subclones isolated from a multipotent intestinal cell line (HT-29) provide new models for cell polarity and terminal differentiation, J Cell Biol., **1987**, 105, 345–357.

19 A. Wikman, J. Karlsson, I. Carlstedt, P. Artursson, A drug absorption model based on the mucus layer producing human intestinal goblet cell line HT29-H, Pharm Res., **1993**, 10, 843–852.

20 V. C. Dias, R. W. Yatscoff, Investigation of rapamycin transport and uptake across absorptive human intestinal cell monolayers, Clin Biochem., **1994**, 27, 31–36.

21 M. J. Cho, D. P. Thompson, C. T. Cramer, T. J. Vidmar, J. F. Schieszka, The Madin-Darby canine kidney (MDCK) epithelial cell monolayers as a model cellular transport barrier, Pharm Res., **1989**, 6, 71–77.

22 K-M.Y. Covitz, G. L. Amidon, W. Sadée, Human dipeptide transporter, hPEPT1, stably transfected into Chinese Hamster Ovary Cells, Pharm Res., **1996**, 13, 1631–1634.

23 A. Braun, S. Hämmerle, K. Suda, B. Rothen-Rotishauser, M. Günther, S. Krämer, Cell cultures as tools in biopharmacy, Eur J Pharm Sci., **2000**, 11, S51–S60.

24 E. Grasset, M. Pinto, E. Dussaulx, A. Zweibaum, Epithelial properties of human colonic carcinoma cell line Caco-2; electrical parameters, Am J Physiol., **1984**, 247, C260–267.

25 A. Blais, P. Bissonnette, A. Berteloot, Common characteristics for Na - dependent sugar transport in Caco-2 cells and human fetal colon, J Membr Biol., **1987**, 99, 113–125.

26 T. Smith, C. Gibson, B. Howlin, J. Pratt, Active transport of amino acids by gamma-glutamyl transpeptidase through Caco-2 cell monolayers, Biochem Biophys Res Commun., **1991**, 178, 1028–1035.

27 M. Yoshioka, P. Erickson, H. Matsumoto, E. Gum, Y. Kim, Expression of dipeptidyl aminopeptidase IV during enterocytic differentiation of human colon cancer (Caco-2) cells, Int J Cancer., **1991**, 47, 916–921.

28 D. W. Rosenberg, T. Leff, Regulation of cytochrome P450 in cultured human colonic cells, Arch Biothem Biophys., **1993**, 300, 186–192.

29 T. Sergent-Engelen, V. Delistrie. Y. Schneider, Phase I and II biotransformations in living Caco-2 cells cultivated under serum-free conditions, Biochem Pharm., **1993**, 46, 1393–1401.

30 V. Carriere, T. Lesuffleur, A. Barbat, M. Rousset, E. Dussauix, P. Costet, I. de Waziers, P. Beaune, A. Zweibaum, Expression of cytochrome P-450 3A in HT29-MTX cells and Caco-2 clone TC7, Fed Eur Biochem Sot Lett., **1994**, 355, 247–250.

31 P. Artursson, A-L. Ungell, J-E. Löfroth, Selective paracellular permeability in two models for intestinal absorption: cultured monolayers of human intestinal epithelial cells and rat intestinal segments, Pharm Res., **1993**, 10, 1123–1129.

32 P. Artursson, K. Palm, K. Luthman, Caco-2 monolayers in experimental and theoretical predictions of drug transport, Adv Drug Deliv Rev., **1996**, 22, 67–84.

33 D. T. Thwaites, G. T. A. McEwan, B. H. Hirst, N. L. Simmons, H^+-coupled α-methylaminoisobutyric acid transport in human intestinal Caco-2 cells, Biochim Biophys Acta., **1995b**, 1234, 111–118.

34 M. Hu, R. T. Borchardt, Mechanism of L-α-methyldopa transport through a monolayer of polarized human intestinal epithelial cells (Caco-2), Pharm Res., **1990**, 7, 1313–1319.

35 L. Z. Benet, T. Izumi, Y. Zhang, J. A. Silverman, V. J. Wacher, Intestinal MDR transport proteins and P-450 enzymes as barriers to oral drug delivery, J Control Release., **1999**, 62, 25–31.

36 C. D. Tran, P. Timmins, B. R. Conway, W. J. Irwin, Investigation of the coordinated functional activities of Cytochrome P450 3A4 and P-glycoprotein in limiting the absorption of xenobiotics in Caco-2 cells, J Pharm Sci., **2002**, 91, 117–128.

37 M. D. Troutman, D. R. Thakker, Rhodamine123 requires carrier-mediated influx for its activity as a P-glycoprotein substrate in Caco-2 cells, Pharm Res., **2003**, 20, 1192–1199.

38 P. Augustijns, R. Mols, HPLC with programmed wavelength fluorescence detection for the simultaneous determination of marker compounds of integrity and P-gp functionality in the Caco-2 intestinal absorption model, J Pharm Biomed Anal., **2004**, 34, 971–978.

39 J. Karlsson, A. Wikman, P. Artursson, The mucus layer as a barrier to drug absorption in monolayers if human intestinal epithelial HT29-H goblet cells, Int J Pharm., **1993**, 99, 209–218.

40 D. E. Leahy, J. Lynch, D. C. Taylor, Mechanisms of absorption of small molecules In: Novel Drug Delivery and its Therapeutic Application. Wiley & Sons, Chichester, **1989**, 33–44.

41 P. Artursson, J. Karlsson, Correlation between oral drug absorption in humans and apparent drug permeability coefficients in human intestinal epithelial cells (Caco-2) cells, Biochem Biophys Res Commun., **1991**, 175, 880–885.

42 S. Yamashita, T. Furubayashi, M. Kataoka, T. Sakane, H. Sezaki, H. Tokuda, Optimized conditions for prediction of intestinal drug permeability using Caco-2 cells, Eur J Pharm Sci., **2000**, 10, 195–204.

43 Y. Quan, K. Hattori, E. Lundborg, T. fujita, M. Murakami, S. Muranishi, A. Yamamoto, Effectiveness and toxicity screening of various absorption enhancers using Caco-2 cell monolayers, Biol Pharm Bull., **1998**, 21(6), 615–620.

44 W. Kamm, J. Hauptmann, I. Behrens, J. Stuzebecher, F. Dullweber, H. Gohlke, M. Stubbs, G. Klebe, T. Kissel, Transport of peptidomimetic thrombin inhibitors with a 3-amino phyenylalanine structure: permeability and efflux mechanism in monolayers of a human intestinal cell line (Caco-2), Pharm Res., **2001**, 18, 1110 –1114.

45 M. Thanou, J. C. Verhoef, M. T. Nihot, J. H. Verheijden, H. E. Junginger, Enhancement of the intestinal absorption of low molecular weight heparin (LMWH) in rats and pigs using Carbopol 934P, Pharm Res., **2001**, 18, 1638–1641.

46 S. Yamashita, H. Saitoh, K. Nakanishi, M. Masada, T. Nadai, T.Kimura, J Pharm Pharmacol., **1985**, 37, 512–513.

47 R. Bhardwaj, H. Glaeser, L. Becquemont, U. Klotz, S. Gupta, M. Fromm, Piperine, a Major Constituent of Black Pepper, Inhibits Human P-glycoprotein and CYP3A4, J Pharmacol Exp Ther., **2002**, 302(2), 645–650.

48 J. R. Turner, J. M. Angle, E. D. Black, J. Joyal, D. B. Sacks, J. L. Madara, PKC-dependent regulation of transepithelial resistance: roles of MLC and MLC kinase, Am J Physiol., **1999**, 277, C554–C562.

49 T. Imai, M. Sakai, H. Ohtake, H. Azuma, M. Otagiri, In vitro and in vivo evaluation of the enhancing activity of glycyrrhizin on the intestinal absorption of drugs, Pharm Res., **1999**, 16, 80–86.

2.4 Pharmacokinetics Studies of Atenolol

In the present section, effect of bioenhancers (PI and GA) on atenolol bioavailability was determined. Bioavailability determination of atenolol in presence of natural bioenhancers was done by performing *in vivo* studies in rats. The prime objectives were,

- To develop simple and cost effective bio-analytical method for atenolol in presence of PI and GA
- To perform *in vivo* studies of atenolol and atenolol with both bioenhancers (PI and GA) using rat as an animal model
- To determine all pharmacokinetic parameters using the data obtained from *in vivo* studies
- To draw significant conclusions by statistical treatment to data obtained

Bioavailability is the most useful pharmacokinetic variable for describing overall quantitative role of all processes influencing absorption, first-pass metabolism and excretion in the gut and liver (1). This pharmacokinetic variable is used to illustrate the fraction of the dose that reaches the systemic circulation, and relate it to pharmacological and safety for oral pharmaceutical products from several different pharmacological classes.

The objective of *pharmacokinetic* is to describe the time course of drug concentrations in blood in mathematical terms so that, the performance of pharmaceutical dosage forms can be evaluated in terms of rate and amount of drug they deliver to the blood, and the dosage regimen of a drug can be adjusted to produce and maintain therapeutically effective blood concentrations with little or no toxicity. Thus when poor absorption improved by incorporating absorption enhancers, *in vivo* absorption experiments give the most comprehensive results.

To understand the achievement of bioavailability enhancement *in vivo* studies were performed in rats. Ready availability, cost, and ease of maintenance make the rat a very

popular experimental animal. Very often simultaneous sampling of bile and urine along with blood are needed in pharmacokinetic studies, which is easily possible with rats.

Various computer programmes and softwares are available for determining pharmacokinetic parameters. In the present study, all pharmacokinetics parameters were calculated in MS Excel (2) using Wagner nelson method (3,4).

The experiments were conducted as per CPCSEA (Committee for Prevention, Control and Supervision of Experimental Animals, Reg. No. 404/01/a/CPCSEA) guidelines. Protocol for the study was approved by the Institutional ethical committee at The M. S. University of Baroda, India.

2.4.1 Calculations for Pharmacokinetic Parameters

Pharmacokinetic parameters estimated were as follows (1,5,6,7),

Maximum plasma concentration (C_{max}): It was determined directly from the plasma concentration time profiles. Maximum concentration obtained in the study was considered to be maximum plasma concentration C_{max}.

Time to maximum plasma concentration (T_{max}): It was determined directly from the plasma concentration time profiles. Time at which the maximum concentration was obtained is said to be time to maximum plasma concentration T_{max}.

Area under the plasma concentration-time curve from time '0' to 't' (AUC_{0-t}): It was calculated by using trapezoidal rule. According to trapezoidal rule, area under the curve from time t_2 to time t_1 is calculated by equation 2.4.1.

Equation 2.4.1

$$AUC_{t1}^{t2} = \left(\frac{C_1 + C_2}{2}\right) \times (t_1 - t_2)$$

Where, C1 and C2 are concentrations at time t_1 and t_2.

Concentration at zero time (C0): Time versus $\log_n$ plasma concentration graph was plotted on MS-Excel graph wizard. The terminal linear phase was extrapolated to zero. It gave intercept. The antilog of intercept was obtained by linear regression wizard, which gave concentration at zero time (C0). C0 = antilog (intercept)

Elimination rate constant ($-K_{el}$): The plot of $\log_n$ of plasma concentration verses time was linear for terminal portion (last three detectable concentrations). Slope of this linear line was calculated. K_{el} = -slope × 2.303

Elimination half life ($t_{1/2}$): It was determined by ($t_{1/2}$ = 0.693/Kel)

Area under the plasma concentration-time from time zero to infinity ($AUC_{0-\alpha}$): The trapezoidal rule was used to determine AUC.

Absorption rate constant ($-K_{ab}$): Terminal linear portion of the curve with slope $-K_{el}$ was extrapolated to t=0. An actual plasma levels were subtracted from corresponding concentrations on the extrapolated linear portions. This gave a series of residual concentration (C_r). The plot of natural log of residual concentration ($\log_n C_r$) versus time gave a straight line with slope ($-K_{ab}$).

Volume of distribution (V_d): It is the volume in which drug would have to be distributed to produce the measured plasma concentration.

Equation 2.4.2 $$V_d = \frac{D_G^0 \cdot K_a}{A\left(K_a - K_{el}\right)}$$ where D_G^0 is dose of drug.

Clearance (Cl): It is the total volume of plasma from which the drug has been removed per unit time.

Equation 2.4.3 $$Clearance(Cl) = \frac{V_d \times 0.693}{t_{1/2el}}$$

Cumulative drug eliminated at t time: It was calculated as, Drug eliminated = 0.434 K_{el} * t

Fraction of drug absorbed at time:

Equation 2.4.4 $$t = \frac{C + K_{el} \times AUC_0^t}{K_{el} \times AUC_0^\infty}$$

Area under momentum curve (AUMC): AUMC is the area under the curve of (Cp x t) versus t.

Mean residence time (MRT):

Equation 2.4.5 $$MRT = \frac{CAUMAC}{CAUC}$$

Where, CAUMC = Cumulative AUMC and CAUC = Cumulative AUC.

Relative Bioavailability (%):

In vivo performance of drugs in presence of bioenhancers was compared in terms of relative bioavailability. It was determined using equation,

Equation 2.4.6 $$\mathrm{Re}lativeBA(\%) = \frac{AUC(test)}{AUC(reference)} X \frac{Dose(reference)}{Dose(test)}$$

2.4.2 Materials

The Model drug atenolol (AT) was procured as a gift sample from Wockhardt Ltd., Mumbai, India. Piperine (PI) and Glycyrrhizic acid ammonium salt (GA) were purchased from Sigma Aldrich Ltd., Mumbai, India. Sodium hydroxide, potassium dihydrogen orthophosphate were purchased from Qualigence fine chemicals, Mumbai, India. Diethyl ether, methanol and water were of HPLC grade (Qualigence fine chemicals, Mumbai, India) and used without further purifications. All the other chemicals and solvents were of analytical grade and were used without any further purification. Deionized double distilled water was used through out the study wherever needed. Animal feed and husk was obtained Amrut Laboratory Animal Feed.

2.4.3 Estimation of Drug in Plasma

2.4.3.1 HPLC method for Atenolol

Atenolol (AT) was determined according to previously reported method (8), which was modified. The method was applied for AT determination in presence of PI and GA from plasma samples. Various parameters for HPLC analysis of AT from plasma samples of in vivo studies are explained in Table 2.4.1.

2.4.3.2 Plasma extraction procedure

Standard or sample of AT was extracted from plasma by modifying previously reported method (9). The plasma sample (100 µl) was alkalinized by adding 1 M NaOH (100 µl) and vortex mixed for 1 min. Diethyl ether (4 ml) was added to it, shaken well and then ether layer was separated by centrifugation (3000 rpm 10 min, 4 °C) and evaporated to dryness in a warm water bath. The residues were dissolved in mobile phase (200 µl). A 20 µl aliquot of final preparation was injected into the HPLC column.

2.4.3.3 Extraction efficiency

The extraction efficiency was calculated by adding known amount of AT (50, 100 and 500 ng/ml; n = 6 per concentration) or internal standard (Metoprolol 50 µl, 4 µg/ml) to 100 µl of blank rat plasma. AT was extracted as described in section 2.4.3.2. The residue was reconstituted in mobile phase. The known amount of aqueous layer was injected into the chromatographic system.

The peak area of sample was compared to those obtained from equivalent volumes of standard solution of drug in mobile phase directly injected into the HPLC system. Determination of un-extracted samples was performed in triplicate for each concentration.

Table 2.4.1 Various HPLC parameters of AT from plasma samples of in vivo studies.

Parameter	Details
System	Merk Hitachi, Lachrom
Pump	Merk Hitachi pump L – 7110, Double piston operated with 10 ml stainless steel pump head
Injector	Rheodyne (Made in USA) manually driven 6 port 3 channel valve with 20 µl fixed loop with 60° rotation.
Detector	UV detector L – 7400 Range of measurement – 0-2 AU Integrator output - ± 1.0 V Auto-zero – Full scale
Software	Computer installed with a multi HSM Manager Software
Stationary Phase	Analytical Column – KR-100 Kromasil C_{18} column, Particle size 5 µm; 250 mm X 4.6 mm i.d. Guard Column – ODS column, Particle size 10 µm; 10 mm X 5 mm i.d.)
Mobile Phase Composition	Methanol : Potassium dihydrogen phosphate 10 mM (70:30 v/v)
Temperature	Ambient
Flow Rate	0.6 ml/min
UV detection wavelength (λ)	228 nm
Retention time	5.3 min
Internal Standard	Metoprolol

The developed methods were validated for following parameters.

2.4.3.4 *Linearity and range*

The linear detector response for the assay was tested as follows. These determination (n=6) from minimum of five concentration levels (25, 50, 100, 300, 500, 1000, and 2000 ng/ml) of the analyte were made. Detector response was correlated against analyte concentration by least squares regression.

2.4.3.5 *Accuracy and precision*

For the determination of intra day and inter day accuracy and precision of the assay, various quantities of AT was added to aliquots of 100 µl rat plasma to yield 50, 100, 500, and 1000 ng/ml. Accuracy was expressed as Mean percent,

Equation 2.4.7

$$Accuracy = \left(\frac{Mean\ measured\ Concentration}{Expected\ Concentration} \right) \times 100$$

Precision was calculated as inter and intra day coefficient of variation,

Equation 2.4.8

$$\%\ CV = \left(\frac{SD}{Mean} \right) \times 100$$

2.4.4 Pharmacokinetic Study

2.4.4.1 Animal treatment

Female Wistar albino rats (weighing about 200-250 gm) were used in all the experiments. Rats were provided by Sun Pharma Advanced Research Company Ltd., Vadodara, India. The animals were housed over two weeks in a temperature (20 – 25 °C) and relative humidity (between 50 and 60 %) controlled room and were given standard rat chow and water which were freely available. The protocol for studies was approved by the Institutional ethical committee at The M S University of Baroda, India. The experiments were conducted as per CPCSEA (Committee for Prevention, Control and Supervision of Experimental Animals, Reg. No. 404/01/a/CPCSEA) guidelines. All the animals were fasted overnight with free access to tap water before experiments.

2.4.4.2 Calculation of dose of the drug in rats

Generally, LD_{50} dose is determined on basis of surface area or weight basis (10). Thus to determine an absolute dose for a species, surface area ratio factor was multiplied with dose of drug (11). Thus for 200 gm rats surface area ratio factor is 0.018. Human dose was multiplied with this factor which will give the dose of rat in mg/kg.

	200 gm Rat
70 Kg Man	0.018

The maximum dose of AT that can be given to human in single day is 100 mg. In this study, dose given to the rats was 2.5 mg/kg which was below LD_{50} dose.

2.4.4.3 Route of administration and withdrawal of blood samples

The different groups of rats were taken for pharmacokinetic studies. Each group has three rats. Table 2.4.2 represents all the groups and dose of AT and bioenhancers administered to rats. All rats were fasted for at least 12 hr prior to the experiment, with free access to water. AT (control), AT along with PI, and AT along with GA were administered orally with gavage needle. AT and GA was dissolved, while PI was suspended in 1% carboxymethyl cellulose (sodium salt – solution was made in hot distilled water).

Table 2.4.2 The Details of groups and dose given to the rats.

Group No.	Group Details (3 rats/group)	Dose (mg/kg)
1	AT (Control)	AT 2.5
2	AT + PI 1	AT 2.5 + PI 0.9
3	AT + PI 2	AT 2.5 + PI 0.45
4	AT + PI 3	AT 2.5 + PI 0.9
5	AT + GA 1	AT 2.5 + GA 0.0225
6	AT + GA 2	AT 2.5 + GA 0.1125
7	AT + GA 3	AT 2.5 + GA 0.225

After oral administration 0.4 ml of blood samples were collected from retro orbital plexus of rat at 0, 0.5, 1, 2, 3, 6, 8, and 24 hr time points into heparinized collection tubes. Blood samples were immediately centrifuged (3000 rpm) for 10 min at an ambient temperature. The supernatant plasma was separated and stored at –20 °C until analyzed. Plasma samples collected from rats were analyzed using modified HPLC method (as described in Section 2.4.3) and drug plasma concentration values were determined from calibration curve.

2.4.4.4 *Statistical analysis*

Primary pharmacokinetic parameters were determined using none compartmental analysis. Maximum plasma concentration C_{max}, and time to reach maximum concentration (T_{max}) were estimated directly from plasma concentration time curve. All other pharmacokinetic parameters were calculated as described in section 2.4.1. All the data were expressed as mean $\pm$ SD. Plasma drug concentrations as well as pharmacokinetic parameters were compared by student's t-test at α= 0.05.

2.4.5 Results and Discussion

2.4.5.1 HPLC method for Atenolol

The chromatograph of rat blank plasma and plasma spiked with AT and internal standard is given in Figure 2.4.1. It also represents chromatogram of rat plasma spiked with PI and GA. It is clearly observed from the chromatogram that there was no interference from blank plasma peaks to peaks of drug and internal standard; as well both bioenhancers PI and GA are not showing any peak at the analytical wavelength of AT. The peaks of AT and internal standard were sufficiently separated with typical retention times of 5.3 min for AT and 10.1 min for internal standard. Usual running time for sample was 12 min.

Figure 2.4.1 The Chromatograph of rat blank plasma, rat plasma spiked with AT and IS, and rat plasma spiked with GA and PI.

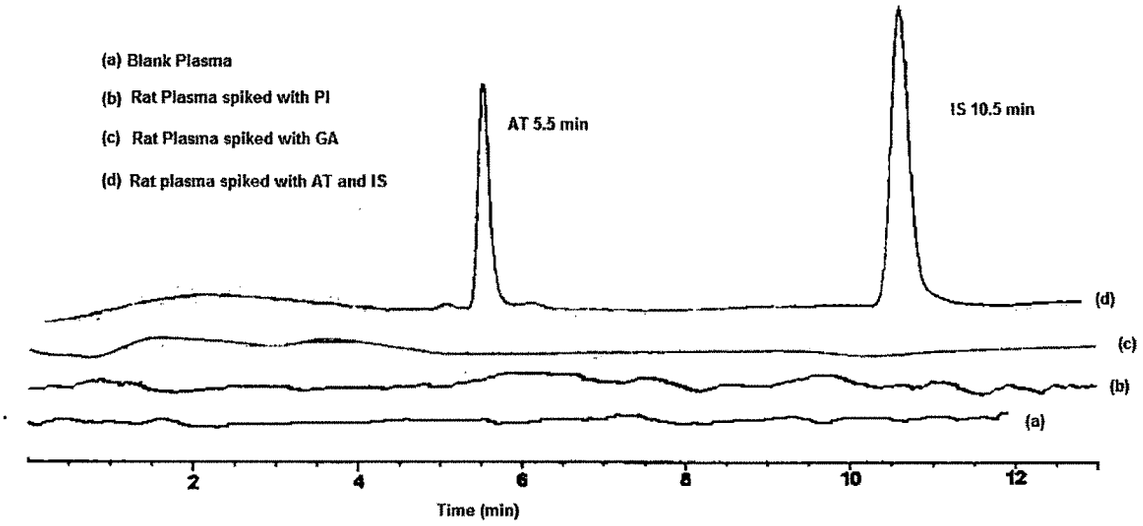

Calibration curve (peak area ratio of AT to IS versus AT concentration) in plasma was constructed by spiking seven different concentrations of AT and fixed concentration of IS. Chromatographic responses were found to be linear over an analytical range of 25–2000 ng/ml and found to be quite satisfactory and reproducible with time. Linear regression equation was calculated by least squares method using Microsoft Excel® program and summarized in Table 2.4.3. Correlation coefficient equals 0.9975, indicating a strong linear

relationship between the variables. Extraction efficiency was greater than 85 % which is represented Table 2.4.4.

Table 2.4.3 The spectral data for determination of AT by proposed HPLC method.

Parameters	**Values**
Linearity Range (ng/ml)	25 – 2000
Coefficient of determination (r^2)	0.9950
Correlation coefficient (r)	0.9975
*Regression equation (Y=m·x + c)	
Slope (m)	0.005
Intercept (c)	0.12
Limit of detection (ng/ml) [a]	7.19 ± 2.3
Limit of quantitation (ng/ml)[a]	21.8 ± 1.4

* Y=m·x + c, where x is the concentration (ng/ml). [a] Data represents Mean ± SD (n = 6).

Table 2.4.4 Mean Extraction Recovery of AT and internal standard from the spiked rat plasma.

	Internal Standard	**AT**		
Concentrations (ng/ml)	200	50	100	500
Mean Extraction* Recovery (%)	94.43 ± 2.43	86.75 ± 5.4	90.66 ± 4.13	91.43 ± 3.6
Average Extraction* Recovery (%)	94.43 ± 2.43		89.61 + 2.50	

*Data represents Mean ± SD (n = 6).

Accuracy data in the present study ranged from 98.38 to 99.87 % (Table 2.4.5) indicates that there was no interference from endogenous plasma components. Inter-day as well as intra-day replicates of AT, gave R.S.D. below 5.0 (should be less than 15 according to CDER guidance for Bio-analytical Method Validation (12)), revealed that proposed method is

highly precise. Accuracy of method was evaluated by using *t*-test at four concentration levels. The *t*-values obtained for 50, 100, 500 and 1000 ng/ml were 0.82, 1.29, 1.03, and 0.50 for inter-day whereas 1.31, 1.10, 1.01, and 0.60 for intra-day, respectively. The *t*-value required for significance at 5 % level at 5 degrees of freedom is 2.57, and obtained values were below this value. Thus no significant difference was observed between amounts of drug added and recovered. Overall, data summarized in Table 2.4.5, enables that an excellent accuracy and high precision was obtained.

Table 2.4.5 The summarised inter-day and intra-day precision and accuracy data of the method for AT estimation in rat plasma.

Concentrations (ng/ml)						
Nominal	**Found mean** [a]	**SD**	**RSD %**	**Mean Accuracy*** **(%)**	t_{cal} #	**CI**
Intra-day precision and accuracy of AT determination in rat plasma (n=6)						
50	49.39	0.78	1.59	98.79	1.31	50 ± 0.63
100	99.13	1.35	1.36	99.13	1.10	100 ± 1.08
500	495.90	4.94	1.40	99.18	1.01	500 ± 5.56
1000	998.74	3.62	0.36	99.87	0.60	1000 ± 2.89
Inter-day precision and accuracy of AT determination in rat plasma (n=6)						
50	49.19	1.69	3.44	98.38	0.82	50 ± 1.35
100	98.89	1.48	1.49	98.89	1.29	100 ± 1.18
500	497.64	3.96	0.80	99.53	1.03	500 ± 3.17
1000	998.63	4.76	0.48	99.86	0.50	1000 ± 3.82

[a] Average of six determinations at four concentration levels for inter-day and intra-day respectively.

*All the mean accuracy was calculated against their nominal concentrations.

$t_{cal} = |100 - R|\sqrt{n} / R.S.D$ Where t_{cal} is the calculated t value, n is the number of replicated, and R is mean accuracy. Tabulated t-value for 95 % two sided confidence interval for 5 degree of freedom was (t_{tab} =) 2.57.

2.4.5.2 *Pharmacokinetic Study of AT with PI*

Plasma samples collected from the rats were analyzed using proposed reverse phase HPLC method and drug (AT) plasma concentration values were determined from calibration curve. Mean plasma concentrations of AT in each of rats i.e. control rat and rats treated with each of three concentrations of PI is shown in Table 2.4.6. The average plasma drug concentrations versus time profiles in presence of each concentrations of PI are represented in Figure 2.4.2, Figure 2.4.3 and Figure 2.4.4. It is clearly observed that plasma drug concentrations with each concentrations of PI are highly significant ($p < 0.001$) and increased than control AT.

Table 2.4.6 The mean plasma concentrations of AT after administrations of AT, AT with three concentrations of PI.

Time (hr)	Observed Mean ± SD Plasma Concentrations of AT (ng/ml) (n = 3)			
	AT (Control)	AT + PI 0.9 mg/kg	AT + PI 0.45 mg/kg	AT + PI 0.9 mg/kg
0.00	0.00 ± 0.00	0.00 ± 0.00	0.00 ± 0.00	0.00 ± 0.00
0.50	42.24 ± 6.42	151.90 ± 7.20	115.15 ± 6.21	90.50 ± 11.41
1.00	80.02 ± 12.79	208.65 ± 11.95	163.90 ± 6.16	217.50 ± 18.60
2.00	60.32 ± 6.84	290.69 ± 9.06	274.02 ± 21.47	252.43 ± 23.08
3.00	56.42 ± 3.61	180.43 ± 18.07	199.09 ± 8.49	181.34 ± 13.22
6.00	42.34 ± 5.55	130.06 ± 14.12	151.43 ± 5.14	142.86 ± 10.04
8.00	32.89 ± 3.00	110.59 ± 3.39	109.23 ± 1.93	116.89 ± 13.40
24.00	10.55 ± 1.31	30.54 ± 2.89	26.59 ± 1.27	25.24 ± 0.90

Figure 2.4.5, Figure 2.4.6, Figure 2.4.7, and Figure 2.4.8 represents the natural log of mean plasma concentrations of AT with time plot for absorption and elimination rate constant. Each Figure indicates there is no much change in elimination rate constant. Table 2.4.7 compares various pharmacokinetic parameters of AT with and without PI administration. It is found that C_{max}, $AUC_{0\text{-}24\ hr}$, $T_{1/2a}$, and K_a were significantly increased, T_{max} also prolonged, whereas no much difference observed in K_{el}, $T_{1/2el}$. Relative bioavailability of AT with PI is almost 3 fold more than the pure drug AT.

Figure 2.4.2 The Mean plasma concentrations versus time profile following a single oral administration of AT, and AT in presence of PI 0.09 mg/kg. Each value is Mean ± SD of three determinations.

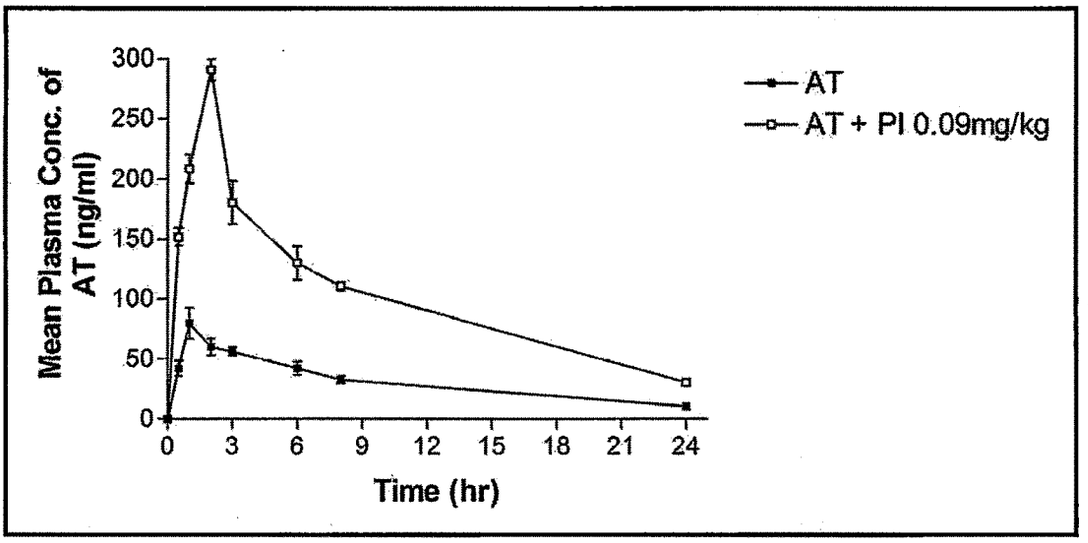

Figure 2.4.3 The Mean plasma concentrations versus time profile following a single oral administration of AT, and AT in presence of PI 0.45 mg/kg. Each value is Mean ± SD of three determinations.

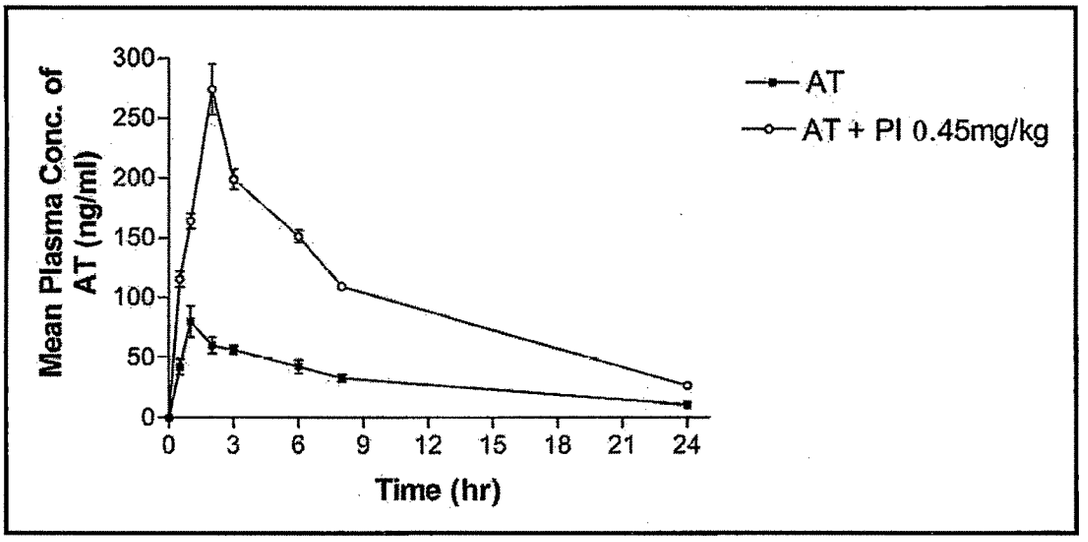

Figure 2.4.4 The Mean plasma concentrations versus time profile following a single oral administration of AT, and AT in presence of PI 0.9 mg/kg. Each value is Mean ± SD of three determinations.

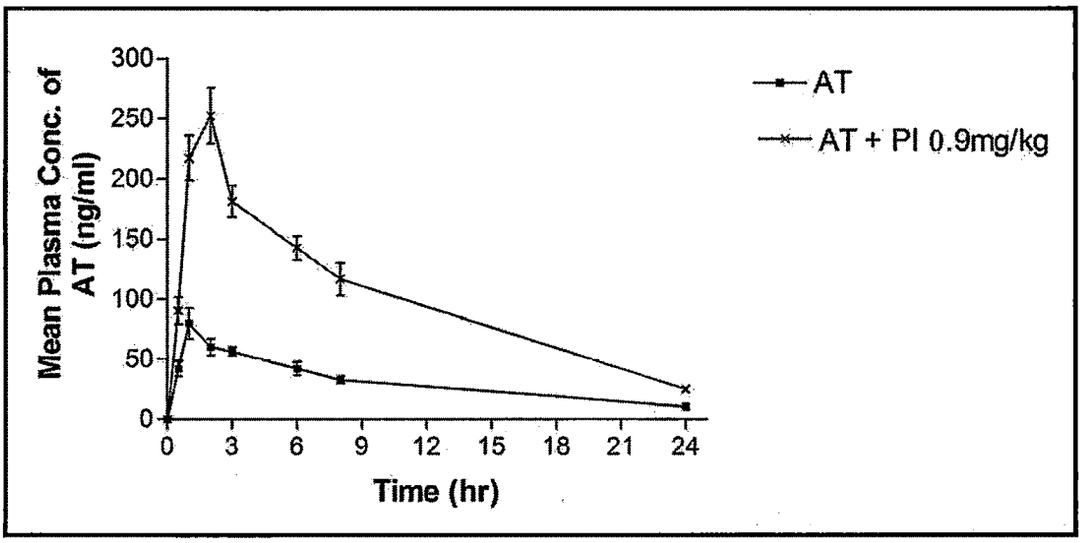

Figure 2.4.5 The Natural log of mean plasma concentrations of AT versus time plot for determination of k_a and k_{el}. Each value is Mean ± SD of three determinations.

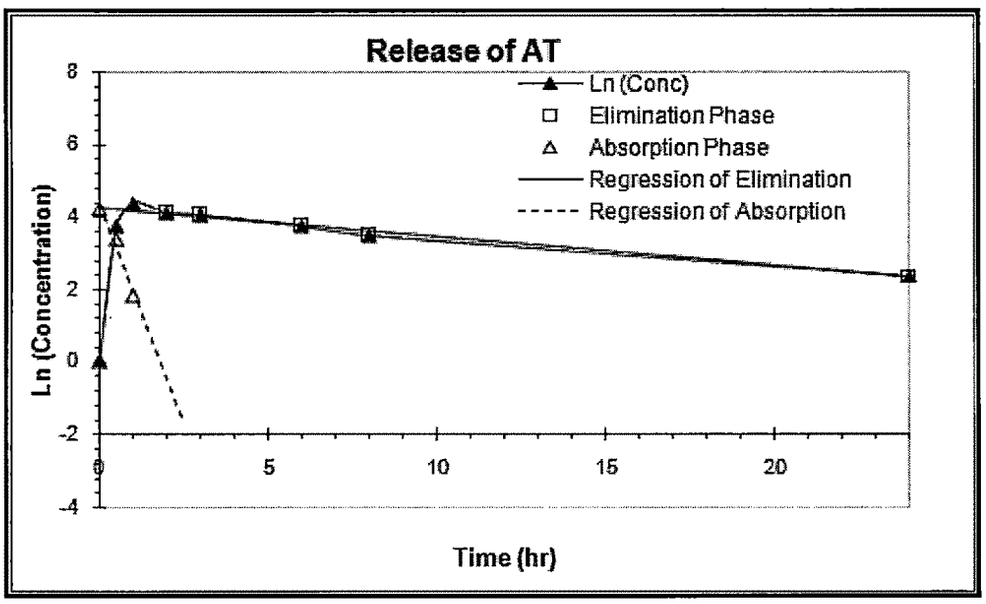

Figure 2.4.6 The Natural log of mean plasma concentrations of AT with PI 0.09 mg/kg versus time plot for determination of k_a and k_{el}. Each value is Mean ± SD of three determinations.

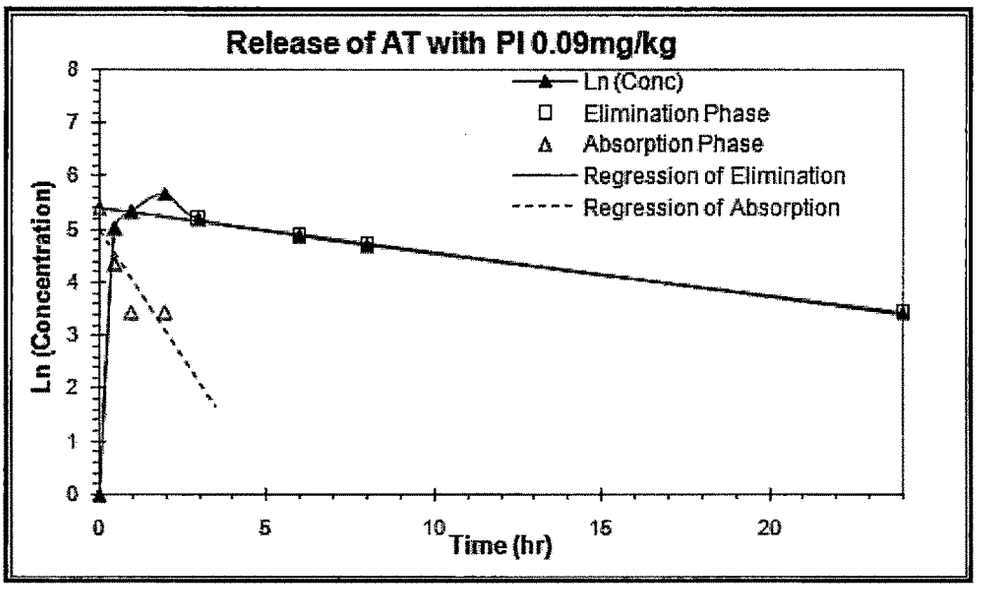

Figure 2.4.7 The Natural log of mean plasma concentrations of AT with PI 0.45 mg/kg versus time plot for determination of k_a and k_{el}. Each value is Mean ± SD of three determinations.

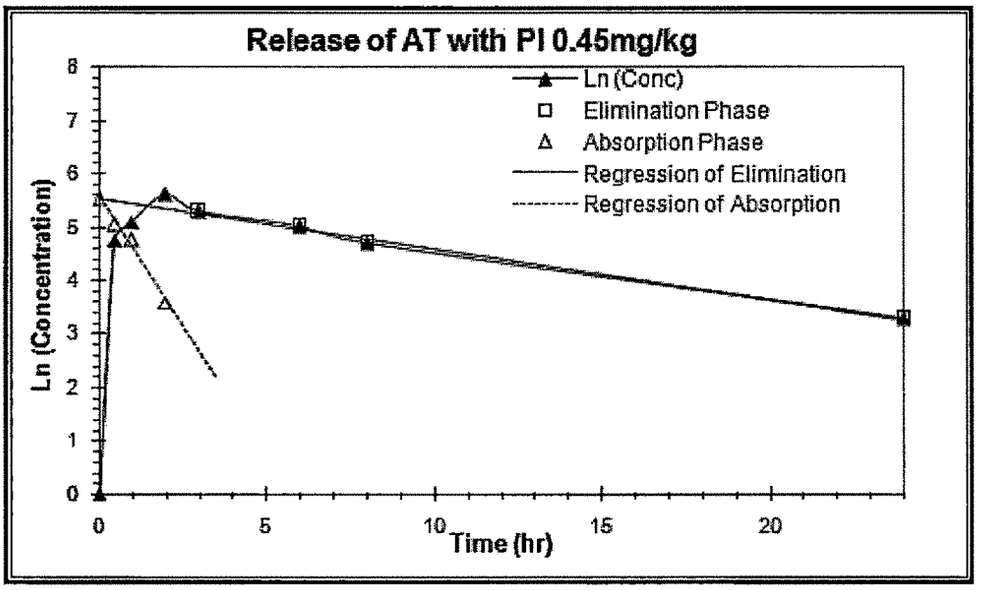

Figure 2.4.8 The Natural log of mean plasma concentrations of AT with PI 0.9 mg/kg versus time plot for determination of k_a and k_{el}. Each value is Mean ± SD of three determinations.

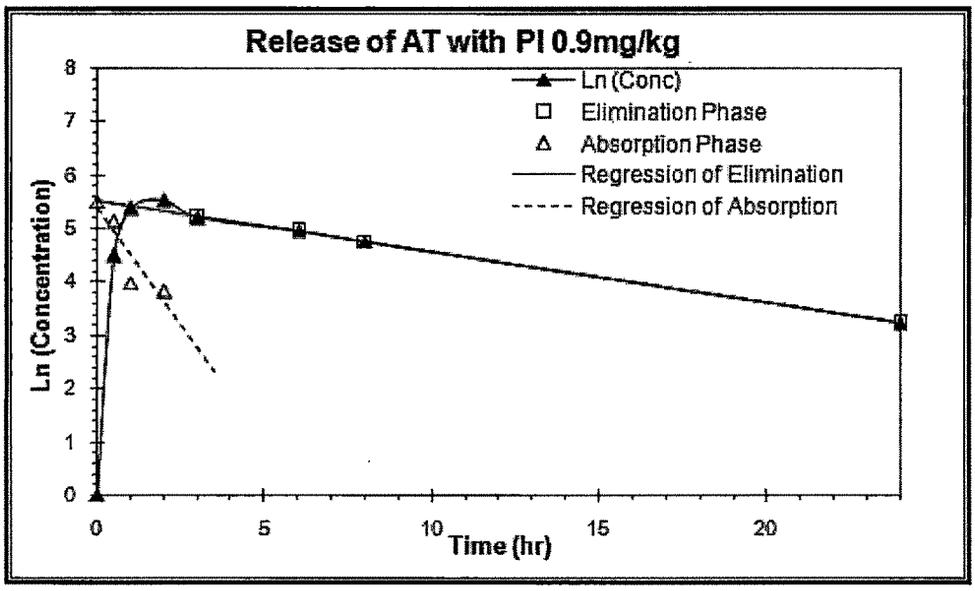

Different concentrations of PI were administered to rats with AT, it significantly increase the mean plasma concentration of AT. It is found that administration of lowest concentration i.e 0.09 mg/kg (5 mg human dose) of PI cause maximum bioenhancement of AT. It cause 3.31 fold increment in permeation of AT. The enhanced absorption could be due to an interaction between PI and AT in gastrointestinal tract. Possible mechanisms proposed are,

(a) The results obtained from the Caco-2 cell line studies postulates that PI can modulate paracellular openings (Section 2.3.4.2) and cause inhibition of P-glycoprotein (plays minor role in AT permeation). This synergistic action (paracellular opening and P-glycoprotein inhibition) increases permeation of AT significantly in presence of PI.

(b) PI can increase splanchnic blood flow, decreased hydrochloric acid secretion, delay in gastric emptying and an alteration of membrane dynamics which aid in efficient permeability through membranes (13). It could modulate membrane dynamics due to its solubility characteristics, by interacting with lipids and hydrophobic portions in the protein vicinity. PI also increases absorption of many drugs due to its easy partitioning ability, induction of synthesis of proteins associated with cytoskeletal functions resulting in an increase in the small intestinal surface, thus assisting efficient penetration through epithelial

barriers (14). An enhanced absorption of AT can be due to brush broader mechanism of PI. It has been found that PI doesn't affect the excretion of AT, but successively enhance permeation and absorption of AT.

Table 2.4.7 The pharmacokinetic parameters of AT after a single oral dose of AT, to rat (each group 3 rats), in absence and presence of each of three concentrations of PI.

Pharmacokinetic parameters	**AT**	**AT + PI 0.09 mg/kg**	**AT + PI 0.45 mg/kg**	**AT + PI 0.9 mg/kg**
Absorption rate constant, K_a (hr^{-1})	-2.42	**-0.95**	-0.97	-0.88
Elimination rate constant, K_{el} (hr^{-1})	0.08	**0.08**	0.10	0.09
Time required for maximum plasma concentration, T_{max} (hr)	1.00	**2.00**	2.00	2.00
Maximum plasma concentration, C_{max} (ng/ml)	80.02	**290.69**	274.02	252.43
Plasma half life, $T_{1/2}$ (hr)	8.78	**8.37**	7.29	7.31
Area under curve at 24hr, $AUC_{(0-24)}$ (ng hr/ml)	740.56	**2448.77**	2427.07	2434.57
Area under curve at infinite time, $AUC_{(0-\infty)}$ (ng hr/ml)	874.23	**2817.44**	2706.77	2700.66
Area under curve at 24hr, $AUMC_{(0-24)}$ (ng hr^2/ml)	5558.52	**17635.48**	17135.58	17183.71
Volume of distribution, V_d (ml)	6.8	**2.2**	1.9	2.1
Mean residence time, MRT (hr)	7.51	**7.20**	7.06	7.06
Total clearance rate, TCR (ml/hr)	0.54	**0.19**	0.19	0.19
Relative Bioavailability (%)	1.00	**3.31**	3.27	3.28

Pharmacokinetic data are Mean values $\pm$ SD (n=3).

Although it is also found from above results that pharmacokinetics data show more enhancing effect of PI on AT permeation than Caco-2 cell line studies and *ex vivo* permeation studies. It can be explained by few observations; there are some differences such as firstly, AT is a hydrophilic drug that is transported via the paracellular route through

tight junctions. A higher permeability with *in-vivo* studies may be due to availability of larger area for absorption (15,16). Secondly, the intestine has mucus producing goblet cells, which influence the tight junctions. Caco-2 cells are lacking in mucus producing cells. It has been found in some previous studies that when Caco-2 cells mixed with mucus producing cells (HT29- MTX) and permeability studies of AT done, it can increase permeation of AT (17). Thus mucus producing cells play important role in AT permeation. Thirdly, differences in extracellular Ca^{++} concentrations can lead to change in the integrity of cell structures, thereby causing a change in paracellular permeability of AT (18). The cell tissue of intestine has a transepithelial electrical resistance (TEER) of 50–100 Ω cm^2 (19) and Caco-2 cell lines have a TEER of >200–300 Ω cm^2. AT, having a low permeability and being paracellularly transported, the higher TEER of Caco-2 cells may contribute to resistance to permeate AT molecules compare to intestinal cell tissue.

2.4.5.3 Pharmacokinetic Study of AT with GA

Plasma samples collected from the rats were analyzed using proposed reverse phase HPLC method and AT plasma concentration values were determined from calibration curve. Mean plasma concentrations of AT in each of rats i.e. control rat and rats treated with each of three concentrations of PI is shown in Table 2.4.8. Average plasma drug concentrations versus time profiles in presence of each concentrations of GA are represented in Figure 2.4.9, Figure 2.4.10 and Figure 2.4.11. It is clearly observed that plasma drug concentrations with each concentrations of GA are highly significant ($p < 0.001$) and increased than control AT.

Table 2.4.8 The mean plasma concentrations of AT after administrations of AT, AT with three concentrations of GA.

Time (hr)	Observed Mean ± SD Plasma Concentrations of AT (ng/ml) (n = 3)			
	AT (Control)	AT + GA 0.0225 mg/kg	AT + GA 0.1125 mg/kg	AT + GA 0.225 mg/kg
0.00	0.00 ± 0.00	0.00 ± 0.00	0.00 ± 0.00	0.00 ± 0.00
0.50	42.24 ± 6.42	93.76 ± 13.19	85.95 ± 2.88	79.67 ± 8.14
1.00	80.02 ± 12.79	158.33 ± 7.82	190.44 ± 14.76	119.46 ± 17.51
2.00	60.32 ± 6.84	296.13 ± 14.65	310.02 ± 16.94	221.03 ± 5.62
3.00	56.42 ± 3.61	213.54 ± 15.08	267.43 ± 13.96	150.01 ± 4.23
6.00	42.34 ± 5.55	145.50 ± 13.44	172.86 ± 8.19	78.79 ± 13.56
8.00	32.89 ± 3.00	114.58 ± 3.87	140.15 ± 2.97	67.51 ± 3.59
24.00	10.55 ± 1.31	33.69 ± 4.11	32.56 ± 9.27	22.56 ± 2.12

Figure 2.4.9 The Mean plasma concentrations versus time profile following a single oral administration of AT, and AT in presence of GA 0.0225 mg/kg. Each value is Mean ± SD of three determinations.

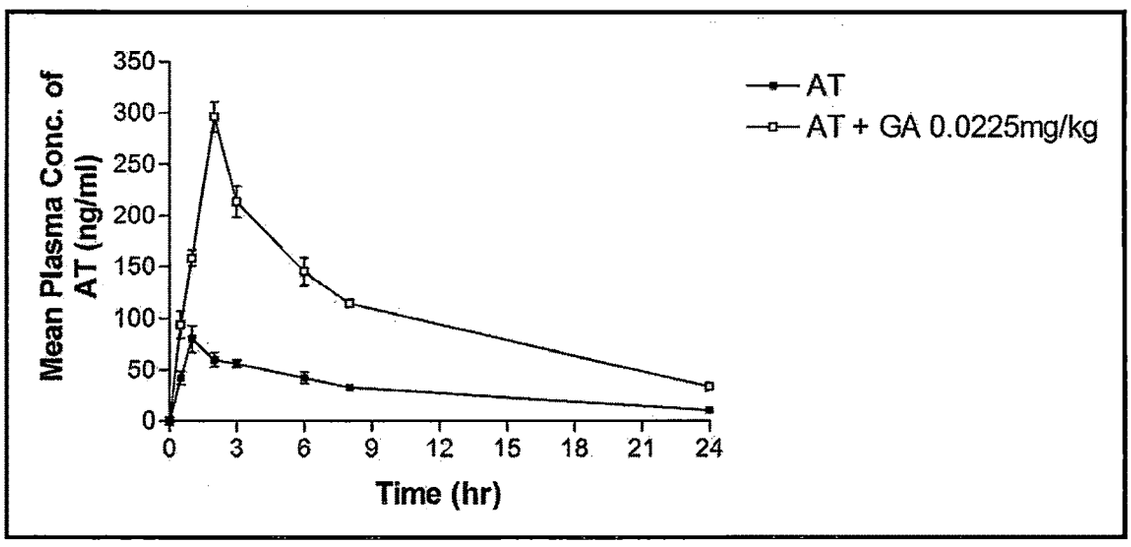

Figure 2.4.10 The Mean plasma concentrations versus time profile following a single oral administration of AT, and AT in presence of GA 0.1125 mg/kg. Each value is Mean ± SD of three determinations.

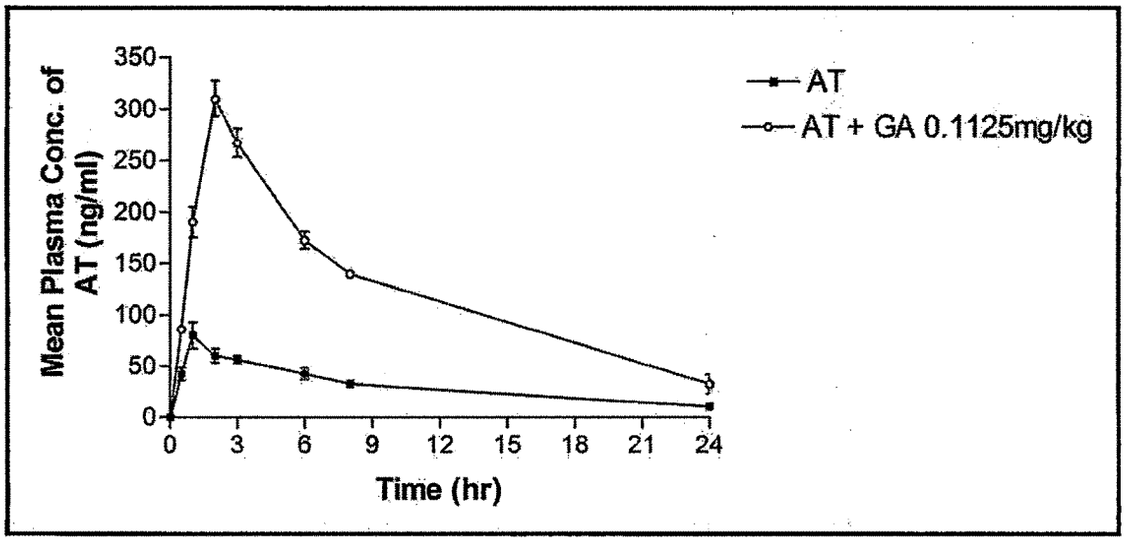

Figure 2.4.11 The Mean plasma concentrations versus time profile following a single oral administration of AT, and AT in presence of GA 0.225 mg/kg. Each value is Mean ± SD of three determinations.

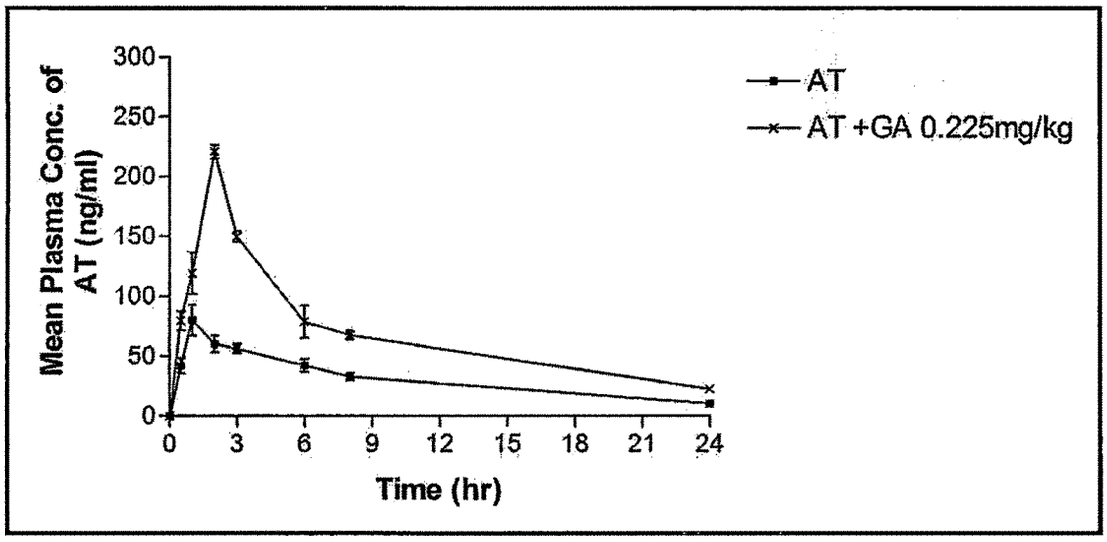

Figure 2.4.12 Figure 2.4.13, and Figure 2.4.14 represents the natural log of mean plasma concentrations of AT with time plot for absorption and elimination rate constant. Each Figure indicates there is no much change in elimination rate constant. Table 2.4.9 compares various pharmacokinetic parameters of AT with and without GA administration. It is found that C_{max}, $AUC_{0\text{-}24\ hr}$, $T_{1/2a}$, and K_a were increased, T_{max} also prolonged, whereas no much difference observed in K_{el}, $T_{1/2el}$. Relative bioavailability of AT with GA is almost 4 fold higher than pure drug AT.

Figure 2.4.12 The Natural log of mean plasma concentrations of AT with GA 0.0225 mg/kg versus time plot for determination of k_a and k_{el}. Each value is Mean ± SD of three determinations.

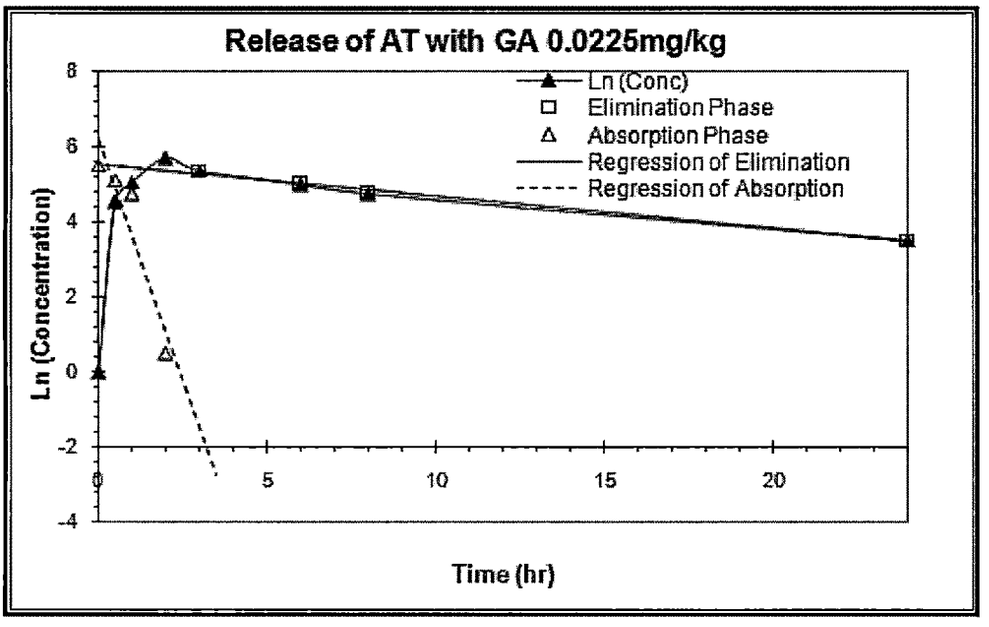

Figure 2.4.13 The Natural log of mean plasma concentrations of AT with GA 0.1125 mg/kg versus time plot for determination of k_a and k_{el}. Each value is Mean ± SD of three determinations.

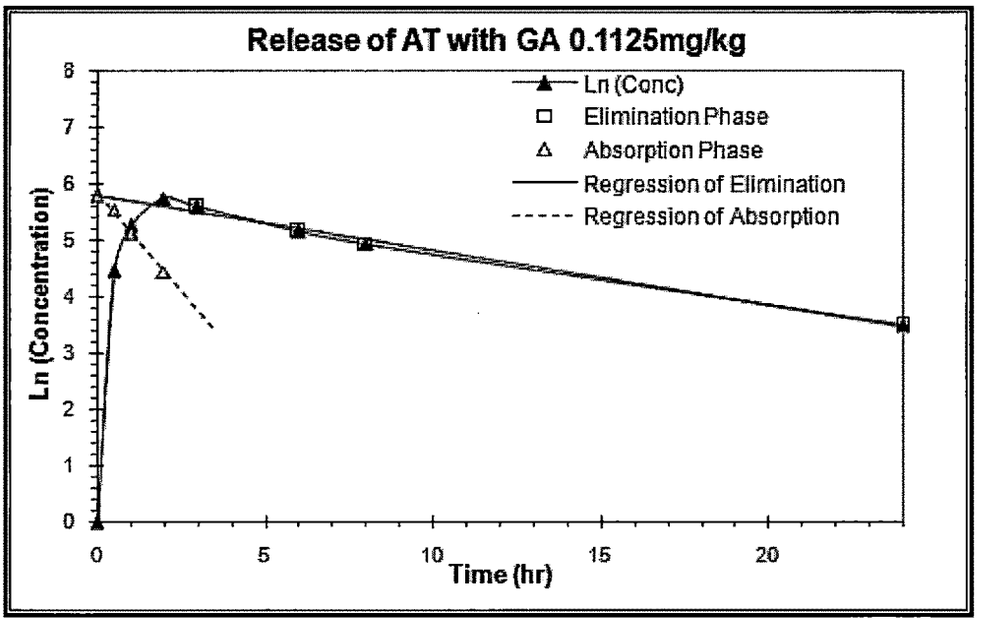

Figure 2.4.14 The Natural log of mean plasma concentrations of AT with GA 0.225 mg/kg versus time plot for determination of k_a and k_{el}. Each value is Mean ± SD of three determinations.

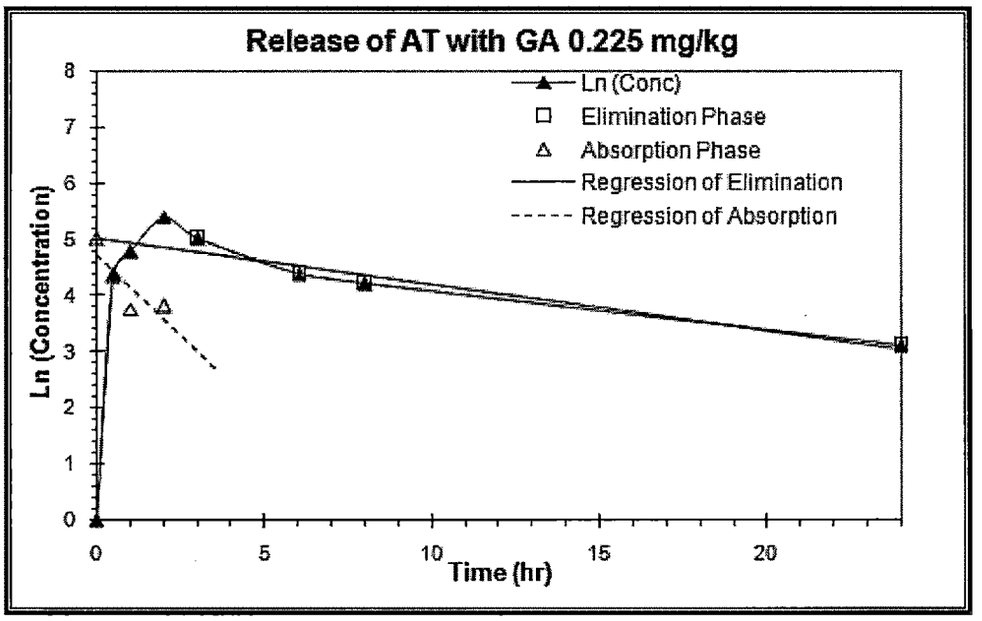

Table 2.4.9 The pharmacokinetic parameters of AT after a single oral dose of AT, to rat (each group 3 rats), in absence and presence of each of three concentrations of GA.

Pharmacokinetic parameters	**AT**	**AT + GA 0.0225mg/kg**	**AT + GA 0.1125mg/kg**	**AT + GA 0.225mg/kg**
Absorption rate constant, K_a (hr^{-1})	-2.42	-2.56	**-0.69**	-0.58
Elimination rate constant, K_{el} (hr^{-1})	0.08	0.08	**0.10**	0.08
Time required for maximum plasma concentration, T_{max} (hr)	1.00	2.00	**2.00**	2.00
Maximum plasma concentration, C_{max} (ng/ml)	80.02	296.13	**310.02**	221.03
Plasma half life, $T_{1/2}$ (hr)	8.78	8.21	**7.15**	8.53
Area under curve at 24hr, $AUC_{(0-24)}$ (ng hr/ml)	740.56	2553.33	**2984.70**	1635.59
Area under curve at infinite time, $AUC_{(0-\infty)}$ (ng hr/ml)	874.23	2952.23	**3320.88**	1913.17
Area under curve at 24hr, $AUMC_{(0-24)}$ (ng hr^2/ml)	5558.52	18916.43	**21324.92**	11826.19
Volume of distribution, V_d (ml)	6.8	1.9	**1.61**	3.49
Mean residence time, MRT (hr)	7.51	7.41	**7.14**	7.23
Total clearance rate, TCR (ml/hr)	0.54	0.16	**0.17**	0.28
Relative Bioavailability (%)	1.00	3.45	**4.03**	2.20

Pharmacokinetic data are Mean values $\pm$ SD (n=3).

Different concentrations of GA were administered to rats with AT, GA significantly increases mean plasma concentration of AT. Maximum bioenhancement (i.e. 4 fold than pure AT) of AT was found with 0.1125 mg/kg of GA (i.e. AT: GA 1:0.05 ratio). Enhanced absorption could be due to an interaction between GA and AT in the gastrointestinal tract.

The results obtained from Caco-2 cell line studies suggest that GA showed negligible effects on TEER and lacks prominent increase in AT permeation. The *in vivo* results suggest significant increase in transport of AT. Thus results of *in vivo* study are not consistent with

Caco-2 cell line studies. Glycyrrhizic acid which is obtained in form of a mixed K-Ca-Mg salt (glycyrrhizin) from the roots of licorice plants of *Glycyrrhiza glabra L.* and *Glycyrrhiza uralensis F.* species (20,21).In the present study ammonium salt of glycyrrhizic acid (GA) was used.

Figure 2.4.15 The stepwise hydrolysis of GA.

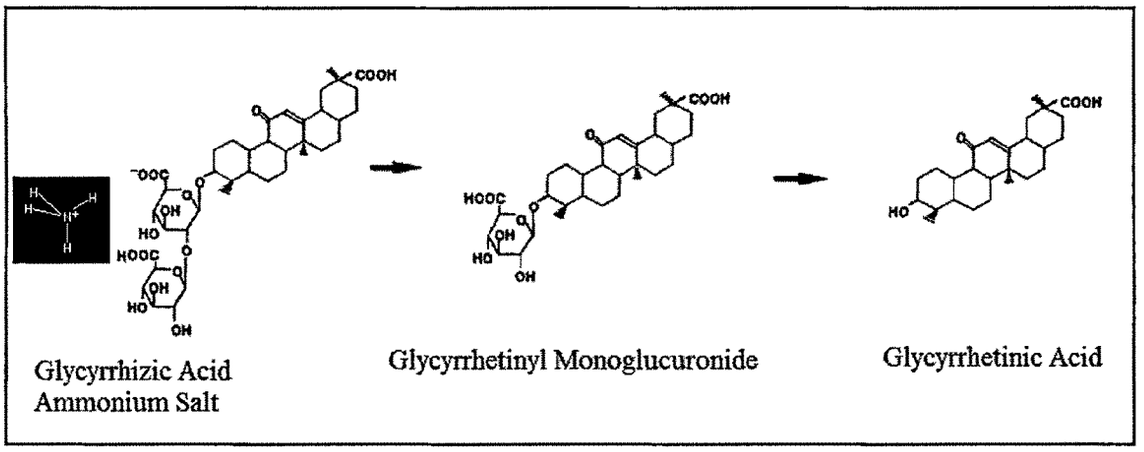

GA contains two glucuronosyl moieties linked to a steroid. GA hydrolysed in a stepwise manner (Figure 2.4.15) to monoglucuronide and then to glycyrrhetinic acid (GTA – aglycon of GA). This hydrolysis proceeds by endogenous (biliary or enteric) and bacterial β-glucuronidases in intestinal lumen (22,23). This GTA may cause activation of inositol triphosphate (IP_3) and calcium-calmodulin complex which cause increase in intracellular calcium concentration, which then provokes concentration of actin-myosin filaments resulting in opening of paracellular route (24). Thus increase in calcium ion concentration can be leading to enhancement of AT though paracellular opening. Thus prominent increase in permeation of AT when administered with GA is due to its hydrolysed product GTA, which can cause paracellular opening and due to its surfactant like effect (section 2.3.4.3) (25,26). It is found that highest concentration of GA – 0.225 mg/kg (10 % weight of AT) is having less enhancement than GA – 0.0225 mg/kg (1 % weight of AT) and GA – 0.1125 mg/kg (5 % weight of AT) that may be due to saturation effect of GA.

2.4.6 Conclusion

The results pharmacokinetic data suggests that both bioenhancers PI and GA effectively cause increment in mean AT plasma concentration. Both bioenhancers PI and GA administration with AT causes increment in area under the curve and absorption rate. They don't affect elimination rate but prolong T_{max}. The results of *in vivo* studies of AT with PI and GA are almost similar but more enhancement of AT found with GA than PI. The *in vivo* results of enhancement in permeation are same as the results obtained in previous studies of *ex vivo* permeation and *in vitro* cell line studies.

In the *in vivo* studies of AT with PI, lowest concentration of PI (AT: PI 5:1 i.e. 0.09 mg/kg of PI) is sufficient enough to act as bioenhancer and cause 3 fold increase in bioavailability. While in *ex vivo* studies it has been found that PI (AT: PI 5:2) cause 2 fold increase in permeation of AT. This suggests that for *in vivo* permeation lowest concentration of PI is more effective as bioenhancer. Therefore binary system of PM method with PI ratio (AT: PI 5:1) was optimised for formulation development.

In the *in vivo* studies of AT with GA, (AT: GA 1:0.05 i.e. 0.1125 mg/kg of GA) is causing 4 fold increase in bioavailability of AT. Same ratio of AT: GA cause 2.5 fold increase in permeation of AT in *ex vivo* permeation studies. Thus in both studies AT: GA 1:0.05 (i.e. 0.1125 mg/kg of GA) is sufficient enough to act as bioenhancer. Therefore binary system of PM method with GA ratio (AT: GA 1:0.05) was optimised for formulation development.

These herbal origin bioenhancers are not causing any toxicity on the intestinal membrane like synthetic bioenhancers. Thus PI and GA can be successfully utilized as bioenhancer for atenolol.

2.4.7 References

1 M. Rowland, T. N. Tozer, Clinical Pharmacokinetics: Concepts and Applications, Edn 3, Lea and Febiger, Phiadelphia, PA, USA, **1995**, 119–134.

2 Microsoft office Excel 2007, Microsoft Press, Redmont, WA, **2007**.

3 J. G. Wagner, E. Nelson, Kinetic analysis of blood levels and urinary excretion in the absorptive phase after single doses of drug, J Pharm Sci., **1964**, 53, 1392–1396.

4 J. G. Wagner, Absorption rate constant calculated according to the one compartment open model with first order-absorption: Implications in in vivo in vitro correlation, J Pharm Sci., **1970**, 59, 1049–1053.

5 D. Bourne, Mathematical Modeling of Pharmacokinetic Data, Technomic Publishing Company, Lancaster, PA, USA, **1995**.

6 L. Shargel, A. Yu, Applied Biopharmaceutics and Pharmacokinetics. Edn 4, CT: Appleton & Lange, Stamford, UK, **1999**.

7 G. Banker, C. Rhodes, Modern Pharmaceutics, Edn 4, Marcel Dekker, New York, USA, **2002**.

8 L. Liu, X. Wang, Solubility-modulated monolithic osmotic pump tablet for atenolol delivery, Eur J Pharm Biopharm.,**2008**, 68, 298–302.

9 Y. Tashiro, M. Sami, S. Shichibe, Y. Kato, E. Hayakawa K. Itoh, Effect of lipophilicity on *in vivo* iontophoretic delivery. II. β –Blockers, Biol Pharm Bull., **2001**, 24, 671–677.

10 G. E. Paget, J. M. Barnes, In Evaluation of Drug Activities: Pharmacometrics, Edn 2, vol 1, Academic press, New York, USA, **1964**.

11 M. N. Ghosh, Fundamentals of Experimental Pharmacology, Edn 3, Hilton & Company, Kolkata, India, **2005**, 192–201.

12 Guidance for the Industry: Bioanalytical Method Validation, Department of Health and Human Services, US Food and Drug Administration, Center for Drug Evaluation and Research (CDER), Rockville, MD, USA, **2001**, (http://www.fda.gov/cder/guidance/4252fnl.pdf).

13 A. Khajuria, U. Zutsi, K. L. Bedi, Permeability characteristic of piperine on oral absorption – an active alkaloid from peppers as a bioavailability enhancer, Indian J Exp Biol., **1998**, 36, 46–50.

14 A. Khajuria, N. Thusu, U. Zutshi, Piperine modulates permeability characteristics of intestine by inducing alterations in membrane dynamics: influence on brush border membrane fluidity, ultrastructure and enzyme kinetics, **Phytomedicine**., **2002**, 9, 224–231.

15 H. Lennerna¨s, O. Ahrenstedt, A-L Ungell, Intestinal drug absorption during induced net water absorption in man: A mechanistic study using antipyrine, atenolol, and enalaprilat, Br J Clin Pharmacol., **1994**, 37, 589–596.

16 H. Lennerna¨s, Human intestinal permeability, J Pharm Sci., **1998**, 87(4), 403–410.

17 S. Louis, Drug, Fact and Comparisons, Edn 55, New York, USA, **2001**, 477–480.

18 P. Artursson, C. Magnussen, Epithelial transport of drugs in cell culture. II: Effect of extracellular calcium concentration on the paracellular transport of drugs of different lipophilicity across monolayers of intestinal (Caco-2) cells, J Pharm Sci., **1990**, 79(7), 595–600.

19 A. Collett, E. Sims, D. Walker, Y-L He, J. Ayrton, M. Rowland, G. Warhurst, Comparison of HT29-18-C1 and Caco-2 cell lines as models for studying intestinal paracellular drug absorption, Pharm Res., **1996**, 13(2), 216–221.

20 S. Ishida, Y. Sakiya, T. Ishikava, S. Awazu, Pharmacokinetics of Glycyrrhetic Acid, a Major Metabolite of Glycyrrhizin, in Rats, Chem Pharm Bull., **1989**, 37(9), 2509–2513.

21 Sakamoto K, Wakabayashi K. Inhibitory effect of glycyrrhetinic acid on testosterone production in rat gonads, EndocrinoL Jpn., **1988**, 35(2), 333–342.

22 S. Takeda, K. Ishihara, Y. Wakui, S. Amagaya, M. Maruno, T. Akao, K. Kobashi, Bioavailability study of glycyrrhetic acid after oral administration of glycyrrhizin in rats; Relevance to the intestinal bacterial hydrolysis. J Pharm Pharmacol., 1996, 48, 902–905.

23 T. Akao, T. Hayashi, K. Kobashi, M. Kanaoka, H. Kato, M. Kobayashi, Intestinal bacterial hydrolysis is indispensable to absorption of 18β-glycyrrhetic acid after oral administration of glycyrrhizin in rats, J Pham Pharmacol., **1994**, 46, 135–137.

24 T. Imai, M. Sakai, H. Ohtake, H. Azuma, M. Otagiri, In vitro and in vivo evaluation of the enhancing activity of glycyrrhizin on the intestinal absorption of drugs, Pharm Res., **1999**, 16, 80–86.

25 N. A. Motlekar, K. S. Srivenugopal, M. S. Wachtel, B. C. Youan, Evaluation of the Oral Bioavailability of Low Molecular Weight Heparin Formulated With Glycyrrhetinic Acid as Permeation Enhancer, Drug Dev Res., **2006**, 67(2), 166–174.

26 S. P. S. Khanuja, S. A. Kumar, M. Singh, Composition comprising pharmaceutical /nutraceutical agent and a bio-enhancer obtained from Glycyrrhiza glabra, U.S. Pat. No. 6, 979, 471, **2005**.

2.5 FORMULATION DEVELOPMENT OF ATENOLOL

In the present section, binary systems of atenolol and both bioenhancers (PI and GA) of physical mixture (PM) method were formulated as single oral powder form. Various compatible excipients were used to formulate the oral powders. The prepared formulations were evaluated for,

- Appearance,
- Angle of repose
- Uniformity of content

Oral powders are preparations consisting of solid, loose, dry particles of varying degrees of fineness. They contain one or more active substances, with or without excipients and, if necessary, colouring matter and flavouring substances which are authorised by competent authority. Generally they are administered in or with water or another suitable liquid. They can be swallowed directly. They are presented as single-dose or multi-dose preparations. In manufacturing of oral powders, means are taken to ensure a suitable particle size with regard to the intended use. To comply with the standards monograph of oral powder includes the test for 'uniformity of dosage units'. Single-dose oral powders comply with the test for uniformity of dosage units or, where justified and authorised, with the tests for uniformity of content and/or uniformity of mass are also done. Herbal drugs and herbal drug preparations present in the dosage form *are not subject* to the provisions of this paragraph (1). Single dose oral powder form is easier to formulate. Absorption is quite quick than that of the tablet and capsule. Administration is also patient compliant and found to be stable.

2.5.1 Materials

The Model drug atenolol (AT) was procured as a gift sample from Wockhardt Ltd., Mumbai, India. Piperine (PI) and Glycyrrhizic acid ammonium salt (GA) were purchased from Sigma Aldrich Ltd., Mumbai, India. Anhydrous lactose NF (direct tableting) was procured as gift sample from Quest International, IL, USA. Magnesium Stearate was purchased from Suvidhinath Lab, Baroda, India. Sodium lauryl sulphate obtained from Alembic Ltd., Baroda, India.

2.5.2 Formulation Development of AT-bioenhancer binary systems

Each of previous studies of bioenhancement of AT by PI suggests that in the physical mixture (PM) method with AT: PI (5:1) ratio shows maximum permeation compared to other two ratios. The studies of bioenhancement of AT by GA suggests that PM method with AT: GA (1:0.05 i.e GA is 5 % w/w of AT) shows maximum permeation. This optimized binary system of AT-PI and AT-GA was selected to formulate single dose oral powder. These single dose oral powders were incorporated into *cachets* to avoid leaching and provide better storage conditions. The formula of powder is summarised in Table 2.5.1. Anhydrous lactose of direct compressible grade was used as diluent. Magnesium stearate was used as lubricant. Sodium lauryl sulphate was used to aid the dissolution of the powder.

Table 2.5.1 Formulation of single dose oral powder.

Drug/Excipients	AT-PI binary system	AT-GA binary system
PM of AT-PI/ AT-GA containing eq. to 25 mg AT (g)	0.600	0.525
Anhydrous Lactose (g)	3.344	3.419
Magnesium Stearate (g)	0.036	0.036
Sodium Lauryl Sulphate (g)	0.020	0.020
Total filled weight per 20 cachet (g)	4.000	4.000

2.5.3 Evaluation Parameters

2.5.3.1 Angle of Repose (Φ)

For measurement of angle of repose, the powder was passed through a funnel on the horizontal surface. The height (h) of the heap formed was measured with a cathetometer and the radius (r) of the cone base was also determined. The angle of repose (Φ) was calculated from the **equation 2.5.1,**

Equation 2.5.1

$$\phi = \tan^{-1}\left(\frac{h}{r}\right)$$

2.5.3.2 Uniformity of Content

The drug eq. to 25 mg of the powder dosage was dissolved in 25 ml methanol. AT was determined using spectrophotometric method. For AT-PI binary system, AT was determined as method described in section 2.1.3.3 and for AT-GA binary system, as per section 2.2.3.3. Each characteristics of oral powder are summarized in Table 2.5.2.

Table 2.5.2 Properties of single dose oral powder of AT-PI and AT-GA binary systems.

Parameters	AT-PI binary system	AT-GA binary system
Appearance	White powder	White powder
Uniformity of Content	99.98 ± 0.04	100.07 ± 0.14
Angle of Repose (°) ± SD*	30.92 ± 2.02	29.41 ± 1.57

* Data represents the Mean ± SD (n = 3)

2.5.4 References

1 British Pharmacopoeia, Vol. 1, HMSO, London, **2005**, 789.